Université de Montréal

A computational fluid dynamic study on the filtering mechanics in suspension feeding marine invertebrates

par
Maureen Vo

Département de sciences biologiques
Faculté des arts et sciences

Mémoire présenté à la Faculté des études supérieures
en vue de l'obtention du grade de Maître en Sciences (M.Sc.)
en sciences biologiques

Août, 2013

Université de Montréal
Faculté des études supérieures et postdoctorales

ce mémoire intitulé:

A computational fluid dynamic study on the filtering mechanics in suspension feeding marine invertebrates

Présenté par:
Maureen Vo

a été evalué par un jury composé des personnes suivantes:

Dr. Anja Geitman, président-rapporteur
Dr. Christopher B. Cameron, directeur de recherche
Dr. Dominique Pelletier, co-directeur de recherche
Dr. Stephane Etienne, membre du jury

Résumé

Les suspensivores ont la tâche importante de séparer les particules de l'eau. Bien qu'une grande gamme de morphologies existe pour les structures d'alimentation, elles sont pratiquement toutes constituées de rangées de cylindres qui interagissent avec leur environnement fluide. Le mécanisme de capture des particules utilisé dépend des contraintes morphologiques, des besoins énergétiques et des conditions d'écoulement. Comme nos objectifs étaient de comprendre ces relations, nous avons eu recours à des études de comparaison pour interpréter les tendances en nature et pour comprendre les conditions qui provoquent de nouveaux fonctionnements. Nous avons utilisé la dynamique des fluides numérique (*computational fluid dynamics*, CFD) pour créer des expériences contrôlées et pour simplifier les analyses. Notre première étude démontre que les coûts énergétiques associés au pompage dans les espaces petits sont élevés. De plus, le CFD suggère que les fentes branchiales des ptérobranches sont des structures rudimentaires, d'un ancêtre plus grande. Ce dernier point confirme l'hypothèse qu'un ver se nourrit par filtration tel que l'ancêtre des deuterostomes. Notre deuxième étude détermine la gamme du nombre de Reynolds number critique où la performance d'un filtre de balane change. Quand le Re est très bas, les différences morphologiques n'ont pas un grand effet sur le fonctionnement. Cependant, une pagaie devient une passoire lorsque le Re se trouve entre 1 et 3,5. Le CFD s'est dévoilé être un outil très utile qui a permis d'obtenir des détails sur les microfluides. Ces études montrent comment la morphologie et les dynamiques des fluides interagissent avec la mécanisme de capture ou de structures utilisées, ainsi que comment des petits changements de taille, de forme, ou de vitesse d'écoulement peuvent conduire à un nouveau fonctionnement.

Mot-clés: suspensivores, filtration, énergétique, biomécanique, dynamique des fluides numérique, évolution, hémichordés, balanes

Abstract

Suspension feeders have the important task of separating particles from the liquid medium surrounding them. Although a wide range of morphologies exist for feeding structures, essentially all consist of arrays of cylinders interacting with their fluid environment. The particle capture mechanism employed depends on morphological constraints, energy requirements, and flow conditions, therefore our objectives were to understand these relationships through comparison studies to interpret trends in nature and to understand the conditions in which novel functioning arises. Our studies used computational fluid dynamics (CFD) to create controlled experiments and to simplify analyses. The first study demonstrates the unfeasibly high energetic costs of pumping in small and medium pharynx sizes of hemichordates, implying the gill pores of pterobranchs are likely vestigial structures from a larger ancestor. This last point further supports the hypothesis of an acorn worm as the ancestor to all deuterostomes. Our second study determined the critical Reynolds number (Re) range where barnacle filters transition from a paddle to a sieve. At very low Re, morphological differences have no major effect on functioning and filters behave as paddles, however, at Re 1 - 3.5, these differences dictate when a paddle becomes a sieve. CFD proved to be a very useful tool for simplifying studies and providing detailed microfluidics. These studies demonstrate how morphology and fluid dynamics interact to dictate the capture mechanisms or appendages employed and how simple changes in size, shape, or flow speed can lead to novel functioning.

Keywords: suspension feeding, filtration, energetics, biomechanics, computational fluid dynamics, evolution, hemichordates, barnacles

TABLE DES MATIÈRES

Liste des tableaux

Liste des Figures

1.80 mm s^{-1}. (C) Twenty-day old *Saccoglossus kowalevskii*. Paired gill pores (inset) of enteropneusts develop sequentially starting from the anterior trunk region, towards the posterior. Initially they are simple circular pores, then elongate into slit shape with the extension of collagenous gill bars. (D) A *Cephalodiscus gracilis* zooid that has been removed from its tube. Its single pair of gill pores (inset) are about 9 μm in diameter and are not heavily ciliated. (E) Pharyngeal filtering morphology of *Harrimania planktophilus*. Suspension enters through the mouth (long arrow) and exits the pharynx through the gill slits. For a more thorough explanation, see Cameron (2002). c, collar; cs, cephalic shield; ft, feeding tentacles; gp, primary gill bar; m, mouth; mi, milk; pip, pipette; ps, posterior extension of metasome; p, proboscis; t, trunk.

Figure 2.2. Finite element model of the reference pharynx, perforated with gill pores showing the mesh of domain elements. There are 271894 finite elements in the reference model. In all models the mass inflow of seawater at the mouth was defined at a constant of 1.608 x10-5 kgs_{-1}, based on video recordings from *Protoglossus graveolens*. (A) side view; (B) front mouth view into pharynx. m, mouth; g, gill depth; l, pharynx length; d, pharynx diameter; p1, pore 1; p2, pore 2; ew, esophageal wall. Arrows denote direction of flow.

Figure 2.3. Velocity profiles and fluid path-lines showing the change in velocity of fluid throughout the reference model with static (A,B,C,E) and sliding gill pores walls (D,F). (A) Path-line of fluid entering the mouth colored by velocity magnitude (ms^{-1}). (B) Velocity contour in a cross sectional plane through the pharynx at the position of the gill pores (i.e., y-axis). (C) Velocity profile of section along the x-axis showing the increase in velocity as water approaches and exits a pore. (D) Fluid velocity profile with sliding gill pore walls. (E) Fluid velocity contour of the inside of a gill pore with a static wall, top-view. (F) Fluid velocity contour of the inside of a gill pore with a sliding wall, top-view. Arrows denote direction of flow.

Figure 2.4. Power output (in watts) required by pumps, of different pharynx and pore sizes and shapes, to overcome friction. (A) Power output with three different pore numbers

(n); (B) power output of a 2 pore simulation using different pore diameters and shapes; (C) power output required at increasing pharynx length (mm); and (D) power output with increasing pharynx diameter (mm).

Figure 2.5. Pressure drop (Pa) between the mouth and gill pores of twelve model calculations in increasing order. Energy usage goes up with pressure drop.

Figure 3.1. Captorial feeding net of sheltered and exposed barnacles. A, exposed barnacle phenotype showing cirri I-VI and B, sheltered barnacle phenotype.

Figure 3.2. Sheltered specimen showing traits measured. A, complete captorial feeding net with boxed area showing central portion of cirri VI used for CFD modeling. B, front view showing intersetal spacing (i.e. from A to B); C, side view; D, cross section through central portion of cirri VI. h, height of segment; l, length of segment; s, setae lengths (measured from base to tip); w, width of segment; Θ, angle of setae protruding from segment

Figure 3.3. CFD section modeled. A) side view of a segment and setae, with setae numbered in descending size order; B) top, cross-section view of segment C) front view of full section. b, base diameter; h, height of segment; i, intersetal spacing; l, length of segment; s, setae length; t, tip diameter; w, width of segment; Θ, angle of setae with respect to segment.

Figure 3.4. Meshed GAMBIT models. Sheltered (A-B) and exposed (C-D) models. A) Sheltered front view; B) Sheltered top view; C) Exposed front view; D) Exposed top view

Figure 3.5. Setae with boxed boundary

Figure 3.6. Velocity contours. Top view of velocity contours passing through intersecting setae with symmetric view applied. A-C sheltered, D-F exposed at corresponding velocities. Symmetry applied to represent scale of simulations.

Figure 3.7. Velocity vectors passing through intersecting setae at increasing velocities. A-

C sheltered vector profiles; D-F exposed vector profiles. Since flow fields are symmetric, only a single enclosed setae section shown. Arrow lengths denote relative velocities.

Figure 3.8. PIV of wake behaviour. Sheltered filter (A-C) and exposed filter (D-F). A, D show slow recirculating vortices; B, flow is passing through the filter, altering wake and flow separation point is pushed rearward; C, full leakiness with a short, turbulent wake and flow separation pushed further rearward; E, flip-flopping wake; F, short, turbulent wake with flow separation.

Figure 3.9. Drag coefficient plotted against Re. A, inner and B, outer setae.

Figure 4.0. CFD percent of mass flow rate passing through setae at increasing Re.

Figure 4.1. PIV leakiness with increasing Reynolds number.

Figure 4.2. PIV flow fields representing paddle and sieve-like behaviour in a sheltered barnacle filter. A-C show paddle-like behaviour as a seeding cloud approaches and passes around the perimeter of filter at slow flow (i.e. 0.027 m/s, Re = 0.46). D-E show sieve-like functioning at faster flow (i.e. 0.13 m/s, Re = 2.24), with arrows denoting movement of a particle passing directly through the center of filter.

Figure 4.3. PIV flow fields of exposed filter at 0.161 m/s (Re = 3.8). Sieve-like behaviour with A, showing flow field before seeding and B, directly after with arrows denoting particles passing directly through the center of filter.

Figure A1. CFD simulation showing the velocity profile of seawater throughout the 2-pore reference model, where the pharynx wall was set to slide posteriorly at a rate of 0.3309 ms^{-1}.

Figure. A2. CFD simulation showing the velocity profile through a half diameter reference model with sliding pharynx wall velocity set to slide posteriorly at 0.3309 ms^{-1}.

Figure. A3. CFD simulation showing the velocity profile through a half diameter reference model with sliding gill and pharynx walls set to slide posteriorly at a rate of 0.020 ms^{-1} and 0.015 ms^{-1} respectively.

Fig. A4. CFD simulation showing the velocity profile through a half diameter reference model using simultaneously sliding gill and pharynx walls, as done in A3, however the pharynx wall has been drastically decelerated. The walls of the gills and pharynx are set to slide posteriorly at a rate of 0.020 ms^{-1} and 0.004 ms^{-1} respectively.

Figure A5. Experimental setup. A, recirculating flume showing camera, laser and barnacle positions. B, laser positioned on top of the flume and pointing down through the optical crystal to create a vertical laser sheet.

Figure A6. Velocity contours at Re = 0.5. A, Through decreasing cylinder diameters and B, through uniform diameter cylinders

Figure A7. Setae Reynolds number with increasing velocities. A, sheltered setae and B, exposed setae.

Liste des vidéos

Vidéo A1. Summary of PIV flow fields in a sheltered barnacle filter. Velocities ranging from 0.027 m/s - 0.13 m/s.

Vidéo A2. Summary of PIV flow fields in an exposed barnacle. Velocities ranging from 0.027 m/s - 0.16 m/s.

Liste des abréviations

A	area
CFD	Computational fluid dynamics
C^d	Coefficient of drag
D	diameter
EPC	Electronic particle counters
FCM	Flow cytometry
FVM	Finite volume methods
$\vec{F}$	surface force
L	gap spaces
L	characteristic length
L/d	center-to-center ratio
ME	million elements
N-S	Navier-stokes
η	pump efficiency
$\hat{n}$	normal vector
PIV	particle image velocimetry
P_{op}	pumping power output
P	pumping rates
ρ	pressure, density
Q	Volumetric flow rate
Re	Reynolds number
R_{tot}	metabolic input
τ	viscous strain tensor
U	viscosity
v	kinematic viscosity
$\vec{V}$	vector force

ACKNOWLEDGEMENTS

My sincerest thanks go to my director Christopher Cameron who had the faith to trust I would succeed despite the many obstacles. It has been a privilege to learn from him and work in his lab. Thanks for all the meaningful discussions and the unforgettable experiences in beautiful Bamfield.

I would like to give a big thanks out to Dominique Pelletier and Fernando Villalpando for their countless guidance with CFD and helpful discussions which have allowed me to achieve these new found skills. Thanks to all the members of the fluid dynamics lab at École Polytechnique for their continual encouragement and helpful advice along the way.

My sincere gratitude to all the wonderful people I have met at Bamfield Marine Sciences Centre for their incredible efforts to help during my many technical difficulties.

Finally, thank you to my friends and family who have provided me with nothing but love and support during this journey.

CHAPTER 1

Suspension feeding in marine invertebrates

1. INTRODUCTION

1.1 Suspension feeding marine invertebrates

Suspension feeding invertebrates have the impressive ability of separating edible particles from the fluid in which they are suspended. These particles can include detritus, protists, or animals and range anywhere in size from sub-micron free-living bacteria (i.e. 0.1 - 2μm) up to long-chains of diatoms or krill (i.e. up to 10 cm across) (Vogel, 2003; Riisgård and Larsen, 2010). Large sponges, for example, have evolved to become effective filter feeders with nearly 100% retention of particles down to 0.1μm diameter (Riisgård and Larsen, 2010). Considering colloidal particles represent the largest pools of organic carbon on the planet (Jørgensen, 1955; Kepkay, 1994), unattainable to most other animals, suspension feeders play a pivotal role in marine ecosystem as energy links between microplankton and higher trophic levels in marine food chains (Koehl, 1996). Calanoid copepods, for example, are a major link in marine food chains whose feeding can alter both the abundance and composition of phytoplankton (Koehl, 1983). Deciphering the functioning of the particle capturing system of suspension feeders improves both our biological and physical understanding of these ecologically important organisms.

1.2 Diversity of organisms and structures

The importance of suspension feeders is represented by the fact that they are found in nearly all animal classes in the marine environment (e.g. sponges, anemones, jellyfish, bryozoans, annelids, microcrustaceans, barnacles, bivalves, polychaetes, ctenophores, and ascidians) and in oceans world wide (Jorgensen, 1975; Riisgård and Larsen, 1995; Riisgård and Larsen, 2000; Vogel, 2003). Sizes can range anywhere from several millimeters, as with the appendicularian *Oikopleura labradoriensis* (Flood, 1991), up to several meters long, as observed in the enteropneust *Balanoglossus gigas,* which sometimes exceed 2 m long (Horst, 1939). With this great diversity of suspension feeders and plankton to capture, a comparable diversity of appendages and particle capture mechanisms have developed (Figure 1.1).

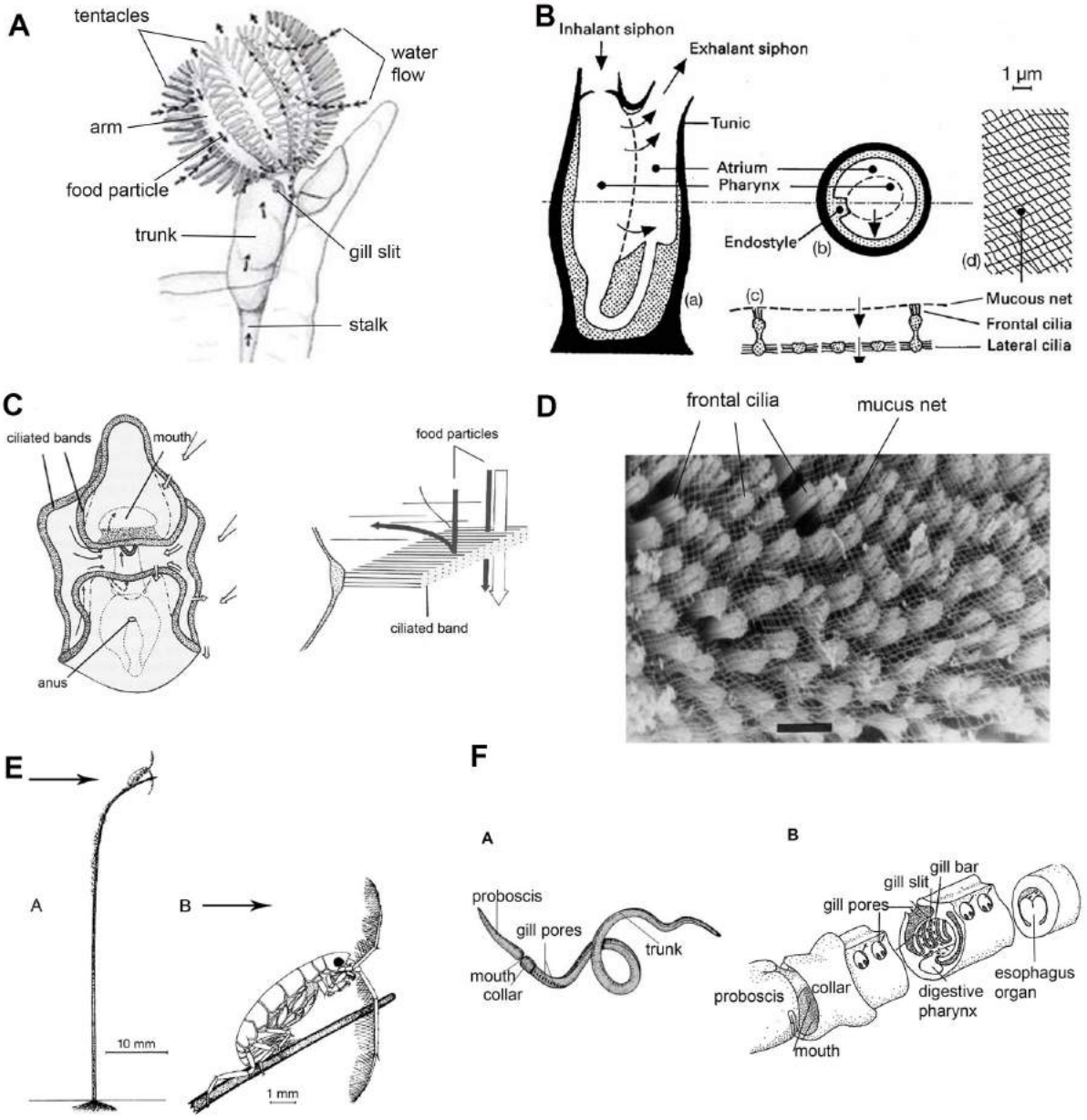

Figure 1.1. Diversity of filtering structures among suspension feeders. A, *Cephalodiscus* with upward-pointing curved arrows denoting movement of water around lophophorate filtering structure and downward arrows denoting particle movement. Reprinted with permission from Lester (1985). B, an ascidian revealing the filtering process through the pharyngeal cavity. Reprinted with permission from Petersen, J.K (2007). C, dipleurula larva. Modified from Ruppert et al. (2004). D, filter net of the ascidian, *Salpa fusiformis,* scale bar = 10µm. Reprinted with permission from Bone et al. (2003). E, amphipod, *Dyopedos monacanthus,* with (A) showing the position of the amphipod high on its mast to reach a higher level in the boundary layer; and (B) a detailed view showing the long setose antennae used for sieving food particles from water. Reprinted with permission from Mattson & Cedhagen (1989). F, enteropneust with (A) general body plan and (B) a cross section through the internal pharyngeal filtering structure. Modified with permission from Cameron (2002a).

Although a wide range of filtering structures exist among classes and even families, essentially all suspension feeding appendages consist of arrays of bristles, or cylinders, beating on feeding organs that function at low Reynolds number (Re) to capture particles or produce water currents (LaBarbera, 1984). The Reynolds number (Re = UL/v, where U is the velocity, L is some characteristic length, and v is the kinematic viscosity of the fluid) represents the ratio of inertial to viscous forces for a particular flow, which informs us of the fluid behaviour around appendages (Vogel, 2003). Filtering elements are all generally very small in size, ranging from 10^{-1} μm diameter cilia and flagella in animals such as bryozoans and copepods to 10^{1}-10^{2} μm diameter tentacles in corals (LaBarbera, 1984).

1.3 Capture mechanisms

Filter feeding and suspension feeding are sometimes synonymously used, however as filter feeding simply implies straining particles with specialized filtering structures and ignores several important processes such as the migration of particles across steep gradients and oscillatory flow patterns, suspension feeding is now the preferred term for all animals living off plankton (Jorgensen, 1983; Vogel, 2003). Regardless of morphology, the feeding process of any suspension feeder includes: i) transport of water to feeding appendages, ii) extraction and retention of particles from suspension, iii) transport of captured particles to the mouth, and iv) ingestion (Strathmann et al., 1972; LaBarbera, 1981; LaBarbera, 1984; Wildish and Kristmanson, 2005).

Various filtering appendages and behavioural tricks are employed by suspension feeders to capture their particles. Barnacles put up passive screens to catch particles and may even reorient or sweep these filters to maximize particle capture depending on flow conditions (Figure 1.2A) (Anderson, 1994). Lateral cilia of cephalochordate create a feeding current which enters the inhalant siphon, passes through the mucus net filter, and exits via the exhalant aperture or siphon (Figure 1.2B) (Riisgård and Svane, 1999). Some sessile organisms living in colonies or stalks (e.g. bryozoans) exposed to the free stream may take advantage of faster flow conditions (Figure 1.2C) (Riisgård and Larsen, 2010). Regardless of the mechanisms used to capture, all have essentially evolved to solve the common basic problem of extracting a sufficient amount of food from the surrounding water.

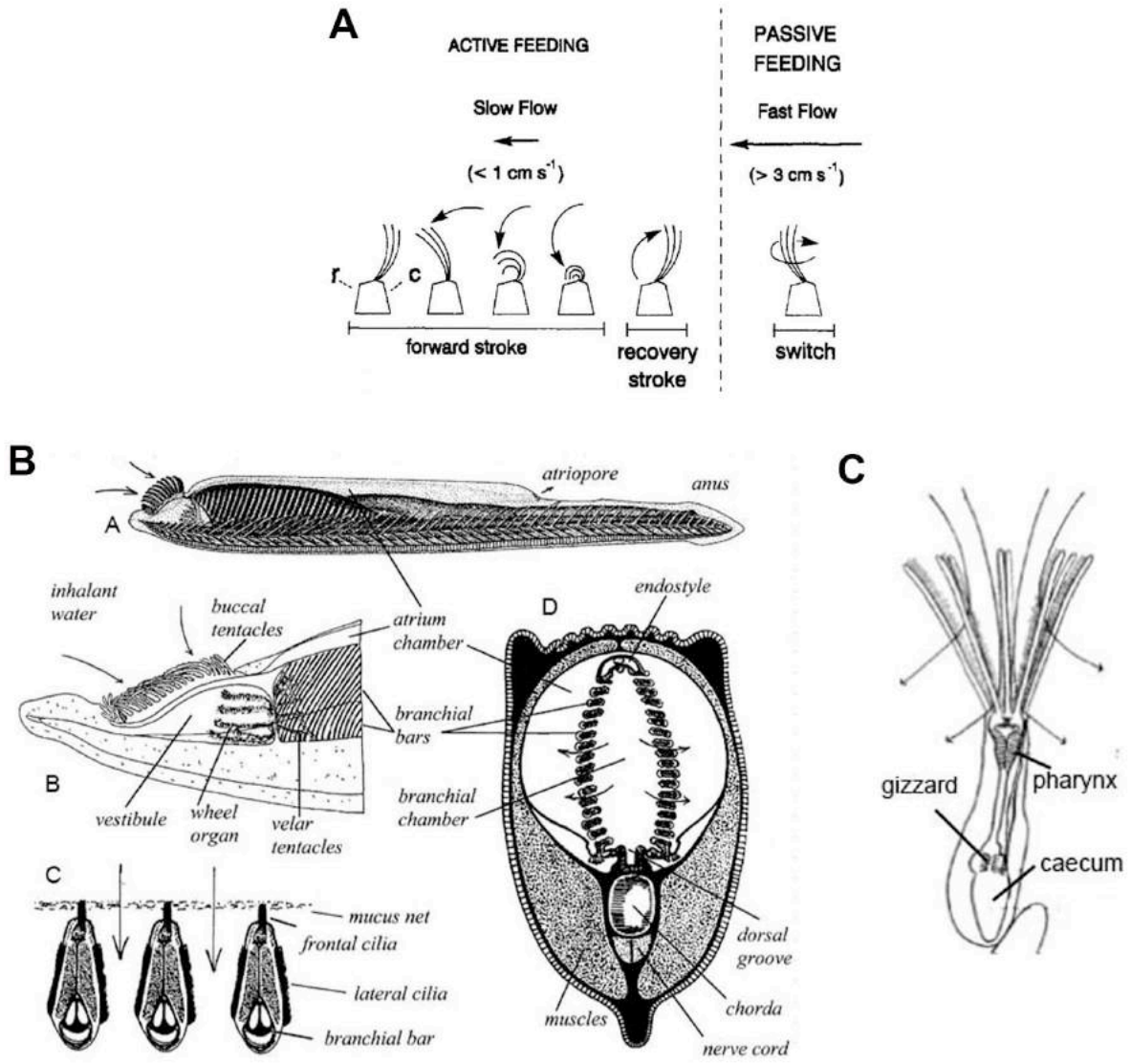

Figure 1.2. Examples of filtering mechanisms. A, Active and Passive feeding behaviour in barnacles. Reprinted with permission from Trager et al. (1990). B, Cephalochordate filter pump structure (A-D). Arrows denote direction of water flow. Reprinted with permission from Riisgård & Svane (1999) (based on various sources). C, Bryozoan *Zoobotryon verticillatum* with lophophorate extended. Arrows denoting feeding currents and fronto-lateral setae drawn approximately to scale. Reprinted with permission from Bullivant (1968).

The physical mechanisms to separate particles from medium prove to be very diverse. Six different ways organisms separate particles from medium have now been identified: simple sieving, direct interception, inertial impaction, gravitational deposition, diffusional deposition, and electrostatic attraction (Figure 1.3) (For a more thorough explanation of each please see Vogel, 2003, Rubenstein & Koehl, 1977, and Labarbera, 1984). Each mechanism works with the predictions from the filtration theory where the assumption is that all particles

that touch and intercept a filtering fiber adhere and are retained (Rubenstein and Koehl, 1977; LaBarbera, 1984).

1.4 Internal versus External suspension feeders

With this large diversity of particle capture mechanisms, two broad categories can further be used to generalize all suspension feeding animals: i) *Internal suspension feeders,* and ii) *External suspension feeders*. Those that use internal filtering mechanisms pass large amounts of water internally to a large cavity, often a pharynx, to process and separate particles (i.e. using mucus nets, choanocytes, or cilated gill bars), followed by release of filtered water out through openings, such as the osculum of sponges or gill pores of ascidians and enteropneusts *(*Fig. 1.1B, D, F) (Riisgård and Larsen, 2010). Those that are external suspension feeders use structures located external to the body, such as ciliated bands, lophophores, or tentacles to capture and transport particles and include animals such as bryozoans, crinoids, pterobranchs, cnidarians, and ciliated larvae (Fig. 1.1A, C, E) (Riisgård and Larsen, 2010).

A survey of internal versus external suspension feeding animals reveals a general trend. Small organisms (i.e. < 5 mm) are more commonly found to feed using external capture mechanisms, whereas large organisms (i.e. >1cm) have a tendency towards internal suspension feeding methods (MacGinitie, 1939; Barnes, 1965; Rosenberg, 1980; Gilmer and Harbison, 1986; Riisgård, 1989; Jorgensen, 1990; Halanych, 1993; Riisgård et al., 1993; Riisgård and Larsen, 1995; Riisgård and Svane, 1999; Larsen and Riisgård, 2002; Vogel, 2003; Marchinko, 2007). There are exceptions to the latter observation including crinoids that trap particles on external tentacles. The reason for this general trend may be revealed by analysing the energetic cost required to pump and process water with different morphologies of decreasing size.

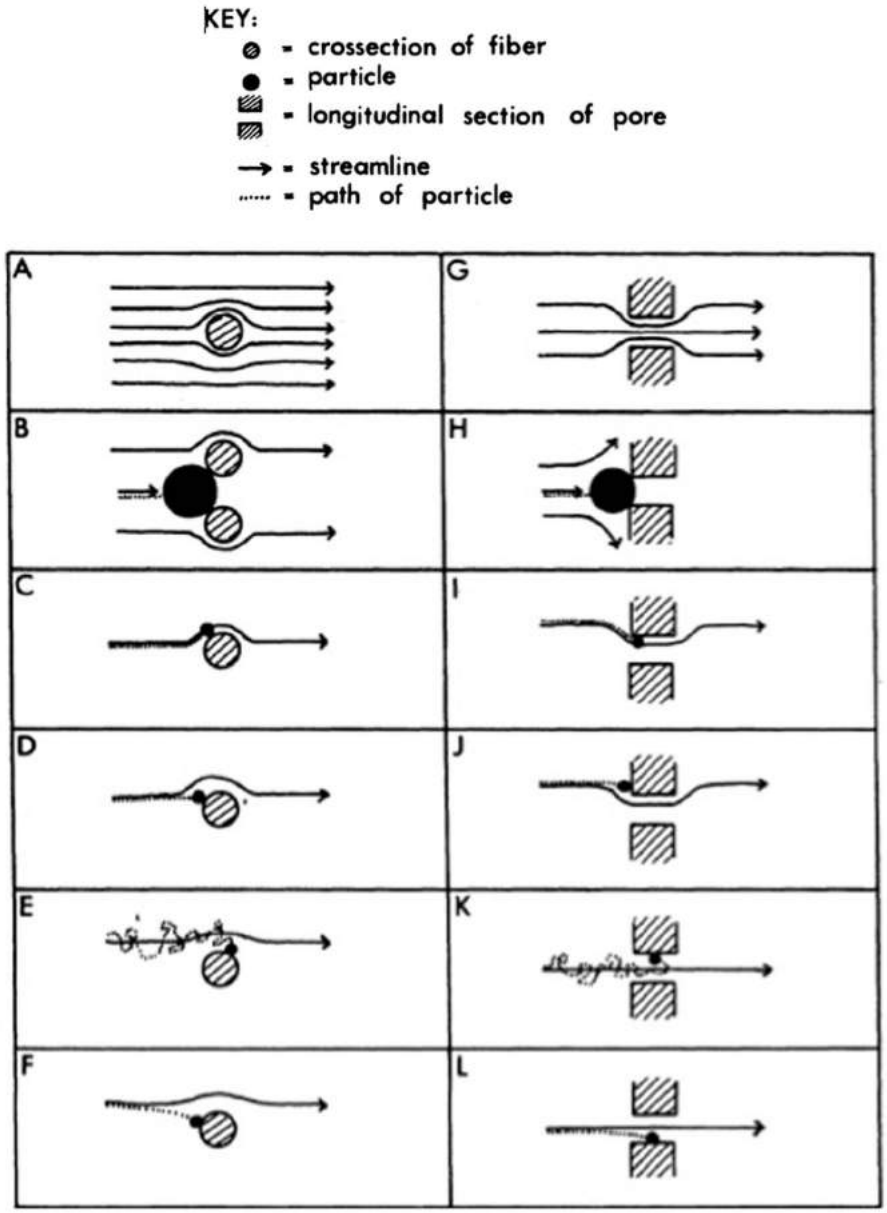

Figure 1.3. Particle-capture mechanisms. A, flow around a fiber; G, flow through a pore; B & H, sieving; C & I, direct interception; D & J, inertial impaction; E & K, diffusional deposition; F & L, gravitational deposition. Reprinted with permission from Rubenstein and Koehl (1977).

1.5 The energetics of pumping in an internal suspension feeder: The hemichordate pharynx

The energetic cost can increase dramatically between animals of different body sizes and shapes, or through ontogeny. Regardless of morphology or filtering mechanism, the energy expended to capture particles must be less than the energy acquired from the filtered food or the alternative would be fatal (Riisgård and Larsen, 1995).

Riisgård and Larsen (1995) attempted to quantify energy efficiencies in several ciliary filter feeders (e.g. sponges, bivalves, ascidians, and polychaetes) and found the energy cost for useful pump work constitutes 0.3 - 4% of the total metabolic expenditure (Riisgård and Larsen 1995). Despite these studies, there still remains a paucity of oxygen consumption rates necessary to calculate energy efficiencies among hemichordates due to their fragile nature and difficulties to measure these rates *in vivo*.

In Chapter 2, we analyse flow, and determine pump energetics through the internal filter feeding pharynx and gill slits of hemichordates of different sizes and shapes. We determine the minimum size a pharynx may be before the cost of pumping becomes lethal, and determine why hemichordates at medium to large sizes have abandoned pharyngeal filter feeding. These results have direct implications on the origin and evolution of deuterostomes (i.e. hemichordates, echinoderms and chordates) (Hyman, 1959; Burdon-Jones, 1962; Romer, 1967; Jefferies et al., 1996; Cameron, 2002a; Brown et al., 2008; Cannon et al., 2009; Gonzalez and Cameron, 2009).

1.6 The fluid mechanics of an external suspension feeder: Barnacle legs - paddles or rakes?

External particle-capturing appendages may function as: 1) sieves or 2) paddles. Most setae, setules, and other biological fibers function at low Re in the order of 10^{-5} -10 (LaBarbera, 1984; Cheer and Koehl, 1987a). As a result, viscous forces dominate, shear gradients are thick, and flow is laminar (Jorgensen, 1983; LaBarbera, 1984). Re determines the flow behaviour around appendages and thus the functional behaviour of appendages. Some setal appendages may function as rakes or sieves with flow passing through spaces between setae to capture and separate particles, whereas others may function as paddles that move pockets of water (Cheer and Koehl, 1987a). Considering the significantly different mechanics of filtering which come about whether an appendage is a sieve or a paddle and the ongoing debates in biological literature about how ecologically important planktonic animals (i.e. copepods, cladocerans, and barnacles) operate (Kerfoot, 1980), it is important to understand what dictates the type of functioning an appendage exhibits. Cheer and Koehl (1987) investigated the circumstances in which bristled appendages function as rakes versus paddles and suggest a change in size or speed of feeding appendage (i.e. Re) can lead to a completely

new function. Flow about cylinders is important not only in filtering, but in many other biologically important functions such as chemoreception, gas exchange, and locomotion in both marine and terrestrial animals and thus flow about these cylinders requires a more thorough examination.

In Chapter 3, I address the question, how does the size and shape of barnacle legs (cirri and setae) determine whether they function as a sieve or a paddle at increasing flow?

This thesis attempts to understand more completely the filtering process of suspension feeding animals including the fluid dynamics through and around suspension feeding appendages, pumping energetics, and how slight morphological modifications can lead to complete functional changes. Consequently, these changes lead to important ecological, ontogenetic, and evolutionary implications.

The conclusion chapter evaluates an innovative and novel technique of studying fluid flow problems in biology using computational fluid dynamics (CFD). CFD is a method of computer-based simulation that solves and analyzes problems of fluid flow. It is primarily used in industrial applications, but more recently, it is revolutionizing fluid biomechanics research. Our study of internal filter feeding in hemichordates and external filter feeding in barnacles relay heavily on CFD and our conclusion chapter assesses its usefulness, limitations, and accuracy in biological studies.

1.7. REFERENCES

Acheson, D. J. (1990). Elementary fluid dynamics: Oxford University Press.

Anderson, D. T. (1994). Barnacles: structure, function, development and evolution. London: Springer. 1-15.

Azariah, J., Ismail, M. M. and Najib, M. A. (1975). Investigation on the ecology and respiratory responses of the hemichordate *Ptychodera flava* to tidal cycles and salinity changes. *The Biological Bulletin* **149**, 455-466.

Barnes, R. D. (1965). Tube-building and feeding in chaetopterid polychaetes. *The Biological Bulletin* **129**, 217-233.

Bone, Q., Carre, C., Chang, P. (2003). Tunicate feeding filters. *Journal of the Marine Biological Association of the UK* **83,** 907-919.

Brown, F. D., Prendergast, A. and Swalla, B. J. (2008). Man is but a worm: chordate origins. *Genesis* **46**, 605-613.

Burdon-Jones, C. (1962). The feeding mechanism of *Balanoglossus gigas*. *Bol. Fac. Filos. Ciênc. Letr. Univ. S. Paulo*, 255-280.

Cameron, C. (2005). A phylogeny of the hemichordates based on morphological characters. *Canadian Journal of Zoology* **83**, 196-215.

Cameron, C. B. (2002a). The anatomy, life habits, and later development of a new species of enteropneust, *Harrimania planktophilus* (Hemichordata: Harrimaniidae) from Barkley Sound. *The Biological Bulletin* **202**, 182.

Cameron, C. B. (2002b). Particle retention and flow in the pharynx of the enteropneust worm *Harrimania planktophilus*: the filter-feeding pharynx may have evolved before the chordates. *The Biological Bulletin* **202**, 192.

Cameron, C. B., Garey, J. R. and Swalla, B. J. (2000). Evolution of the chordate body plan: new insights from phylogenetic analyses of deuterostome phyla. *Proceedings of the National Academy of Sciences* **97**, 4469.

Cannon, J. T., Rychel, A. L., Eccleston, H., Halanych, K. M. and Swalla, B. J. (2009). Molecular phylogeny of hemichordata, with updated status of deep-sea enteropneusts. *Molecular Phylogenetics and Evolution* **52**, 17-24.

Caron, J.-B., Morris, S. C. and Cameron, C. B. (2013). Tubicolous enteropneusts from the Cambrian period. *Nature* **495**, 503-506.

Cheer, A. and Koehl, M. (1987). Paddles and rakes: fluid flow through bristled appendages of small organisms. *Journal of Theoretical Biology* **129**, 17-39.

Etienne, S., Garon, A., Pelletier, D. and Cameron, C. (2010). *Philiadium Gregarum* versus *Aurelia aurita*: on propulsion efficiency in jellyfish. From the 48th *American Institute of Aeronautics and Astronautics Meeting,* 1-8.

Flood, P.R., Fiala-Médioni, A. (1981) Ultrastructure and histochemistry of the branchial sac of benthic filter-feeding invertebrates (Ascidians). *Acta Zoologica* **59**:1–9.

Flood, P. R. (1991). Architecture of, and water circulation and flow rate in, the house of the planktonic tunicate *Oikopleura labradoriensis*. *Marine Biology. Berlin, Heidelberg* **111**, 95-111.

Gilmer, R. and Harbison, G. (1986). Morphology and field behavior of pteropod molluscs: feeding methods in the families Cavoliniidae, Limacinidae and Peraclididae (Gastropoda: Thecosomata). *Marine Biology* **91**, 47-57.

Gonzalez, P. and Cameron, C. B. (2009). The gill slits and pre oral ciliary organ of *Protoglossus* (Hemichordata: Enteropneusta) are filter feeding structures. *Biological Journal of the Linnean Society* **98**, 898-906.

Halanych, K. M. (1993). Suspension feeding by the lophophore-like apparatus of the pterobranch hemichordate *Rhabdopleura normani*. *The Biological Bulletin* **185**, 417.

Horst, C. J. van der. 1939. Hemichordata. *Kl. Ordn. Tierreichs* **4,** 1- 737.

Hou, X.-g., Aldridge, R. J., Siveter, D. J., Siveter, D. J., Williams, M., Zalasiewicz, J. and Ma, X.-y. (2011). An early Cambrian hemichordate zooid. *Current Biology* **21**, 612-616.

Hyman, L. H. (1959). The invertebrates: smaller coelomate groups, Chaetognatha, Hemichordata, Pogonophora, Phoronida, Ectoprocta, Brachipoda, Sipunculida, the coelomate Bilateria. New York: McGraw-Hill Book Company Inc. Volume **V**, 735-747.

Jefferies, R. P. S., Brown, N. A. and Daley, P. E. J. (1996). The early phylogeny of chordates and echinoderms and the origin of chordate left–right asymmetry and bilateral symmetry. *Acta Zoologica* **77**, 101-122.

Jørgensen, C. (1975). Comparative physiology of suspension feeding. *Annual Review of Physiology* **37**, 57-79.

Jørgensen, C. (1983). Fluid mechanical aspects of suspension feeding. *Marine Ecology Progress Series* **11**, 89-103.

Jørgensen, C., Kiorboe, T., Mohlenberg, F. and Riisgard, H. (1984). Ciliary and mucus-net filter feeding, with special reference to fluid mechanical characteristics. *Marine Ecology Progress Series* **15**, 283-292.

Jørgensen, C., Larsen, P., Møhlenberg, F. and Riisgård, H. (1988). The mussel pump: properties and modelling. *Marine Ecology Progress Series.* **45**, 205-216.

Jørgensen, C., Famme, P., Kristensen, H. S., Larsen, P., Møhlenberg, F. and Riisgård, H. (1986). The bivalve pump. *Marine Ecology Progress Series.* **34**, 69-77.

Jørgensen, C. B. (1990). Bivalve filter feeding: hydrodynamics, bioenergetics, physiology and ecology: Olsen & Olsen.

Jørgensen, C. B. (1955). Quantitative aspects of filter feeding in invertebrates. *Biological Reviews* **30**, 391-453.

Kepkay, P. E. (1994). Particle aggregation and the biological reactivity of colloids. *Marine Ecology Progress Series* **109**, 293-293.

Kerfoot, W. C. (1980). Evolution and ecology of zooplankton communities. Hanover, New Hampshire: University Press of New England.

Koehl, M. (1983). The morphology and performance of suspension-feeding appendages. *Journal of Theoretical Biology* **105**, 1-11.

Koehl, M. (1996). When does morphology matter? *Annual Review of Ecology and Systematics* **27**, 501-542.

LaBarbera, M. (1981). Water flow patterns in and around three species of articulate brachiopods. *Journal of Experimental Marine Biology and Ecology* **55**, 185-206.

LaBarbera, M. (1984). Feeding currents and particle capture mechanisms in suspension feeding animals. *American Zoologist* **24**, 71-84.

LaBarbera, M. and Vogel, S. (1982). The Design of Fluid Transport Systems in Organisms: Despite their apparent diversity, fluid transport systems display a fundamental unity of organization resulting from the constraints of a few design principles on natural selection. *American Scientist* **70**, 54-60.

Larsen, P. S. and Riisgård, H. U. (2002). On ciliary sieving and pumping in bryozoans. *Journal of Sea Research* **48**, 181-195.

Lester, S.M. (1985). *Cephalodiscus sp*. (Hemichordata: Pterobranchia): observations of functional morphology, behaviour and occurrence in shallow water around Bermuda. *Marine Biology* **85,** 263-268.

Liu, H. (2002). Computational biological fluid dynamics: digitizing and visualizing animal swimming and flying. *Integrative and Comparative Biology* **42**, 1050-1059.

Liu, H., Wassersug, R. and Kawachi, K. (1996). A computational fluid dynamics study of tadpole swimming. *Journal of Experimental Biology* **199**, 1245-1260.

Liu, H., Ellington, C. and Kawachi, K. (1998). A computational fluid dynamic study of hawkmoth hovering. *Journal of Experimental Biology* **201**, 461-477.

MacGinitie, G. (1939). The method of feeding of tunicates. *The Biological Bulletin* **77**, 443-447.

Marchinko, K. B. (2007). Feeding behavior reveals the adaptive nature of plasticity in barnacle feeding limbs. *The Biological Bulletin* **213**, 12-15.

Mattson, S., Cedhagen, T. (1989) Aspects of the behaviour and ecology of *Dyopedos monacanthus* (Metz ger) and *D. porrectus* Bate, with comparative notes on *Dulichia tuberculata Boeck* (Crustacea: Amphipoda: Podoceridae). *Journal of Experimental Marine Biology Ecologica* **127**:253–272.

Peteresen, J.K. (2007) Ascidian suspension feeding. *Journal of Experimental Marine Biology and Ecology* **342**: 127-137.

Riisgård, H. (1988). The ascidian pump: properties and energy cost. *Marine Ecology Progress Series* **47**, 129-134.

Riisgård, H. (1991). Suspension feeding in the polychaete *Nereis diversicolor*. *Marine Ecology Progress Series* **70**, 29-37.

Riisgård, H. and Larsen, P. S. (1995). Filter-Feeding in marine macro-invertebrates: pump characteristics, modelling, and energy cost. *Biological Reviews* **70,** 67-106.

Riisgård, H. and Larsen, P. S. (2000). Comparative ecophysiology of active zoobenthic filter feeding, essence of current knowledge. *Journal of Sea Research* **44**, 169-193.

Riisgård, H. U. (1989). Properties and energy cost of the muscular piston pump in the suspension feeding polychaete *Chaetopterus variopedatus*. *Marine Ecology Progress Series* **56**, 157-168.

Riisgård, H. U. and Ivarsson, N. M. (1990). The crown-filament pump of the suspension-feeding polychaete *Sabella penicillus*: Filtration, effects of temperature, and energy cost. *Marine Ecology Progress Series.* **62**, 249-257.

Riisgård, H. U. and Larsen, P. S. (1995). Filter-Feeding in marine macro-invertebrates: pump characteristics, modelling, and energy cost. *Biological Reviews* **70**, 67-106.

Riisgård, H. U. and Svane, I. (1999). Filter feeding in lancelets (amphioxus), *Branchiostoma lanceolatum*. *Invertebrate Biology* **118**, 423-432.

Riisgård, H. U. and Larsen, P. S. (2010). Particle capture mechanisms in suspension-feeding invertebrates. *Marine Ecology Progress Series* **418**, 255-293.

Riisgård, H. U., Vedel, A., Boye, H. and Larsen, P. S. (1992). Filter-net structure and pumping activity in the polychaete *nereis*-diversicolor effects of temperature and pump-modeling. *Marine Ecology Progress Series* **83**, 79-89.

Riisgård, H. U., Thomassen, S., Jakobsen, H., Weeks, J. and Larsen, P. S. (1993). Suspension-Feeding in Marine Sponges *Halichondria-Panicea* and *Haliclona-Urceolus*-Effects of Temperature on Filtration-Rate and Energy-Cost of Pumping. *Marine Ecology Progress Series* **96**, 177-188.

Romer, A. S. (1967). Major steps in vertebrate evolution. *Science* **158**, 1629.

Rosenberg, G. G. (1980). Filmed observations of filter feeding in the marine planktonic copepod *Acartia clausii*. *Limnology and Oceanography* **25**, 738-742.

Rubenstein, D. I. and Koehl, M. (1977). The mechanisms of filter feeding: some theoretical considerations. *American Naturalist* **111**, 981-994.

Ruppert E.E., Fox R.S., Barnes R.D. (2004). Invertebrate zoology: a functional evolutionary approach, 7th ed. Thomas Brooks/Cole, Belmont, CA.

Strathmann, R. R., Jahn, T. L. and Fonseca, J. R. C. (1972). Suspension feeding by marine invertebrate larvae: clearance of particles by ciliated bands of a rotifer, pluteus, and trochophore. *The Biological Bulletin* **142**, 505-519.

Trager, G. C., Hwang, J.S., and Strickler, J.R. (1990). Barnacle Suspension feeding in variable flow. *Marine Biology* **105,** 117- 127.

Vogel, S. (2003). Comparative biomechanics: life's physical world. New Jersey: Princeton Univ Press.

Wildish, D. and Kristmanson, D. (2005). Benthic suspension feeders and flow: Cambridge Univ Press.

Worsaae, K., Sterrer, W., Kaul-Strehlow, S., Hay-Schmidt, A. and Giribet, G. (2012). An anatomical description of a miniaturized acorn worm (Hemichordata, Enteropneusta) with asexual reproduction by paratomy. *PloS one* **7**, e48529.

CHAPTER 2

2. Article: A computational fluid dynamic analysis of hemichordate pharyngeal filter feeding reveals pump constraints at small and medium sizes

Maureen Vo, Fernando Villalpando, Dominique Pelletier,
Chris B. Cameron

Article submitted on July 24, 2013 and currently under review with the
Royal Society Interface journal

2.1 ABSTRACT

Pharyngeal filter feeding in invertebrates typically occurs in organisms within a specific size range (i.e. ~ 5 mm -100 mm), suggesting a size limitation exists for this method of feeding. To determine the size constraints of pharyngeal filter feeding, a comparative analysis of the energetic costs of pumping fluid in various sized and shaped pharynxs was performed. Twelve models varying in pharynx length and diameter and pore number, shape, and area were constructed and used to represent a range of hemichordate pharynges for comparisons. The power to pump water through each system was determined using finite volume methods and computational fluid dynamics. Pore number and area have the largest effect on flow rates, pressure, and power consumptions required to pump water through the systems. It was also found that an inefficient central reverse flow develops in the pharynx at medium pharynx diameters, flow out miniscule pore sizes comparable to those of the pterobranch, *Cephalodiscus* was unattainable, and velocity profiles at the mouth of our simulations and those observed in vivo were similar when the pumping of the system was limited to within the walls of the gill pores. These results suggest why filter feeding is absent in large acorn worms, how the pterobranch gill pores may have been inherited from a larger gilled ancestor, and that cilia of the gill pores likely constitute the primary pump of the filter system. We conclude by exploring reasons for low values of overall pump efficiency of our models.

2.2 INTRODUCTION

Suspension feeding invertebrates have the daunting task of separating a sufficient amount of particles, including small phytoplankton and zooplankton, from dilute environments. This ability is critical for a suspension feeders survival, but in addition, it allows for an important energy link between suspended phytoplankton and higher trophic levels in marine food webs. Considering phytoplankton encompass the major primary production in the sea, it is understandable that suspension feeders are found in almost all animal classes in aquatic environments worldwide (e.g. sponges, bivalves, polychaetes, ascidians, bryozoans, crustaceans, cnidarians and ctenophores (Jørgensen 1975, Riisgård & Larsen 1995, 2000, 2001).

These animals display a wide range of particle capturing mechanisms. Some swim around, seeking out rich patches and intercepting particles in the process, while others, such as many invertebrate larvae, consist of a stage where they exist as plankton and feed on smaller plankton (Vogel, 2003). A few (e.g. goose neck barnacles) attach to floating objects, mostly living as sessile animals at the interface between solid substratum and a body of water.

Pharyngeal filter-feeding, is a specific feeding mechanism, which typically involves separating particles from ambient water by pumping fluid using a ciliary current into a mouth, through a pharynx, and out gill pores in order to meet daily food requirements (Fig. 2.1A,B, E). In invertebrate chordates, the water current is maintained by the pumping of cilia that line the walls of the gill slits (Fig. 2.1E). The pump drives water against various resistances to flow present in the system including viscosity, friction, and pressure. This method of feeding is characteristic of several tunicates, cephalochordates, and hemichordates, though in the latter case, the precise location of the ciliated pump has not been observed.

Generally speaking, animals under a very small size range (i.e. <5 mm), or over a moderate size (i.e. >1 cm pharynx diameter), do not filter feed using a ciliated pharynx perforated with gill slits. Small animals capture food particles using structures external to the body including ciliary bands or tentacles as observed in many invertebrate larvae, ectoprocts, polychaetes, and lophophorates, while large filter feeders typically use externally located arms and tentacles (e.g., crinoids and polychaetes). Exceptions to the latter exist in the case of some fish (e.g., herring, whale sharks, and other fish) that use ram feeding or a muscular buccal pump to pharyngeal filter feed.

Fluid mechanics is a strong selective force that dramatically changes between animals of different body sizes and shapes, or as individuals grow. Small marine filter-feeders in particular must cope with low Reynolds numbers dominated by high viscous forces, whereas in larger animals, momentum dominates flow. Ultimately, the optimal size of an organism must maximize the difference between energy intake and energetic costs. Fluid physics largely accounts for very different body plans between small larvae and the corresponding adult body plans.

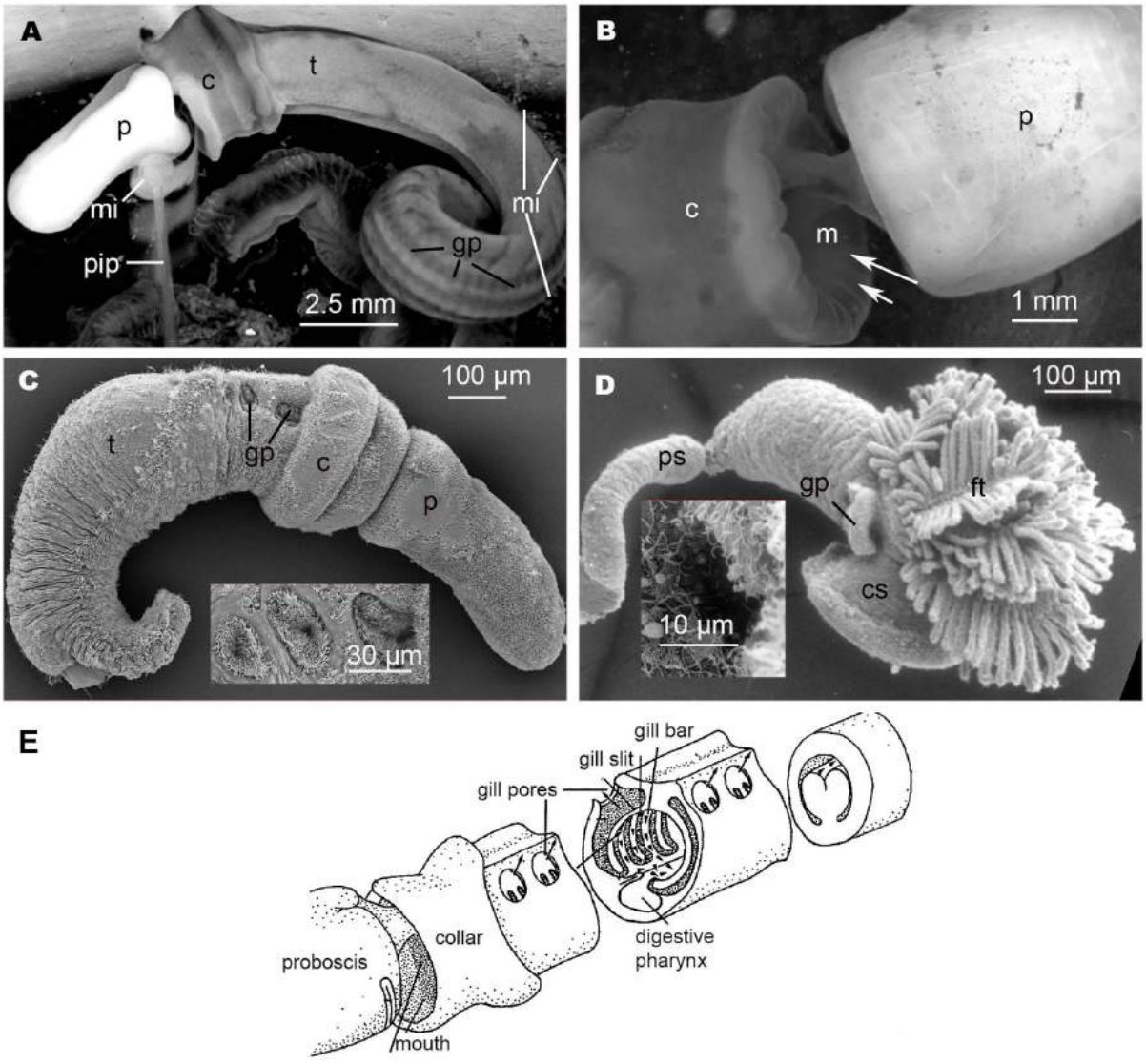

Figure 2.1. Light micrographs showing (A) the flow of diluted milk entering the mouth and exiting the gill pores of *Protoglossus graveolens*. (B) Close-up of the mouth. Arrows represent flow speeds with the long arrow equal to 4.05 mm s^{-1} and the short arrow equal to 1.80 mm s^{-1}. (C) Twenty-day old *Saccoglossus kowalevskii*. Paired gill pores (inset) of enteropneusts develop sequentially starting from the anterior trunk region, towards the posterior. Initially they are simple circular pores, then elongate into slit shape with the extension of collagenous gill bars. (D) A *Cephalodiscus gracilis* zooid that has been removed from its tube. Its single pair of gill pores (inset) are about 9 μm in diameter and are not heavily ciliated. (E) Pharyngeal filtering morphology of *Harrimania planktophilus*. Suspension enters through the mouth (long arrow) and exits the pharynx via gill slits. For a more detail, see Cameron (2002b). c, collar; cs, cephalic shield; ft, feeding tentacles; gp, primary gill bar; m, mouth; mi, milk; pip, pipette; ps, posterior extension of metasome; p, proboscis; t, trunk.

Hemichordates, the deuterostome phylum most closely related to the chordates, are providing insight into the evolutionary origins of chordate traits including the gill slits. The phylum consists of two classes: i) the solitary, mobile, enteropneusts (acorn worms) and ii) the sessile, colonial, tube-twelling pterobranchs. The pterobranch *Cephalodiscus* exhibit a single pair of non-functional gill pores, whereas *Rhabdopleura,* lack them. Their absence in *Rhabdopleura* may be correlated with its diminutive size (Barrington, 1965). What then, is the role of the single pair of pharyngeal pores of *Cephalodiscus*?

Traditional hypotheses of hemichordate origins posit that the ancestor was a colonial pterobranch, suggesting the *Cephalodiscus* pores were elaborated in the larger enteropneusts. This hypothesis has been challenged by molecular phylogenetic trees constructions and fossil data that conversely suggests an enteropneust worm better represents the basal group (1-4). This would imply a switch from a solitary, worm-like, pharyngeal filter-feeder to a colonial, tentacle-feeding pterobranch, correlated with a decrease in body size. The single pores of *Cephalodiscus,* in this case would be regarded as vestigial structures of a larger ancestor.

Among hemichordates, internal filter feeding has been observed in the small harrimaniid worms (Cameron, 2002b), but not the larger ptychoderids (Dilly, 1993 and Swalla, 2009). Observations are difficult in enteropneusts because the worms are stressed outside of the burrow, easily damaged, secrete copious amounts of mucus and undergo ciliary arrest *in vivo*. Unlike cephalochordates and some tunicates, enteropneust bodies are not transparent, and so the location of the ciliary pump remains a mystery. Internal filter feeding has not been observed in the pterobranch *Cephalodiscus*, a zooid of minute size (1mm) that lives inside of tubes (Fig. 2.1D). Here we model flow through the *Cephalodiscus* pharynx and demonstrate that friction, and related to that the power required to pump water through a very small pharynx and gill pores, are too great to support the idea that the gill pores of *Cephalodiscus* create a feeding current.

Examining and understanding the allometry in filter-feeders requires knowledge of the fluid mechanics of filtering including fluid velocity through filters, as well as pressure heads generated by water-transporting structures. The difficulty of obtaining empirical data on fluid flow inside the hemichordate pharynx has led us to adopt a novel computational approach to address our questions. Computer-based simulations using finite volume methods (FVM) in

concert with computational fluid dynamics (CFD) is a relatively new and promising avenue to approach questions not easily answered by direct observation. In this study, we use FVM and CFD to numerically solve for fluid flow into the mouth, through the pharynx, and out the gill pores of twelve generalized filter-feeding models to determine and examine the relationship between the pharynx diameter and length, and the gill pore number, size and form, and fluid mechanics, including velocity profiles, pressure changes, and pump energetics.

The models evaluated were designed to represent a range of pharynx sizes and shapes characteristic of hemichordates. The smallest model represents a juvenile enteropneust (Fig. 2.1C), or the adult pterobranch *Cephalodiscus* (Fig. 2.1D). The largest model represents the inner pharynx of a large adult ptychoderid worm (e.g. *Balanoglossus*), and the intermediate sizes may represent medium sized worms or an ontogenetic stage during the growth of an individual animal. The hemichordate pharynx begins development with a mouth and a single pair of circular gill pores. During growth, the pharynx increases in diameter and length and additional pairs of gill pores are added posteriorly (Fig. 2.1C). The pharynx terminates at the esophageal organ (Fig. 2.1E), which forms a barrier to water flow into the intestine. As the pores continue to develop, they enlarge and extend into a slit shape, caused by the downward extension of dorso-lateral collagenous gill bars (Fig. 2.1C).

In this study, a comparative analysis of the power required to pump fluid through the twelve hemichordate pharynx models uncovers both an upper and lower size limit for internal feeding. The location of the ciliary pump in the hemichordate pharynx is also predicted using the sliding wall feature of CFD to emulate the velocity profile observed at the mouth of the acorn worm *Protoglossus graveolens*. We conclude by discussing the significance of these simulations on our understanding of body plan evolution in the deuterostomes.

2.3 MATERIALS AND METHODS

In situ observations of filter feeding

Protoglossus graveolens was collected from Lowes Cove (43°56'N, 69°34'W), a tidal mudflat in the Damariscotta River estuary, Maine. Specimens were kept in their natural sediments in an aquarium under a flow of ambient seawater. One at a time, three worms were removed from their sediment and placed in a dish where they were cleaned of sediment and

fed orange-colored plastic particles (Dayglo Color Corp., Cleveland, OH, USA) or diluted milk, in order to visualize and record the flow profile at the mouth and flow velocity exiting the gill pores. Particle velocity was measured for three individuals using still images taken at a regular interval and analyzed with ImageJ. Videos and photographs were taken with a QImaging Retiga 2000 camera mounted on an Olympus SZX16 microscope.

Pharynx Modeling

Twelve three-dimensional models representing a variation in size and shape of filter-feeding pharynges and gill pores of hemichordates were created using the mesh generator GAMBIT 2.4 (Ansys, 2002), a pre-processor for the CFD solver ANSYS FLUENT. Due to constraints with CFD and inherent problems with calculating power consumption of a bed of cilia, we defined an external pump to provide flow through the models. We calculated relative power consumption based on the energy required to overcome friction through each model system. We did not add to this number the power required to drive the pump and therefore our power estimates are conservative. The consumption of biological pumps varies depending on density and number of monociliated cells, the arrangement and coordination of the cells, and the shape and length of cilia. For this reason, a simplified numerical calculation of power consumption by a pterobranch vs. an enteropneust pump would be meaningless. Instead, we assume the pump is perfectly efficient (i.e., zero Watts) and regards friction (i.e., the load on the pump) as the most relevant and useful variable to compare among pump efficiencies.

Model construction incorporates the pre-processing stage of CFD and consists of four main components: i) definition of geometry; ii) discretize the solution into finite elements; iii) specify boundary conditions; and iv) specify continuum, which we elaborate here.

i) *Definition of the geometry*

A reference model representing the shape and size of a general pharynx perforated by gill pores was constructed. It consisted of a cylinder with a diameter of 4 mm and length of 4 mm, open at one end and closed at the other (Fig. 2.2A, B). A single pair of cylindrical gill pores that permeate the pharynx were placed 2 mm along the pharynx, and had a depth of 1 mm.

The pores were circular in cross section with a diameter of 0.8 mm (Fig. 2.2). For comparisons, each of the subsequent eleven models differed in a single feature from the reference model, while all other parameters remained constant (Table 1). Seventeen simulations total were conducted for comparisons using the twelve models constructed. In 5 simulations, the reference model and half pharynx model were defined with sliding walls to emulate pumping done by cilia to observe velocity profiles at the mouth and gills. Each model was created to explore the effects of size and shape on fluid flow and the pump resistance (or power) by altering four variables: (i) number of pores, (ii) pharynx diameter, (iii) pore diameter and shape, and (iv) pharynx length (Table 1).

ii) *Discretize the solution domain into finite elements*

Each wireframe model was sub-divided into nodes along the mouth, back wall, and pores, from which a number of non-overlapping sub-domain tetrahedral and hexahedral shaped elements were generated, transforming each of our models into a grid of finite elements (ie. mesh) (Fig. 2.2A,B). A grid dependence test, in which successive refinements of an initially coarse grid was performed, until–flow velocity into the mouth remained constant. After several trials using a range of mesh densities, the minimal number of elements, for which increasing the number of cells showed no further fluctuations in velocity, was determined to be 271894 for our reference model. The ideal number of elements determined for each of the 12 models is provided in Table 1.

iii) *Specify boundary conditions* - Each face of a model that touches a domain boundary (i.e. fluid) must be defined in order to solve the governing equations and simulate fluid flow. The mouth was defined as the '*mass flow inlet'*; pores as '*pressure outlets'*; and the pharynx, gills, and back wall were each defined as a '*wall*'. Flow through the pores satisfied a free exit (continuative) boundary condition and the inflow and exit flow satisfied the condition of conservation of mass. The mass flow inlet at the mouth was defined at a constant of 1.608 x10-5 kg s^{-1} for all models tested. This rate was chosen as it is the observed average mass flow into the mouth of the enteropneust *Protoglossus graveolens* (Gonzales and Cameron, 2009).

iv) *Specify Continuum*

The interior was defined as a fluid, in this case, seawater with density = 1.024 x 10^3 kg m^{-3} and a viscosity = 1.072 x 10^{-3} kg ms^{-1} (Vogel, 2003).

Solver types and numerical method

Solving for the Navier-stokes (N-S) equation can provide valuable information on the steady-state, incompressible fluid including flow patterns from velocity and pressure calculated at discretized points (Acheson, 1990). Numerical integrations over all meshed elements constituting the mouth and gill pores exist. Finite volume methods and commercial computational fluid dynamic (CFD) software package ANSYS FLUENT were used for three-dimensional solving of the N-S equation. FLUENT solves the conservation equations for mass and momentum for all flows. Each of the 12 meshed models created was imported into FLUENT to numerically solve for fluid flow, which was assumed to be laminar and in steady-state. The numerical solutions obtained on different grids fell within a level of tolerance specified by us, and is referred to as 'grid converged' solutions. Two hundred iterations were necessary for each model to achieve the flow field convergence characterized by the total, normalized residuals of 0.0001. The governing equations are discretized using the finite volume method and solved using a pressure based solver in steady time. The SIMPLE algorithm, Green-Gauss cell based solver, second order pressure, second order upwind momentum, and pressure-velocity coupling methods were applied for solving the governing equations.

The internal, cylindrical portion of the mesh was treated as '*stationary*' with '*no-slip*' conditions imposed at solid boundaries (i.e., at the wall of the pharynx and gill pores). The '*sliding wall*' function in FLUENT was used on the reference model (Table 1) and a model of 2 mm diameter pharynx. In 3 simulations, moving walls were imposed on the internal surface of: i) the gills, ii) the pharynx, and iii) both gills and pharynx simultaneously. This simulation was run to emulate the pumping position of cilia, which uniformly line the interior of the hemichordate pharynx. Our objective here was to examine velocity profiles at the mouth to determine the precise location of the hemichordate ciliary pump, which we have failed to

characterize in live animals. All other parameters remained consistent with the reference model.

Post-Processor

Versatile data visualization tools and calculation options allowed us to determine the power output and pump efficiency of each of the fifteen models. The diameter of the pores and pharynx (defined in the pre-processor), pressure, volumetric flow rates (defined in the solver), velocity profiles (determined from direct observation), and oxygen consumption rates (determined from literature) once determined, were used to calculate:

The Power Consumption (watts) of Each Model

The minimum power output required to pump fluid through our models was considered as a summation of work done by hydrodynamic forces including pressure and viscosity on the model inlet and outlet sections such that:

$$\text{Power} = \vec{V} \cdot \vec{F} = \vec{V} \cdot [-p\hat{n} + \tau \cdot \hat{n}] \quad (1)$$

where $\vec{V}$ denotes the velocity; $\vec{F}$ the surface force (ie. the sum of the pressure and viscous forces); p is the pressure; $\hat{n}$ the normal vector; and τ the viscous strain tensor.

$$\text{Total Power for all surfaces} = \iint_S \vec{V} \cdot [-p\hat{n} + \tau \cdot \hat{n}] \quad (2)$$

This approach is useful, as it does not enter into the difficulty of accounting for power differences between pump designs of different animals. Instead it assumes the pump efficiencies as perfectly efficient at zero watts, and regards friction and viscosity as the most important variables that determine system design. A consequence of this approach is that our power calculations are conservative.

Pump Efficiency

Physiologists define biomechanical efficiency as the energy output/energy input. In our case, the pump mechanical efficiency (η) for each model was determined by dividing the pumping power output, P_{op} (from equation (1)), by the metabolic input of an acorn worm, R_{tot}.

$$\eta = P_{op} / R_{tot} \quad (3)$$

where R_{tot} is the total respiration rate calculated from measurements of total oxygen consumption rate. We used a rate of 0.0092 ml O_2 h^{-1} that was determined for the acorn worm *Ptychodera flava* (Azariah et al., 1975). To convert oxygen consumption to watts, we used the conversion factor of 1.0 μl O_2 h^{-1} = 5.22 μW (Riisgård and Larsen, 1995) This estimate, albeit rough, indicates the power demand of the pharyngeal pump with respect to the animal's overall metabolism.

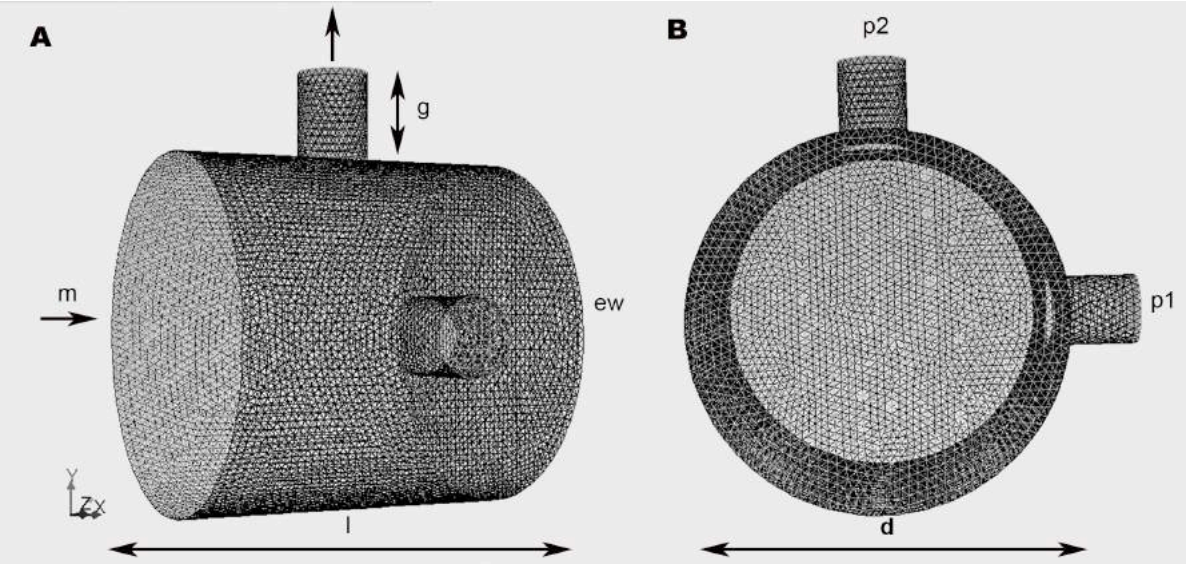

Figure 2.2. Finite element model of the reference pharynx, perforated with gill pores showing the mesh of domain elements. There are 271894 finite elements in the reference model. In all models the mass inflow of seawater at the mouth was defined at a constant of 1.608 x10-5 kgs^{-1}, based on video recordings from *Protoglossus graveolens*. (A) side view; (B) front mouth view into pharynx. m, mouth; g, gill depth; l, pharynx length; d, pharynx diameter; p1, pore 1; p2, pore 2; ew, esophageal wall. Arrows denote direction of flow.

Table 1. Summary of parameters and element sizes used in CFD models.

Model	Pharynx Diameter, *D* (mm)	Pharynx length, *L* (mm)	Gill depth, *g* (mm)	Pore area (mm^2) (diameter in mm)	Pore number (n)	Pore shape	Element size
2-pore reference	4	4	1	2.01 (0.80)	2	circular	271894
VARIABLES							
Pores							
4-pore	4	4	1	2.01 (0.80)	4	circular	246287
6-pore	4	4	1	2.01 (0.80)	6	circular	291239
2x (large) pore	4	4	1	8.04 (1.60)	2	circular	235271
½ (small) pore	4	4	1	0.503 (0.40)	2	circular	207463
slit shaped pore	4	4	1	2.01	2	slit	212882
Cephalodiscus	0.21	0.625	0.035	0.000254 (0.009)	2	circular	223786
Pharynx diameter							
1/3 wider	6	4	1	2.01 (0.80)	2	circular	83813
2x wider	8	4	1	2.01 (0.80)	2	circular	348310
1/2 wide	2	4	1	2.01 (0.80)	2	circular	131702
1/4 wide	1	4	1	2.01 (0.80)	2	circular	167288
Pharynx length							
2x long	4	8	1	2.01 (0.80)	2	circular	167288
3x long	4	12	1	2.01 (0.80)	2	circular	336287

2.4 RESULTS

In vivo observations of flow

When filter feeding, the mouth of *Protoglossus* functions as an inhalant siphon. Plastic particles (0.1 to 2.5 mm, average 0.78 ± 0.57 mm, n=100) placed up to 4 millimeters away from the mouth accelerate as they are sucked towards the mouth (Fig. 2.1A,B). Maximum velocities at the entrance to the mouth varied between individuals ranging from 1.80 to 4.05 $mm \cdot s^{-1}$ (mean v_{max} = 3.19 ± 1.21 $mm \cdot s^{-1}$, n=3). The Reynolds number (Re) in the pharynx is approximately 13, indicating flow is laminar and dominated by viscous forces. The average mouth area is A = 9.46 ± 1.15 mm^2 (n=3). Average estimated pumping rates (volumetric flow rates) are $P = vA = 0.031 \pm 0.013$ $ml \cdot s^{-1}$ (n=3). Observations of diluted milk at the entrance to the mouth show a concave velocity profile where the highest flow is at the center and decreases to zero at the wall of the buccal cavity.

In silico observations of flow

The 2-pore model served as a reference to which the remaining eleven model simulations were compared. Twelve models were used for static wall simulations and 5 sliding wall simulations were conducted using the reference and half reference model for a total of 17 simulations. All twelve models were initially defined with the 'no-slip' boundary condition (i.e., the walls remained stationary) and revealed low Reynolds numbers (<20), laminar flow, and similar flow profiles, varying solely in the water velocity into the mouth (Table 2). Fluid was released from the mouth surface and travelled posteriorly towards the gills and back wall (Fig. 2.3A,C,D). For all models, flow increased in velocity between the mouth and the gill pores with a maximum velocity inside the pharynx varying from 4.19×10^{-4} m s^{-1} in the widest pharynx to 3.92×10^{-2} m s^{-1} in the smallest diameter pharynx (Fig. 2.3A-D). Flow velocity to the posterior wall decreased close to zero and then re-circulated anteriorly, increasing as it approached and exited the pores (Fig. 2.3A). Velocity profiles of the gills revealed the highest flow in the center, decreasing to zero at the gill walls (Fig. 2.3B,E). Maximum velocities for all models inside the gills ranged from 3.88×10^{-3} m s^{-1} to 6.17×10^{-2} m s^{-1} with the double pore area and half pore area models defining the limits

respectively (Table 2). Table 2 summarizes the volumetric flow rates (Q), velocities, power output (P_{op}), and overall pump efficiency (η) for each model tested.

A model based on the pterobranch *Cephalodiscus* pharynx parameters, with a defined pore diameter of 9 μm, or an area of 63.6 μm^2 (Fig. 2.1D inset), was created to observe the overall flow pattern. At this miniscule pore diameter, resistance prevented flow out the pores and water instead re-circulated throughout the pharynx (data not shown).

VELOCITY PROFILE

Sliding Walls

In FLUENT, walls within a model can either be defined as stationary or made to slide in a particular direction. The sliding wall function was used to emulate and approximate the 'pump' of the system, a bed of cilia that uniformly line the walls of the internal pharynx and gill pores of hemichordates (Fig 2.1E). These simulations allowed us to examine velocity profiles at the mouth, to compare with those gathered from live animal recordings. Our objective here was to establish the probable position of the ciliary pump, on the pharynx wall and/or on the gill pore walls. The reference pharynx diameter and the half reference pharynx diameter models were used to investigate these flow dynamics. The power output (P_{op}) of the moving wall models was not calculated because it is not directly comparable with the power of a ciliated pump.

Gills

In the first simulation, using the reference model, the walls of the gill pores were set to slide at a rate of 0.022109 m s^{-1} in order to maintain the same mass flow rate into the mouth as the previous stationary wall model simulations. Gill velocity profiles of the sliding gill wall model were significantly different from the external pump models with static walls (compare Fig. 2.3E,F). Fluid inside the gill pores flowed fastest along the gill wall, at a max speed of 2.20 x $10^{-2}ms^{-1}$, and slowest towards the center with a speed of 1.27 x $10^{-2}ms^{-1}$ (Fig. 2.3F). A concave rather than a convex velocity profile was observed at the mouth.

Pharynx

In the second and third sliding wall simulation, the pharynx wall was set to slide in the reference model and half diameter reference model respectively and velocity profiles were examined for comparisons (Fig. A1,A2). A pharynx sliding wall rate of 0.3309 ms^{-1} was necessary to maintain the same mass flow rate at the mouth as the stationary wall model simulations. In both simulations, the flow was greatest at the pharynx walls, but as flow approached the back wall, a large volume reversed and flowed anteriorly through the central part of the pharynx, exiting the mouth at a relatively high maximum velocity of 1.21 x 10^{-1} ms^{-1} (Fig. A1,A2). Flow through the gill pores with a sliding pharynx differed substantially between these two model simulations. In the reference model simulation, water flowed from the exterior, through the pores, and into the pharynx (i.e., reversed flow) (Fig. A1), whereas in the half-sized model, water exited the pores to the external environment from inside the pharynx (Fig. A2).

Pharynx + Gills

As the half reference model revealed a more feasible flow pattern for filtering, it was used for further observations of flow, this time to test velocity profiles using sliding pharynx and gill walls working simultaneously. In one simulation, the gill pores were set to slide at a rate of 0.020 ms^{-1}, and the pharynx wall was set to slide at 0.015 ms^{-1}, again, set to maintain the mass flow rates into the mouth as the static models (Fig. A3). In another simulation, the pores were set to slide at the same rate as the previous simulation, however the pharynx wall was decelerated to 0.004 ms^{-1} (Fig. A4). In the first simulation, flow entered the mouth, with the fastest velocity along the walls of the pharynx and a large volume of reverse flow occurred centrally in the pharynx, most notably posterior to the gill pores (Fig. A3). This central reverse flow was eliminated by drastically reducing the pharynx sliding wall velocity to nearly zero in the second simulation (Fig. A4). In this latter case, the flow was similar to our sliding gill wall simulation with flow moving into the mouth, through the pharynx, and out of the pores (Fig. 2.3F).

Table 2. Summary of the volumetric flow rates (Q), pore velocities, pressure drop (Pa), power output (P_{op}), and overall pump efficiency (P_{op}/R_{tot}) for each model tested.

Model	Volumetric Flow Rate, Q (m^3/s)	Mouth Velocity (m/s)	Avg pore velocity (m/s)	Pressure drop, ΔP (Pa)	Pumping power, P_{op} (watts)	Overall pump efficiency P_{op}/R_{tot} (%)
2-pore reference	7.85E-09	1.25E-03	1.57E-02	1.45	2.30E-08	0.0479
Variables						
Pore						
4-pore	3.93E-09	1.25E-03	7.63E-03	0.66	1.04E-08	0.0216
6-pore	2.62E-09	1.25E-03	5.14E-03	0.43	6.70E-09	0.0140
2x (large) pore	7.85E-09	1.25E-03	3.88E-03	0.12	1.87E-09	0.0039
½ (small) pore	7.85E-09	1.25E-03	6.17E-02	21.7	3.42E-07	0.7120
slit shaped pore	7.85E-09	1.25E-03	1.52E-02	2.51	3.97E-08	0.0826
Pharynx Diameter						
1/3 wider	7.85E-09	5.56E-04	1.63E-02	1.45	2.29E-08	0.0478
2x wider	7.85E-09	3.12E-04	1.54E-02	1.42	2.24E-08	0.0467
1/2 wide	7.85E-09	5.00E-03	1.58E-02	1.59	2.51E-08	0.0524
1/4 wide	7.85E-09	2.00E-02	1.53E-02	3.13	4.93E-08	0.1028
Pharynx Length						
2x long	7.85E-09	1.25E-03	1.54E-02	1.46	2.29E-08	0.0478
3x long	7.85E-09	1.25E-03	1.54E-02	1.46	2.29E-08	0.0478

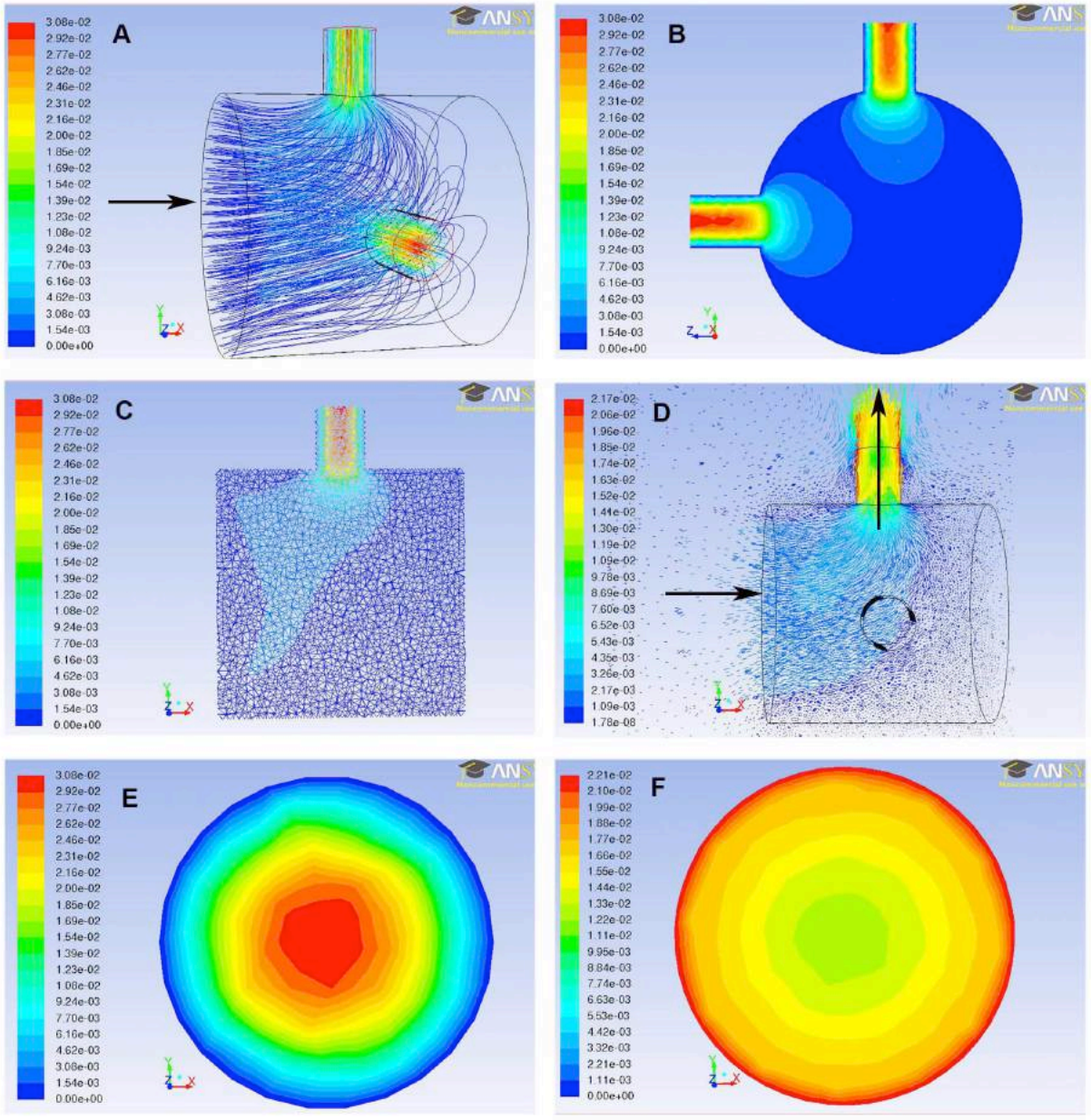

Figure 2.3. Velocity profiles and fluid path-lines showing the change in velocity of fluid throughout the reference model with static (A,B,C,E) and sliding gill pores walls (D,F). (A) Path-line of fluid entering the mouth colored by velocity magnitude (ms^{-1}). (B) Velocity contour in a cross sectional plane through the pharynx at the position of the gill pores (i.e., y-axis). (C) Velocity profile of section along the x-axis showing the increase in velocity as water approaches and exits a pore. (D) Fluid velocity profile with sliding gill pore walls. (E) Fluid velocity contour of the inside of a gill pore with a static wall, top-view. (F) Fluid velocity contour of the inside of a gill pore with a sliding wall, top-view. Arrows denote direction of flow.

POWER

Modifications of pore number and shape

Pore Number

The addition of pores reduced the volumetric flow rate, velocity, and pressure drop (measured as the change in pressure between the pores and the mouth) out of the pores (Table 2). Overall power decreased in relation to the number of pores added (Table 2, Fig. 2.4A). The addition of 2 pores (i.e., 4-pore model) to the reference model reduced all previously mentioned factors by approximately half, the 6-pore model roughly reduced all factors by 1/3. In theory, an 8-pore model would decrease all factors by 1/4 and so on (Table 2, Fig. 2.4A).

Pore Size

The reduction of pore area to half that of the reference model resulted in a dramatic increase in water velocity out the pore by nearly 4 times and a significantly higher increase in pressure of nearly 15 times to 21.7 Pa (Table 2, Fig. 2.5). Related to this was the dramatic increase in power required to push the water through (Table 2, Fig. 2.4B).

Doubling the reference pore area decreased the pore velocity by more than 4 times and significantly decreased the pressure at the pores by approximately 12 times. Consequently, the overall power decreased by nearly 12 times (Table 2; Fig. 2.4B) to 1.87E-09 watts.

Pore Shape

Modifying the conformation of the pore from circular to an oval, slit shape while maintaining the same cross sectional area nearly doubled the pressure drop (Table 2; Fig. 2.5). The volumetric flow rates (and velocities) exhibited no significant changes, while the overall power consumption nearly doubled (Table 2; Fig. 2.4B).

Modifications in the pharynx size

Pharynx length

Increasing the length of the pharynx to double and 3 times that of the reference model showed no significant change across all factors (Table 2, Fig. 2.4C, 2.5). We can predict from this pattern, therefore, that a shorter pharynx would result in no significant change of power consumption due to constant pressures and friction as the reference model.

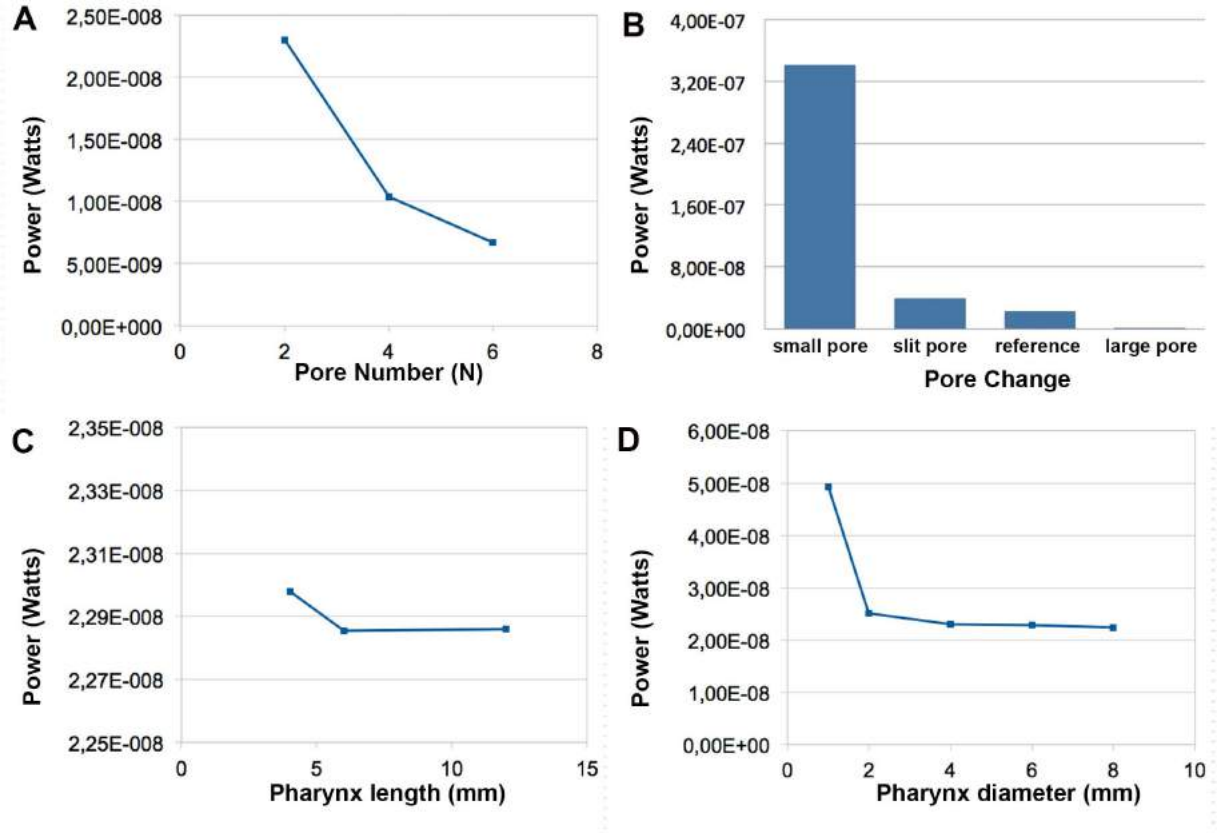

Figure 2.4. Power output (in watts) required by pumps, of different pharynx and pore sizes and shapes, to overcome friction. (A) Power output with three different pore numbers (n); (B) power output of a 2 pore simulation using different pore diameters and shapes; (C) power output required at increasing pharynx length (mm); and (D) power output with increasing pharynx diameter (mm).

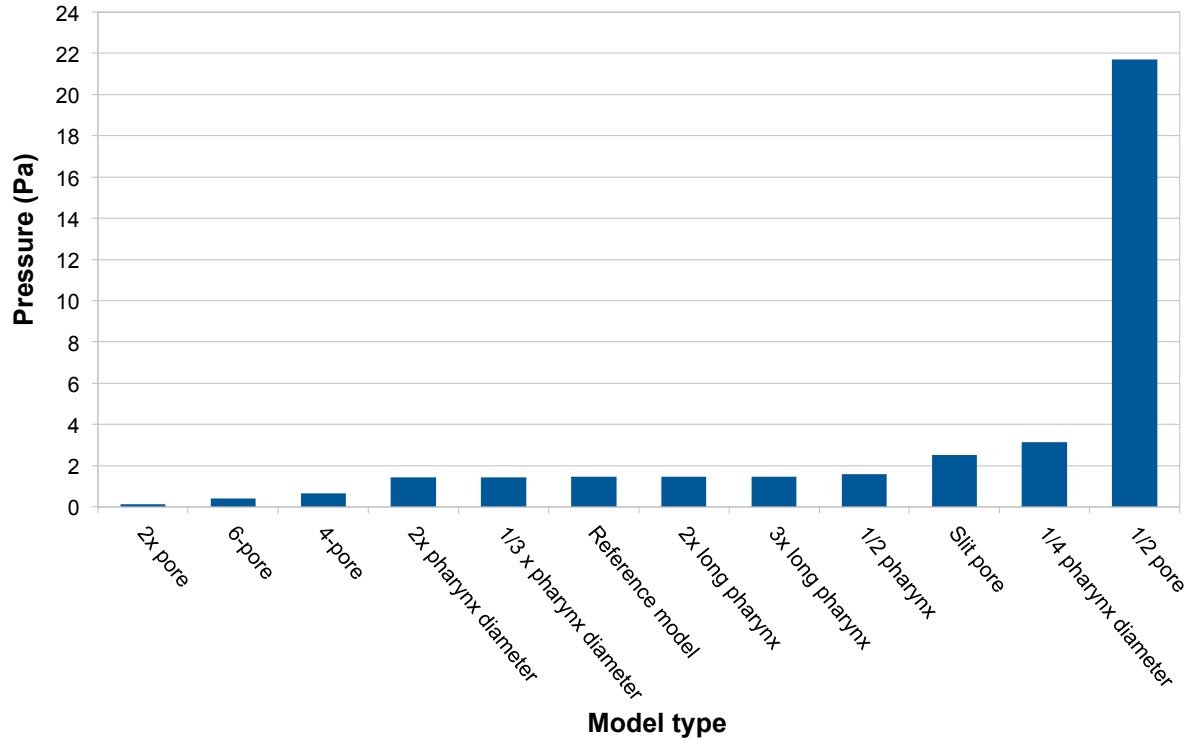

Figure 2.5. Pressure drop (Pa) between the mouth and gill pores of twelve model calculations in increasing order. Energy usage goes up with pressure drop.

Pharynx diameter

Increasing the pharynx diameter by one third that of the reference model decreased the mouth velocity by more than half (Table 2). The volumetric flow rate was held constant, and the pressure remained constant with the reference model and thus power did not vary (Table 2; Fig. 2.4D).

Doubling the pharynx diameter decreased the mouth velocity four-fold but, predictably, the mean pore velocity remained consistent with the reference model. The pressure drop only slightly decreased, thus the total power remained consistent with that of the reference model (Fig. 2.4D, 2.5).

Reducing the pharynx diameter by half that of the reference model, while maintaining the volumetric flow rate, increased the velocity at the mouth four-fold. Pressure drop slightly increased and thus power increased, but the increase was negligible (Fig. 2.4D, 2.5).

Decreasing the pharynx diameter to one quarter that of the reference model while maintaining the volumetric flow rate increased the velocity at the mouth by sixteen times and the velocity out the pores, predictably, remained constant (Table 2). Pressure drop doubled and therefore total power doubled (Fig. 2.4D, 2.5).

Pump Efficiency with Respect to Metabolic Energy

The energetic cost of filter feeding was evaluated in terms of the total oxygen consumption of the animal, which we took as 0.0092 ml O_2 h^{-1} using rates recorded for the acorn worm *Ptychodera flava* (Azariah et al., 1975). The useful pumpwork to metabolic power expenditure of our models represented an overall pump efficiency ranging from 0.004 - 0.712% with the large and small gill pore models representing the extremes respectively (Table 2).

2.5 DISCUSSION

Our primary goal was to simulate flow inside the pharynges of an ontogenetic (or phylogenetic) range of hemichordates. Perhaps most significantly, power consumption analysis demonstrated a low feasibility of filter feeding at very small gill pore diameters, and flow profiles at medium pharynx diameters showed inefficient back-flow out the mouth.

As in any modeling study, the model only approximates the system. In our case, our models were, computationally speaking, smooth, rigid, and static in their conformation. In live animals the pharynx is lined by a dense bed of beating cilia, the viscosity is complicated by mucus, the walls of the pharynx are soft, pliable and more complex than that of our models. An animal pharynx also changes conformation with the contraction of muscles around the pharynx or the gill pores. A significant implication of this is that our calculations of increases (or decreases) in power due to friction and pressure differences across a model, which requires an increase (or decrease) in pump output, are presumably less than those of a living, pumping pharynx. This means that the power consumption results presented here are likely underestimates, and thus the ratio of energy consumption of the pump to the metabolic energy available is conservative. Despite these limitations, our models are the most complex models of filter feeding to date. A benefit of this approach is that comparisons of flow profiles and

pump outputs can be made between hypothetical models, allowing the flexibility to control specific changes among models while maintaining all other conditions constant, providing insight into the expected trends one might observe among acorn worms and the pterobranch *Cephalodiscus*.

Sliding wall simulations

The walls of the pharynx and gill pores of hemichordates are uniformly lined by cilia, and the flow dynamics and location of the pump, whether on the walls of the pharynx and/or the walls of the gill pores, was evaluated. First we quantified the velocity profile of seawater at the entrance to the mouth of *Protoglossus graveolens,* as well as the velocity out of the gill pores. Flow rate into the mouth is highest at the center of the mouth and slowest, and at times reversed, along the pharyngeal walls. In our reference model, water exited the gill pores at the same velocity as diluted milk observed in live animals. We then did four moving wall simulations until we emulated the flow profile observed at the mouth of *P. graveolens*. We used the reference model and the half-sized pharynx diameter model (2 mm). The flow velocity into the mouth was 1.25 x 10-3 ms^{-1} with the pharynx wall sliding at 0.3309 ms^{-1}. Our assumption was that the sliding walls would provide a good proxy of the pump provided by cilia that line these same walls *in natura*. Simulations where only the pharynx wall move results in a large volume of reverse flow in the medial pharynx and out the mouth with no water exiting the pores (Fig. A1). The simulation of a half-sized pharynx diameter model represented a more feasible model as it resulted in water exiting the pores (Figs. A2), but a high pressure of nearly 29 Pa (data not shown) was calculated at the back wall, well above the normal operating pressure of bivalve gills (9.8 Pa) (Jorgensen et al., 1984), suspension feeding polychaete worms (0.19-6.7 Pa) (Riisgård, 1991) and the maximum operating pressure of the ascidian *Styela clava* (11.8 Pa) (Riisgård, 1988) and sponges (6.6 Pa) (Wildish and Kristmanson, 2005).

Further simulations were done where the gill pore walls were set to slide, in conjunction with the pharynx wall, though the latter wall at a very slow rate (ie. 0.004 ms^{-1}). In these simulations, water exited the gill pores and resulted in a concave flow profile at the mouth, similar to what we observed *in natura* (Fig. A4). In the larger reference model, little to

no flow was observed in the medial pharynx, representing an ineffective pump system. Large pharyngeal filter feeders, including many fish, have overcome this upper size constraint by abandoning the ciliary pump for a muscular buccal pump or ram feeding (e.g., herring, whale sharks). These simulations suggest that cilia on the gill pores provide the primary pumping mechanism. The pharynx wall may supplement this flow, but only if the pump velocity is very low.

Power Consumption

Pharynx length

Changes to pharynx length have little effect on power consumption. Power is directly correlated with pressure drop (Table 2). When the mouth and pore diameter are held constant, the pressure loss per unit length throughout the system remained constant and did not change with length changes. Velocity gradients come to steady state independent of the distance downstream. The slightly larger pressure drop between the reference model and longer pharynx models is due to the increased surface area and corresponding energy loss (or head loss) due to water flow (friction) that is proportional to the pipes length (Table 2). It is lower than expected because the volume between the pores and back wall exhibited little flow, approaching zero at the back wall (Fig. 2.3C,D). Most flow, and requisite output power, is confined to the anterior half of the model.

Pharynx diameter

Changes in pharynx diameter influence pressure drop and thus power consumption. The pressure and power differences are negligible from the largest diameter model down to the model that was half the diameter of the reference model (i.e., from 4 mm to 2 mm). A further decrease to a quarter of the reference model (i.e., 1 mm), however, more than doubled the pressure drop and power consumption. According to the principle of continuity, constant volume flow rate requires that any reduction in cross-sectional area of a pipe be associated with an increase in velocity of flow. At larger pipe sizes, small reductions will have a slow increase in velocity, however the reduction of the cross-sectional area is inversely proportional to the square of the reduction factor so at very small pipe sizes, the velocity

increases rapidly (LaBarbera and Vogel, 1982). For a given speed of flow, the cost of the pump is inversely proportional to the square of the radius of the pipe (LaBarbera and Vogel, 1982). Loss due to friction, drag, energy relations, and compressibility are all conventionally assumed to be related to the square of the mean velocity and thus, at very small pipe sizes, the cost to move fluid through is vastly more than through a large one (Vogel, 2003).

Pore size, shape and number

Change in pore size, pore number, and pore shape had the largest effect on power consumption. Increasing the cross-sectional area for water to escape through a pore works on the same principles as increasing the pharynx diameter; increases in pore diameter results in a reduced velocity and pressure inside the pharynx, facilitating the steady, unidirectional flow of water (Table 2).

Correspondingly, the addition of pores decreased the pressure drop and power consumption. The addition of pores increased outlet surface area and the relative volume of water capable of exiting. The benefits of filtering with increased ciliated surface area would result in a more efficient pump. *In natura* we suspect that an increase in pore number would correspond with an increase in mass flow rate. It is not known if it increases the gill pore flow velocity. In either scenario, this increase would translate into an increase in resistance acting against flow, and therefore an increase in power output required of the pump.

A reduction in the radius of the pore diameter increased fluid velocity and pressure drop. The global pressure of the system is determined by the pore size, therefore the smaller the pore, the higher the pressure drop and the harder it is to pump at a given mass flow rate. Interestingly, our simulations of the model with the very small pore diameter, in the micrometer size range (8-10 μm) of *Cephalodiscus* (data not shown), resulted in no flow out the pores due to viscous forces, high-pressure head losses, and high power demands. Instead, fluid remained in the pharynx in a recirculating pattern, representing an ineffective filtration system. This result has two significant evolutionary implications. First, *Cephalodiscus* bypassed the constraint of filter feeding with very small gill pores by evolving tentacles that capture particles external to the pharynx. Second, it rejects the hypothesis that a cephalodiscid-sized zooid might have been the ancestor to the Enteropneusta (unless it was

very large, see (Hou et al., 2011)). In this scenario, pterobranch gill pores would need to be regarded as a *pre-adaptation* for a pumping function, later realized in acorn worms, a theoretical heresy. Interestingly, the exceptionally small harrimanid enteropneust, *Meioglossus psammophilus,* at 611μm in total body length, has a single pair of gill pores that lack both the cilia and gill bars (Worsaae et al., 2012), suggesting that it also may have abandoned filter feeding with a corresponding reduction in size.

Our simulation of slit-shaped pores showed an increase in pressure and power by nearly double (Table 2) as compared to the circular pores of the reference model. The slits maintained the same cross-sectional area as the reference model, but friction losses increased as the relative surface area to volume increased. In live animals, the increase in power associated with gill slits is presumably traded off against a greater surface area for pumping water and for capturing food particles.

Oxygen consumption and overall pump efficiency

Our results demonstrate that a decrease in pharynx diameter, pore diameter and pore number increase relative power output. Our overall pump efficiency rates calculated using our CFD pumps were significantly lower in comparison with those of traditional models of invertebrate filter feeders, showing 0.1- 4% of total metabolic expenditure for useful pump work (Jørgensen et al., 1986; Riisgård, 1988; Riisgård and Larsen, 1995; Riisgård and Larsen, 2000; Wildish and Kristmanson, 2005). We have already discussed that our models have smooth, rigid walls and are thus low on friction, pressure differences and power, effectively lowering the pump consumption calculations, but in this respect our models are no different than those that preceded us. Two reasons likely account for our low pump output calculations, i) Oxygen consumption rates in the literature are reported from large and most probably stressed worms, effectively elevating the numerator (equation 4), and ii) our largest CFD model is comparatively small at 12 mm in length. Like most models, ours does not account for the real output of the fluid pump, but only the energy required to overcome the shear stress of moving seawater through the model. An advantage of this simplification is that direct comparisons can then be made between pump systems (i.e., from a bivalve to a sponge to a pharynx with gill pores), because the models are unimpeded by pump efficiency between

systems (i.e., a sponge flagellar pump may be more or less metabolically demanding than a pharyngeal ciliary pump moving an equivalent volume of water). In any case, a quantification of oxygen consumption rates across a size range of hemichordates is needed to compare and refine further energy calculations.

Validity of current models

Previous estimates of pump power and efficiencies in filter feeders are based on models calculated using estimated resistances, pressure heads, and volume flow rates (Jørgensen et al., 1986; Jørgensen et al., 1988; Riisgård, 1988; Riisgård, 1989; Riisgård and Ivarsson, 1990; Riisgård et al., 1992; Riisgård and Larsen, 1995). This indirect approach is used to arrive at theoretical estimates, which in itself presents several possibilities for miscalculations. Fully developed laminar flow is assumed in most model calculations, yet the small scale of organisms may not allow for flow to fully develop. Such calculations often assume the most optimal pumping in undisturbed conditions of an individual, however suboptimal conditions and/or mechanical disturbances may yield results that differ considerably. Riisgård and Larsen (1995) calculated pumping power and energy costs of filter-feeding macroinvertebrates using a series of equations and incorporated total head losses. The calculations for pumping power, however, still require actual measurements of volume flow and pump head from specimens in normal conditions. Although volumetric flow is easily measured, the pump head was not measured directly and therefore may only be an approximate.

2.6 CONCLUSIONS

Fluid mechanics is a potent selective force that determines the design principles that characterize organismal fluid transport systems at different sizes. Modeling of pumping water through the pharynx and miniscule gill pores of the pterobranch *Cephalodiscus* results in ineffective flow circulation, and is associated with high power costs. These results suggest that the gill pores of pterobranchs are non-functional, vestigial structures, retained from an ancestor that had larger gill pores, arguably, a filter feeding acorn worm (Cameron, 2002b; Gonzalez and Cameron, 2009). The mucous house of appendicularians and the laterally

placed mouth of cephalochordate larvae, both evolutionary novelties, may be modifications to capture particles at very small body sizes. The external house of appendicularians filters the bulk of the food-laden seawater, the tiny pharyngeal pump only operating periodically, to bring food-laden mucus into the mouth (Flood, 1991). The laterally placed mouth of cephalochordate larvae may be a modification to increase mouth diameter and decrease pharynx length, effectively reducing power consumption of the pharyngeal pump. According to Gilmore (1996) these larvae trap particles on mucous threads external to the pharynx, another adaptation to reduce volumetric flow into the mouth. In our study, the ciliary pump was emulated by sliding walls of the pharynx and gill pores until we arrived at a velocity flow profile into the mouth observed from recordings on live animals. This approach allowed us to narrow the location of the primary pump to the gill pores. In this respect the hemichordate pump is spatially identical to the pump of invertebrate chordates. CFD simulations of larger diameter pharynges resulted in a reversed flow field in the pharynx, reducing the systems efficiency. This result may explain why pharyngeal filter feeding has not been observed in large ptychoderid acorn worms, but only the smaller harrimanids. Larger pharyngeal feeders appear to have bypassed the limitations of a ciliary pump by adopting a muscular pump (i.e., herring to whales). In this study the need of published and reliable oxygen consumption rates, coupled with limitations of our CFD models, are the most probable reasons for our unusually low pharyngeal pump power consumption values.

2.7 ACKNOWLEDGEMENTS.

We would like to thank colleagues in the fluid mechanics laboratories at École Polytechnique for helpful discussions with the FVM and CFD analysis. This research was supported by National Sciences and Engineering Research Council of Canada (NSERC) Discovery Grants to C.B.C. and D. P.

2.8 AUTHOR CONTRIBUTIONS

The concept for this study was developed by C.B.C and in concert with D.P, the experimental approach designed. M.V and F.V performed experimental CFD modeling, simulations, and analysis. M.V, C.B.C, and D.P prepared and edited the manuscript prior to submission.

2.9 REFERENCES

Acheson, D. J. (1990). Elementary fluid dynamics: Oxford University Press.

Azariah, J., Ismail, M. M. and Najib, M. A. (1975). Investigation on the ecology and respiratory responses of the hemichordate *Ptychodera flava* to tidal cycles and salinity changes. *The Biological Bulletin* **149**, 455-466.

Cameron, C. (2005). A phylogeny of the hemichordates based on morphological characters. *Canadian Journal of Zoology* **83**, 196-215.

Cameron, C. B. (2002a). The anatomy, life habits, and later development of a new species of enteropneust, *Harrimania planktophilus* (Hemichordata: Harrimaniidae) from Barkley Sound. *The Biological Bulletin* **202**, 182-191.

Cameron, C. B. (2002b). Particle retention and flow in the pharynx of the enteropneust worm *Harrimania planktophilus*: the filter-feeding pharynx may have evolved before the chordates. *The Biological Bulletin* **202**, 192-200.

Cameron, C. B., Garey, J. R. and Swalla, B. J. (2000). Evolution of the chordate body plan: new insights from phylogenetic analyses of deuterostome phyla. *Proceedings of the National Academy of Sciences* **97**, 4469-4474.

Cannon, J. T., Rychel, A. L., Eccleston, H., Halanych, K. M. and Swalla, B. J. (2009). Molecular phylogeny of hemichordata, with updated status of deep-sea enteropneusts. *Molecular Phylogenetics and Evolution* **52**, 17-24.

Caron, J.-B., Morris, S. C. and Cameron, C. B. (2013). Tubicolous enteropneusts from the Cambrian period. *Nature* **495**, 503-506.

Dilly, P.N. (1993). Feeding and gut contents in *Cephalodiscus nigrescens* (Hemichordata, Pterobranchia) from the Weddell Sea. *Journal of Zoology* **230,** 63-67.

Etienne, S., Garon, A., Pelletier, D. and Cameron, C. (2010). *Philiadium gregarum* versus *Aurelia aurita*: on propulsion efficiency in jellyfish. From the 48th *American institute of aeronautics and astronautics meeting,* 1-8.

Flood, P. R. (1991). Architecture of, and water circulation and flow rate in, the house of the planktonic tunicate *Oikopleura labradoriensis*. *Marine Biology* **111**, 95-111.

Fluent 13, Ansys (Software) (2012). Canonsburg, Pennsylvania: Ansys. http://www.ansys.com.

Gambit (version 2.4) (Software) (2002). Canonsburg, Pennsylvania: Ansys. http://www.ansys.com.

Gonzalez, P. and Cameron, C. B. (2009). The gill slits and pre oral ciliary organ of *Protoglossus* (Hemichordata: Enteropneusta) are filter feeding structures. *Biological Journal of the Linnean Society* **98**, 898-906.

Hou, X.-g., Aldridge, R. J., Siveter, D. J., Siveter, D. J., Williams, M., Zalasiewicz, J. and Ma, X.-y. (2011). An early Cambrian hemichordate zooid. *Current Biology* **21**, 612-616.

Jørgensen, C., Kiorboe, T., Mohlenberg, F. and Riisgard, H. (1984). Ciliary and mucus-net filter feeding, with special reference to fluid mechanical characteristics. *Marine Ecology Progress Series* **15**, 283-292.

Jørgensen, C., Larsen, P., Møhlenberg, F. and Riisgård, H. (1988). The mussel pump: properties and modelling. *Marine Ecology Progress Series* **45**, 205-216.

Jørgensen, C., Famme, P., Kristensen, H. S., Larsen, P., Møhlenberg, F. and Riisgård, H. (1986). The bivalve pump. *Marine Ecology Progress Series* **34**, 69-77.

Jørgensen, C. (1975). Comparative physiology of suspension feeding. *Annual Review of Physiology* **37,** 57-79.

LaBarbera, M. and Vogel, S. (1982). The design of fluid transport systems in organisms: Despite their apparent diversity, fluid transport systems display a fundamental unity of organization resulting from the constraints of a few design principles on natural selection. *American Scientist* **70**, 54-60.

Liu, H. (2002). Computational biological fluid dynamics: digitizing and visualizing animal swimming and flying. *Integrative and Comparative Biology* **42**, 1050-1059.

Liu, H., Wassersug, R. and Kawachi, K. (1996). A computational fluid dynamics study of tadpole swimming. *Journal of Experimental Biology* **199**, 1245-1260.

Liu, H., Ellington, C. and Kawachi, K. (1998). A computational fluid dynamic study of hawkmoth hovering. *Journal of Experimental Biology* **201**, 461-477.

Riisgård, H. U. and Larsen, P. S. (1995). Filter-Feeding in marine macro-invertebrates: pump characteristics, modelling, and energy cost. *Biological Reviews* **70**, 67-106.

Riisgård, H. U. and Larsen, P. S. (2000). Comparative ecophysiology of active zoobenthic filter feeding, essence of current knowledge. *Journal of Sea Research* **44**, 169-193.

Riisgård, H. U. and Larsen, P.S. (2001). Mini-review: Ciliary filter feeding and bio fluid mechanics - present understanding and unsolved problems. *Limnology and Oceanography* **46,** 882-891.

Riisgård, H. U. and Ivarsson, N. M. (1990). The crown-filament pump of the suspension-feeding polychaete *Sabella penicillus*: Filtration, effects of temperature, and energy cost. *Marine Ecology Progress Series.* **62**, 249-257.

Riisgård, H. U. (1988). The ascidian pump: properties and energy cost. *Marine Ecology Progress Series* **47**, 129-134.

Riisgård, H. U. (1991). Suspension feeding in the polychaete *Nereis diversicolor*. *Marine Ecology Progress Series* **70,** 29-37.

Riisgård, H. U. (1989). Properties and energy cost of the muscular piston pump in the suspension feeding polychaete *Chaetopterus variopedatus*. *Marine Ecology Progress Series* **56**, 157-168.

Riisgård, H. U., Vedel, A., Boye, H. and Larsen, P. S. (1992). Filter-net structure and pumping activity in the polychaete nereis-diversicolor-effects of temperature and pump-modeling. *Marine Ecology Progress Series* **83**, 79-89.

Swalla, B.J. (2009). Development and Evolution of Ptychoderid Hemichordates. *Integrative and Comparative Biology.* Cary: Oxford University Press. E166 pp.

Vogel, S. (2003). Comparative biomechanics: life's physical world. New Jersey: Princeton Univ Press.

Wildish, D. and Kristmanson, D. (2005). Benthic suspension feeders and flow. New York: Cambridge Univ Press.

Worsaae, K., Sterrer, W., Kaul-Strehlow, S., Hay-Schmidt, A. and Giribet, G. (2012). An anatomical description of a miniaturized acorn worm (Hemichordata, Enteropneusta) with asexual reproduction by paratomy. *PloS one* **7**, e48529.

3.0 APPENDIX

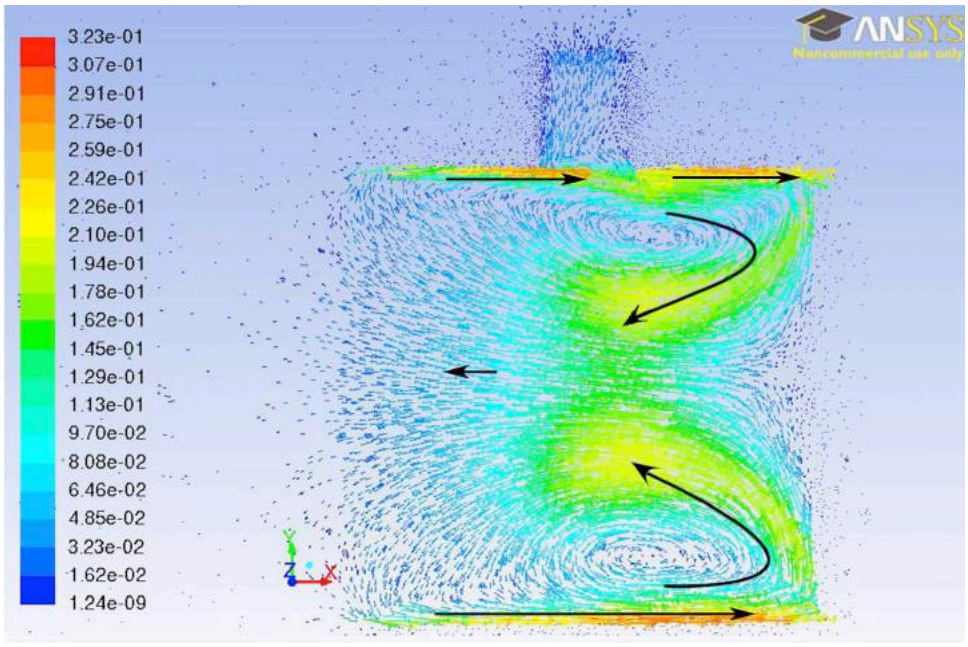

Figure A1. CFD simulation showing the velocity profile of seawater throughout the 2-pore reference model, where the pharynx wall was set to slide posteriorly at a rate of 0.3309 ms^{-1}.

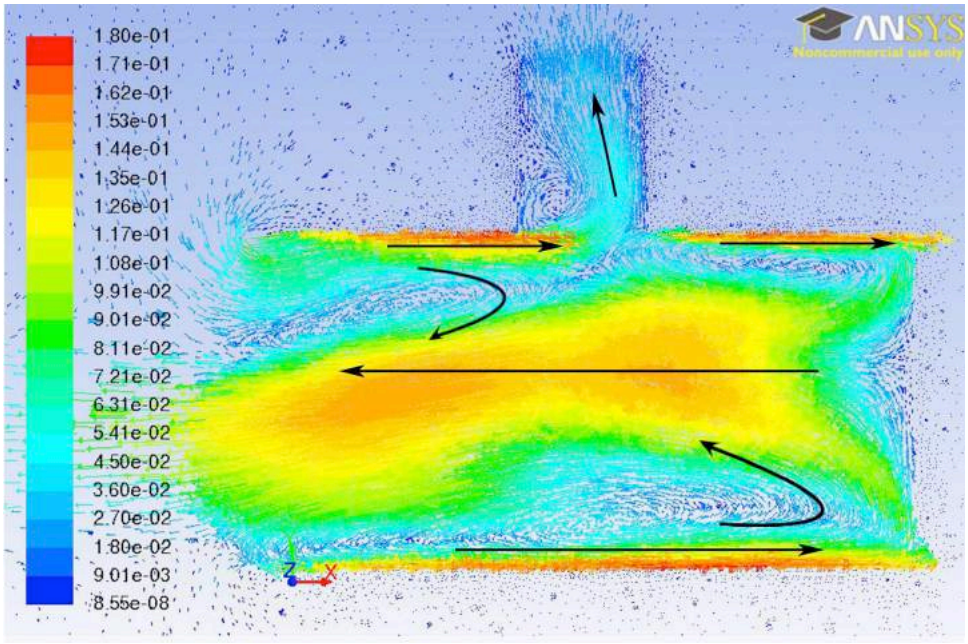

Fig. A2. CFD simulation showing the velocity profile through a half diameter reference model with sliding pharynx wall velocity set to slide posteriorly at 0.3309 ms^{-1}.

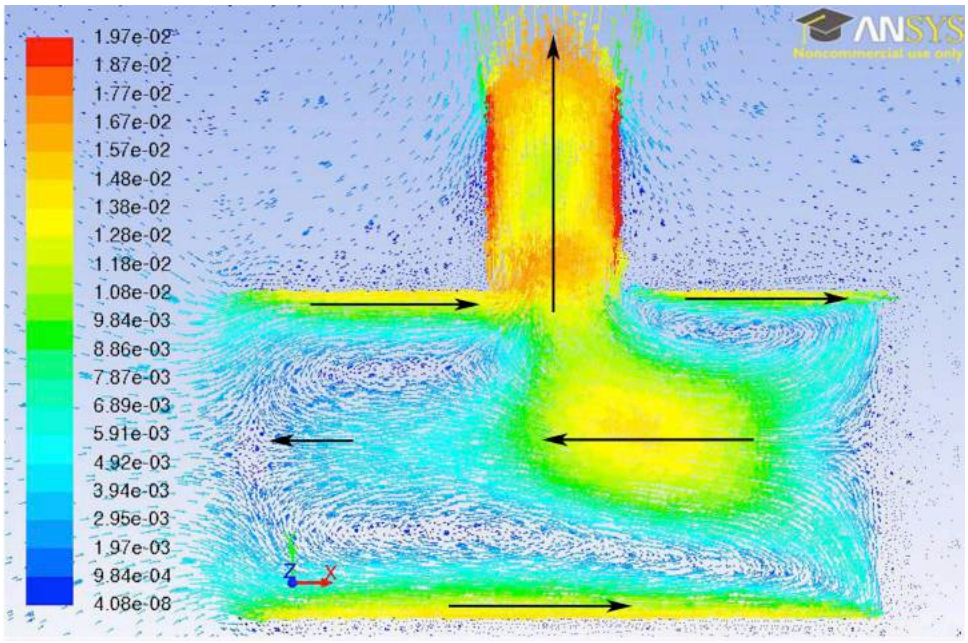

Fig. A3. CFD simulation showing the velocity profile through a half diameter reference model with sliding gill and pharynx walls set to slide posteriorly at a rate of 0.020 ms^{-1} and 0.015 ms^{-1} respectively.

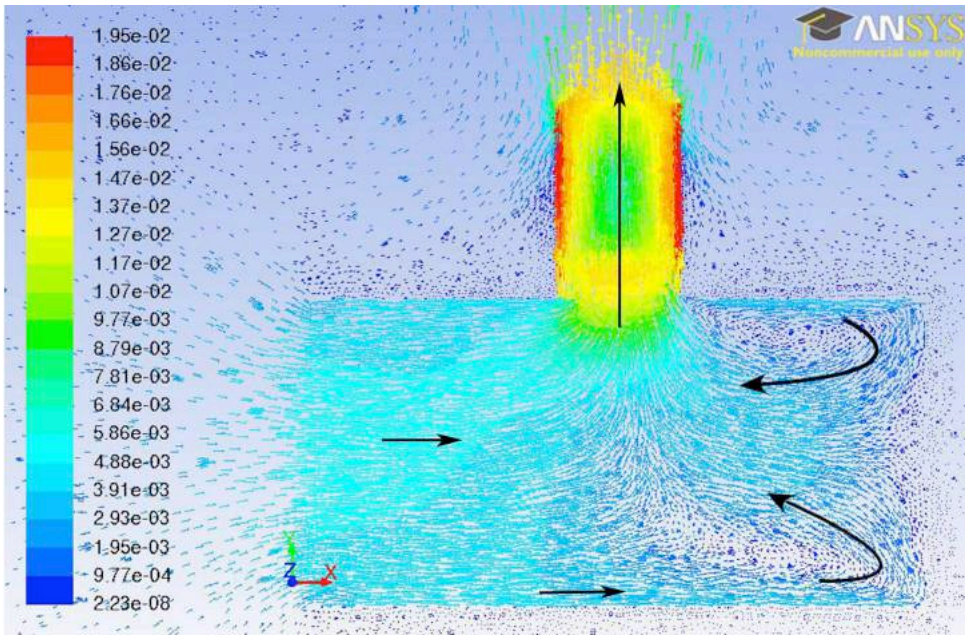

Fig. A4. CFD simulation showing the velocity profile through a half diameter reference model using simultaneously sliding gill and pharynx walls, as done in A3, however the pharynx wall has been drastically decelerated. The walls of the gills and pharynx are set to slide posteriorly at a rate of 0.020 ms^{-1} and 0.004 ms^{-1} respectively.

CHAPTER 3

3. Article: Paddles to rakes: A computational fluid dynamic analysis on the leakiness of wave-extreme barnacle legs reveal the low Reynolds number transitioning

Maureen Vo, Fernando Villalpando, Dominique Pelletier, and Christopher B. Cameron

Manuscript in preparation for submission

3.1. Abstract

Suspension feeders use a wide range of hair-bearing appendages to capture particles from the surrounding fluid. Their functioning, either as a paddle or a sieve, depends on the leakiness, or amount of fluid that passes through the gaps between hairs. *Balanus glandula* is the most common species of barnacle distributed along the Pacific coast of North America. Their filter feeding appendages show a strong phenotypic response to flow, with short and robust filters in high flow environments and long spindly appendages in low flow environments. Computational fluid dynamic models of barnacle filters representing these two extremes were modeled and simulated at low to high Reynolds numbers and flow fields were calculated to determine leakiness. Particle image velocimitry (PIV) was performed at low to medium flow velocities and corroborated results from CFD. Barnacles from sheltered environments transition from paddles to sieves at Re 2.24 while barnacles from high glow environments transition at Re of 3.5. Morphological differences have the greatest effect on function in the critical Re range where transition occur and each wave-extreme barnacle appears to be well adapted to its environment.

3.2 Introduction

Suspension feeders use a diverse range of hair-bearing appendages to capture particles from the surrounding water (Riisgård and Larsen, 2010). Although all essentially consist of arrays of bristles or cylinders, some appendages behave as sieves to intercept particles from suspension passing through (e.g. bands of stiff cilia, filter setae or through mucus nets), while others create feeding currents or act as paddles to direct pockets of suspension for further processing (e.g. flagellum, cirri, or tentacles) (Vogel, 2003; Riisgård and Larsen, 2010). The performance of these appendages (i.e. paddle vs. sieve) depends on their interactions with the surrounding medium. Fluid can either pass readily through the gaps between hairs, creating a 'leaky' appendage or may move around the perimeter of the whole array. If the leakiness of a filtering appendage is high, the appendage functions as a sieve and in contrast, if the leakiness is low, the filter functions as a paddle.

Several mathematical and physical models of fluid velocity profiles around rows of cylinders of finite width have demonstrated that this transition to leakiness depends largely on

the Reyonld's number and setae spacing ratio (Tamada and Fujikawa, 1957; Cheer and Koehl, 1987a, b; Hansen and Tiselius, 1992; Koehl, 1993; Loudon et al., 1994). The Reynolds number (Re) (Re= UL/v, where U is velocity, L is some characteristic length, and v is the kinematic viscosity of the fluid) represents the ratio of inertial to viscous forces determining the motion of fluid around a hair (Vogel, 2003). With most biological fibers functioning in the Re range of 10^{-5}-10 (Rubenstein and Koehl, 1977; Jorgensen, 1983; LaBarbera, 1984; Cheer and Koehl, 1987a; Shimeta and Jumars, 1991), viscous forces dominate, velocity boundary layers are thick relative to the dimensions of the body, and flow about appendages is laminar (Happel and Brenner, 1965; Vogel, 1996). Similarly, setae spacing ratio, G/D (described by the ratio of the cylinder center-to-center spacing, G, to the diameter, D, of the cylinder) can have large effects on leakiness with any changes occurring in the critical Re range of 10^{-2}- 1 (e.g. high leakiness observed at G/D>>5 for Re = 0.5 (Cheer and Koehl, 1987a; Koehl, 1996, 2001). At very low Re (i.e. $<10^{-3}$) however, changes to this ratio has little influence on leakiness (i.e. morphological and behavioural diversity without performance consequences) (Koehl, 1996). The mechanisms and rates of particle capture by filter feeding appendages depend on the flow fields around individual hairs of a filter (Rubenstein and Koehl, 1977; Shimeta and Jumars, 1991). Specific morphological changes and novel functions can result simply from changes in size, shape, stiffness or habitat of an organism, therefore to understand the relationships between morphology and functioning and the basic physical rules governing how a biological structure operates, a mechanistic study is required.

Balanus glandula, or acorn barnacles, are a common Northeastern Pacific species found in a wide range of wave-exposure habitats whose feeding legs demonstrate a great degree of phenotypic plasticity varying both within the species and during developmental stages (Fig. 2.1) (Southward, 1955; Marchinko and Palmer, 2003; Marchinko, 2007). Their sessile nature facilitates observations without environmental effects being complicated by blurring from animal movements and they are easily manipulated in the field or transplanted because they settle on such a wide variety of substrata (Arsenault et al., 2001). The parameters of feeding structures and velocity ranges for individuals found in flow extremes are also known, simplifying analysis studies (Arsenault et al., 2001; Marchinko and Palmer, 2003). Barnacles therefore provide ideal subjects to explore questions about how morphology

and fluid dynamics affect appendage functioning. Although the feeding behaviour and general descriptions of flow have been described in several species of barnacles (Southward, 1955; Trager et al., 1990; Marchinko and Palmer, 2003; Marchinko, 2007; Miller, 2007; Geierman and Emlet, 2009), a detailed comparison of the fluid dynamics through and around the cirral legs of wave-extreme barnacles at varying speeds is lacking. The primary challenge has been documenting fluid interactions of small appendages at realistic high flow speeds. Understanding the fluid dynamics around different morphological structures also allow us to determine physical limits to the distribution and abundance of barnacles along wave-exposure gradients and better assess their role in aquatic communities and ecosystems.

Velocity and flow visualization in very small spaces can be difficult to access without excessively disturbing the animal and flow fields. Advances in technology have therefore been required to advance biological research (Frank et al. 2008 and references therein). Biomechanics, or the application of quantitative engineering techniques to study interactions between organisms and their mechanical functioning, is an interdisciplinary approach which can provide insight on functional morphology. Computational fluid dynamics (CFD), which uses computer-based simulations systems to solve and analyze problems involving fluid flow, was used in our study to analyze the details of flow fields around two disparate barnacle filters at increasing flow velocities. Due to the novelty of CFD as a biological technique, CFD predictions were compared with experimental flow observations using particle image velocimetry (PIV), a technique known to accurately depict feeding activity in a variety of suspension feeding invertebrates (Frank et al., 2008). Comparisons allow a more in-depth analysis, with detailed view on the microfluidics near structures. Here, we use CFD to address a vexing problem in biological fluid mechanics that had previously been elusive.

The objective of this study is to compare i) flow dynamics, ii) coefficients of drag, and iii) leakiness between barnacles from exposed and protected shores at increasing flow velocities.

3.3 Materials and Methods

In-vitro observations using PIV

Collection Sites

Balanus glandula specimens were collected from two wave-extreme sites in Barkley Sound, Vancouver Island, British Columbia between May - July, 2013 (Table 3). Rocks and mussels (*Mytilus californianus*) with attached barnacles were collected from the sheltered and low flow shoreline of Grappler Inlet, and from the wave exposed and high flow coast of Seppings Island (Table 3). Careful attention was paid to choosing barnacles from microniches that were not obviously obstructed from flow by adjacent obstacles. These collection locations are the same as those used by Marchinko & Palmer (2003) and therefore their water velocity measurements informed our study. Barnacles were transported to the Bamfield Marine Sciences Centre and maintained in flow through sea tables (181 cm long x 84 cm wide x 8 cm deep).

Fixing of barnacles

Barnacle specimens were removed from their shells and placed in a solution of $MgCl_2$ to relax feeding legs. Specimens were than transferred to Bouin's fixative for 24 hours to fix legs in the open, passive feeding position and stored in 70% ethanol.

Cirral anatomy measurements

The posterior three cirri (IV, V, VI) of *Balanus glandula* individuals were characterized because they are the longest and primary food capturing appendages (Anderson, 1994; Marchinko and Palmer, 2003) (Fig. 3.1A). Individual barnacles were viewed with an Olympus Q color 5 camera mounted on an Olympus SZX16 dissecting microscope and images captured using QCapture (Surrey, BC). The longest ramus, cirrus VI, was removed, straightened into the feeding position, and ventral surfaces and profiles photographed (Fig. 3.2A-D). Morphometric analysis using ImageJ (Schneider et al., 2012) of enhanced micrographs and scanning electron microscope images of central segments of cirri VI produced values for segment length, width, and height, setae lengths and widths (at the tip and base), angle of setae protruding from segments, intersetal spacing, and distance between cirri (Fig. 3.2A-D, Table 4).

Actual measurements averaging six individuals from each wave-extreme site along with incorporation of the percentage differences described by Marchinko and Palmer (2003) between sheltered and exposed barnacles, provided us with our final parameters for our CFD models representing two wave-extreme forms (Table 4). As phenotypic plasticity varies greatly among the barnacles, our goal was simply to create two drastically different wave-extreme representatives for flow observations.

Laser-illuminated flow visualization

Flow visualization was performed in a laboratory flume with the dimensions 107 cm long x 18 cm wide x 19 cm deep (Fig. A5). Extracted barnacle bodies were held with tweezers in plasticine so the feeding legs were free to open in the passive feeding position. A class IIIb, wavelength 532 nm laser (Laserglow technologies) was passed through a concave crystal to create a two dimensional sheet across the mid-section of the barnacles cirri for flow field observations (Fig. A5). The flume water was seeded with silver-coated hollow glass particles 11μm in diameter (110P8, LaVision GmbH) at a concentration of 10.50 g/ml. At times, the density of particles was increased by injecting them directly upstream of the feeding barnacle using a pipette. A variable speed motor (90 volt, 7.6 amp) and propeller was used to control flow velocity. Fully developed flow fields around filters were recorded using a Sony HDV (1080i HVR-Z1U/Z1N, 60i) video recorder at a rate of 30 frames per second.

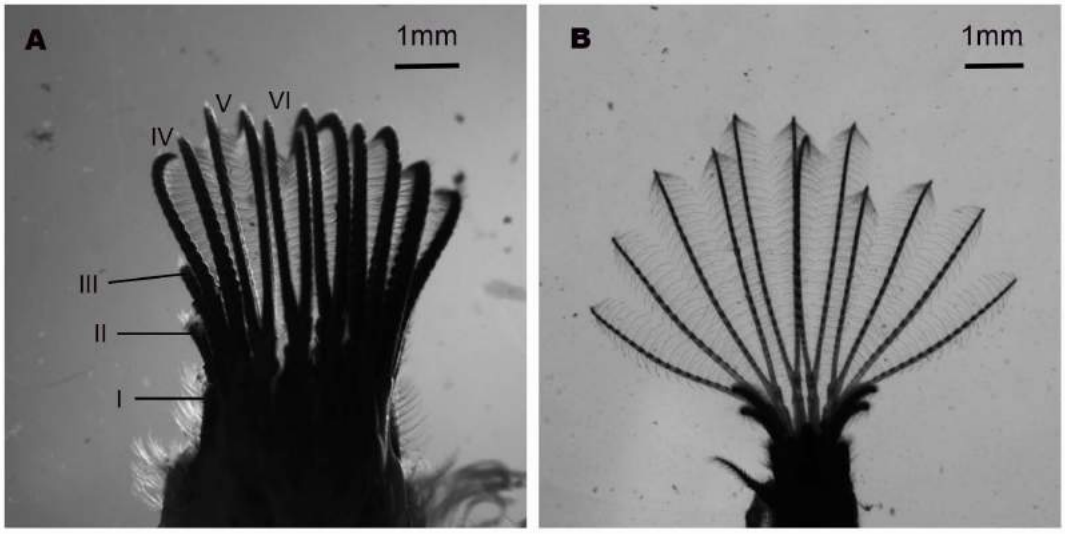

Figure 3.1. Captorial feeding net of sheltered and exposed barnacles. A, exposed barnacle phenotype showing cirri I-VI and B, sheltered barnacle phenotype.

Table 3. Collection sites and descriptions

Barnacles collected from Barkley Sound, Vancouver Island, British Columbia, Canada.

Wave exposure	Site	Location description	North latitude*	West longitude*	Water velocity* (m/s)
Sheltered	Grappler Narrows	west-facing shore	48˚49'91"	125˚07'65"	0.0066
Exposed	Seppings Island	western-most rocks on southwest facing	48˚ 50'50"	120˚12'50"	4.41

*Adapted from Marchinko & Palmer 2003.

Table 4. Summary of sheltered and exposed barnacle dimensions

Barnacle Type	Setae (n)	length, l (µm)	base diameter, D (µm)	tip diameter, t (µm)	setae spacing ratio (G/D)	setae angle (°)	mesh Size
Sheltered (n = 6)	1	515 ± 58	15 ± 4	4±0.78	1.5	47± 2	6808487
	2	362 ± 39	16 ± 3	4±0.78	1.69		
	3	224 ± 21	13 ± 2	2±0,50	1.71		
	4	147 ± 17	11 ± 1	2±0,50	1.82		
	5	90 ± 11	8 ± 1	2±0,50	2.29		
	6	62 ± 12	5 ± 1	0.5±0.20	3.00		
		length, l (µm)	height, h (µm)	width, w (µm)			
	Segment	186±13.7	216±19	93.4±9.4		51± 3	7439983
Exposed (n = 6)	1	445 ± 63	20 ± 2	5 ± 1.30	1.2		
	2	314 ± 87	20 ± 2	5 ± 0.82	1.08		
	3	275 ± 68	18 ± 1	4 ± 0.69	1.09		
	4	161 ± 64	15 ± 2	3 ± 1.30	1.25		
	5	106 ± 28	10 ± 2	3 ± 0.79	1.45		
	6	65 ± 20	6 ± 1.5	2 ± 0.50	2.50		
		length, l (µm)	height, h (µm)	width, w (µm)			
	Segment	280 ± 44	164 ± 24	98 ± 8			

Flow velocity

Velocities ranged from 0.04 m/s to 0.50 m/s in CFD simulations and 0.027 m/s - 0.19 m/s in PIV studies with Re ranging from 0-12 (Fig. A7). Frame-by-frame video analysis of suspended particle movement across an image scale and knowledge of camera speed allowed for the calculation of particle velocities around the passively positioned barnacle filter and determination of leakiness of barnacles from the two disparate morphologies. At a Reynolds number > 6, particle movement became too rapid to calculate velocity vectors. IMovie '11 (version 9.0.4) and ImageJ (Schneider et al., 2012) were used to analyze video footage.

CFD Modeling and fluid simulations

Barnacle filter models were generated using GAMBIT, a Fluent CFD preprocessing program. To simplify studies and minimize computational costs and time, we limited CFD models to the central portion of a barnacle filter (Fig. 3.2A).

Three-dimensional modeling

Setae and Segments

Two elliptical cylinders spaced at a defined distance were computationally constructed to represent the cirri of barnacle feeding legs. Each ramus is divided into six segments varying in height, width, and length depending on barnacle phenotype (Fig. 3.3A-C, Table 4). Projecting anterio-laterally from each segment were six pairs of conical-shaped setae, which protruded from the segments at an angle, with respect to the corresponding pair of 47˚ (sheltered) and 51˚ (exposed) (Fig. 3.3, Table 4). It was important to model the conical shape of setae as leakiness varies according to the position of flow across setae. Specific segment parameters are summarized in Table 4. The first two sets of setae intermingled with those of adjacent segments, while the decreasing sizes of setae towards the base of a segment created a gap (Fig. 3.4A,C). In order to minimize model size and computational calculation, one of the elliptical cylinders was divided in half and reflected as a mirror image using the '*symmetrical*' function when defining boundary conditions. The other segment was left whole to examine flow behaviour around the outermost setae, open to the free flow stream and independent of intermingling setae (Fig. 3.4A-D).

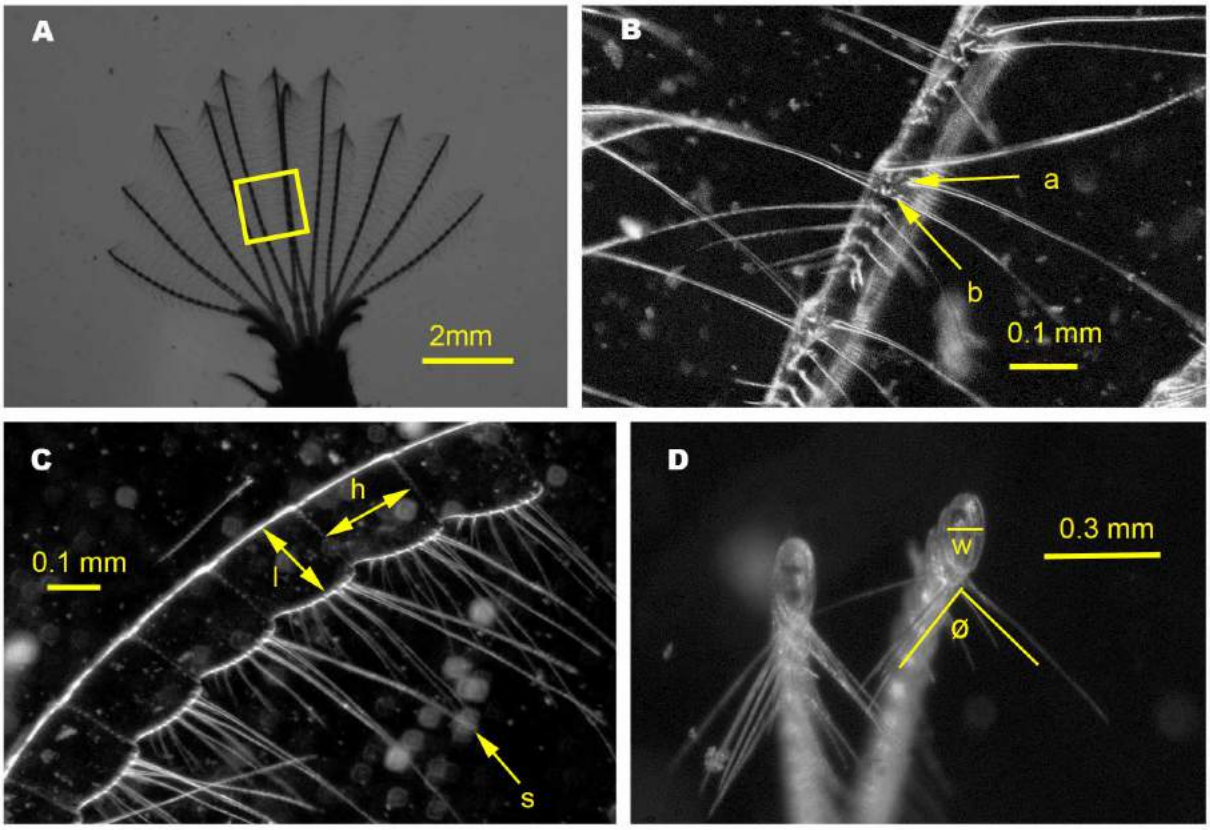

Figure 3.2. **Sheltered specimen showing traits measured.** A, complete captorial feeding net with boxed area showing central portion of cirri VI used for CFD modeling. B, front view showing intersetal spacing (i.e. from A to B) used to calculated spacing ratio; C, side view; D, cross section through central portion of cirri VI. h, height of segment; l, length of segment; s, setae lengths (measured from base to tip); w, width of segment; Θ, angle of setae protruding from segment.

Meshing Models

Each wire-frame model was sub-divided into nodes along the edge of the setae tips and bases and along the length of the setae upon which a number of non-overlapping sub-domain tetrahedral and hexahedral shaped elements were generated. The number of nodes along each setae tip and base was set to 20, while the nodes along the length of each setae ranged from 250 – 45 from longest to shortest setae respectively. Each setae tip and base were defined with 20 nodes and nodes along the length of setae ranged from 250 to 45 from longest to shortest setae respectively. All setae and the region directly surrounding setae represent critical areas of interest and therefore fine elements were placed in this region. Boxed areas were created around the filter structures to control for element size in critical areas (Fig. 3.5). A size function using setae as the source of growth allowed element size to grow increasingly coarser

farther away from the source at a growth rate of 1.05. Mesh sizes used are summarized in Table 4.

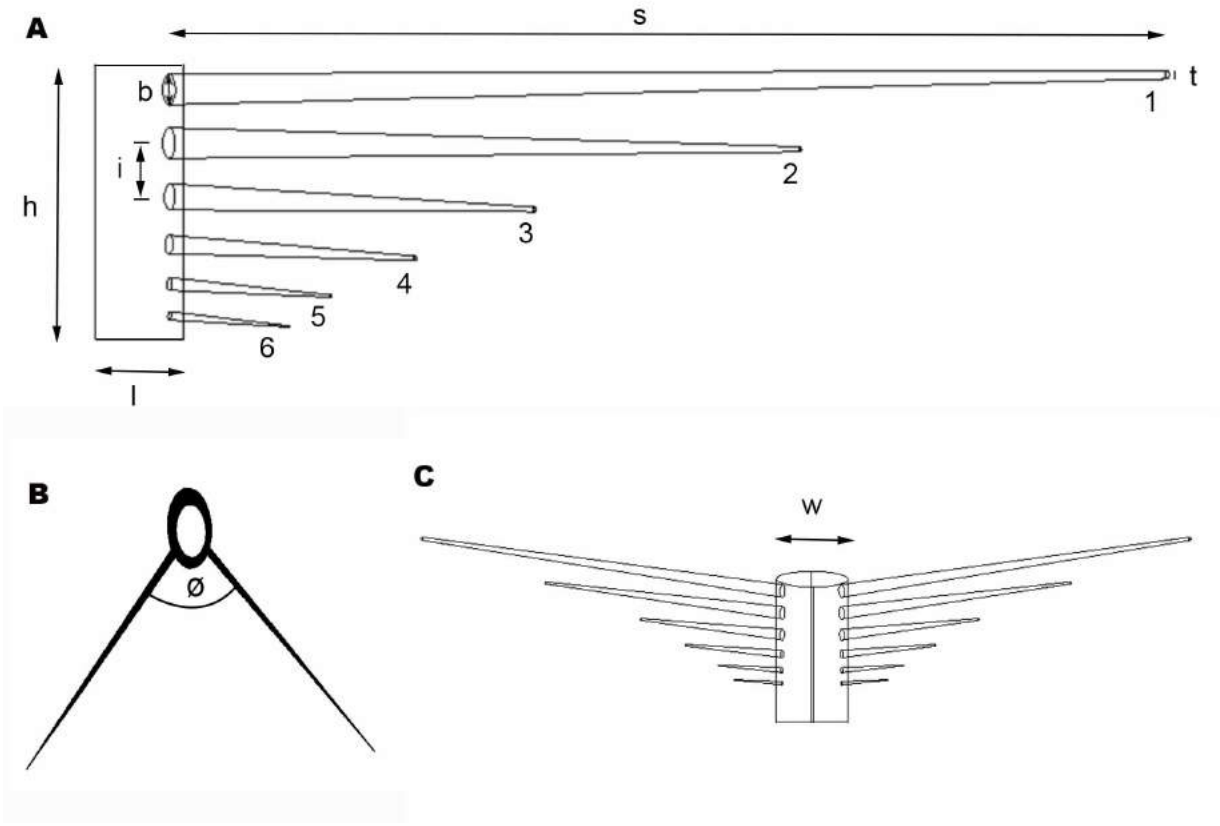

Figure 3.3. CFD section modeled. A) side view of a segment and setae, with setae numbered in descending size order; B) top, cross-section view of segment C) front view of full section. b, base diameter; h, height of segment; i, intersetal spacing; l, length of segment; s, setae length; t, tip diameter; w, width of segment; Θ, angle of setae with respect to segment.

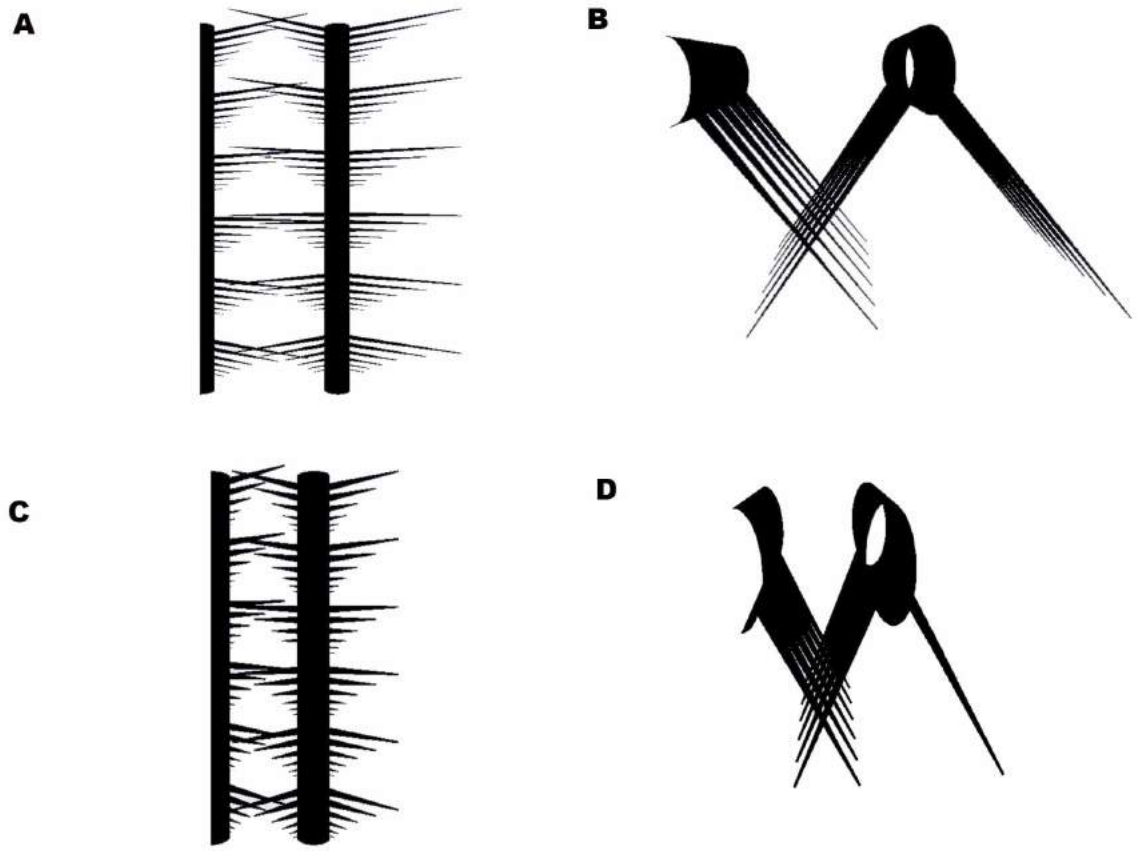

Figure 3.4. Meshed GAMBIT models. Sheltered (A-B) and exposed (C-D) models. A) Sheltered front view; B) Sheltered top view; C) Exposed front view; D) Exposed top view

Dimensionless scaling

Geometries were converted to dimensionless for simulations as it facilitates scale-up of obtained results to real conditions as well as simplified and generalized the calculations. The base diameter of the longest setae from the sheltered barnacle was used as the reference number to divide all parameters of both models. This converted all our models from dimensional to dimensionless scale for simulations. Dimensionless equations provide insight into the behaviour of a complex flow by regrouping dimensional parameters into a smaller set of non-dimensional numbers. For instance, flow around a circular cylinder depends on four parameters: i) the cylinder diameter, D; ii) the upstream velocity, U; iii) the fluid's density, ρ; and iv) viscosity, μ. Dimensional analysis shows flow is completely determined by one dimensionless number, the Reynolds number (Re) calculated as:

$$Re = \rho v L/U \quad (1)$$

where ρ is the density of fluid, v is the velocity of fluid relative to the body, L is the characteristic length, and U is the dynamic viscosity of the fluid.

Boundary Conditions

Each face of the model encountering a domain boundary (i.e. fluid) must be defined in order to simulate and to solve the governing equations for fluid flow. Box faces directly upstream of setae were defined as '*velocity inlets*'; box faces directly downstream of setae as '*pressure-outlets*'; setae and segments as '*walls*' and all remaining box faces as '*symmetry*' (Fig. 2.5).

Simulations were performed to represent three inlet velocities of U = 0.04 m/s, 0.21 m/s, and 0.50 m/s because these velocities represent a velocity range that has been measured *in situ* (Trager et al., 1990; Geierman and Emlet, 2009) and have also been used in previous barnacle studies (Marchinko, 2003, 2007).

The interior of the box, aside from the setae and segments was defined as a '*fluid*', in this case, an incompressible fluid representing seawater with density 1024 kg/ m^3 and viscosity 1.072e-03 kg/m-s (Vogel, 2003). Flow was released from the velocity inlet and was free to move through and around the setae and segments towards the posterior, pressure outlets. Flow through and around the setae and segments satisfied a free exit (continuative) boundary condition and the condition of conservation of mass.

Solver types and Numerical Method

Solving for the Navier-Stokes (N-S) equation can provide valuable information on the steady-state, incompressible fluid including flow patterns from velocity and pressure calculated at discretized points. Finite volume methods and the commercial CFD software package ANSYS FLUENT (version 13.0) were used for three-dimensional solving of the N-S equation. FLUENT solves the conservation equations for mass and momentum for all flows. Flow of fluid was assumed to be laminar, steady-state and isothermal. The mesh contained 6808487 cells in the sheltered model and 7439983 cells in the exposed models (Table 4). The governing equations were discretized using the finite volume method and solved using a

pressure based solver in steady time. The SIMPLE algorithm with QUICK scheme momentum, 'green-gauss cell based' gradient and pressure-velocity coupling method were used. The sum of normalized residuals of all variables converged to less than 1x 10^{-4} within 900-3000 iterations for all models tested.

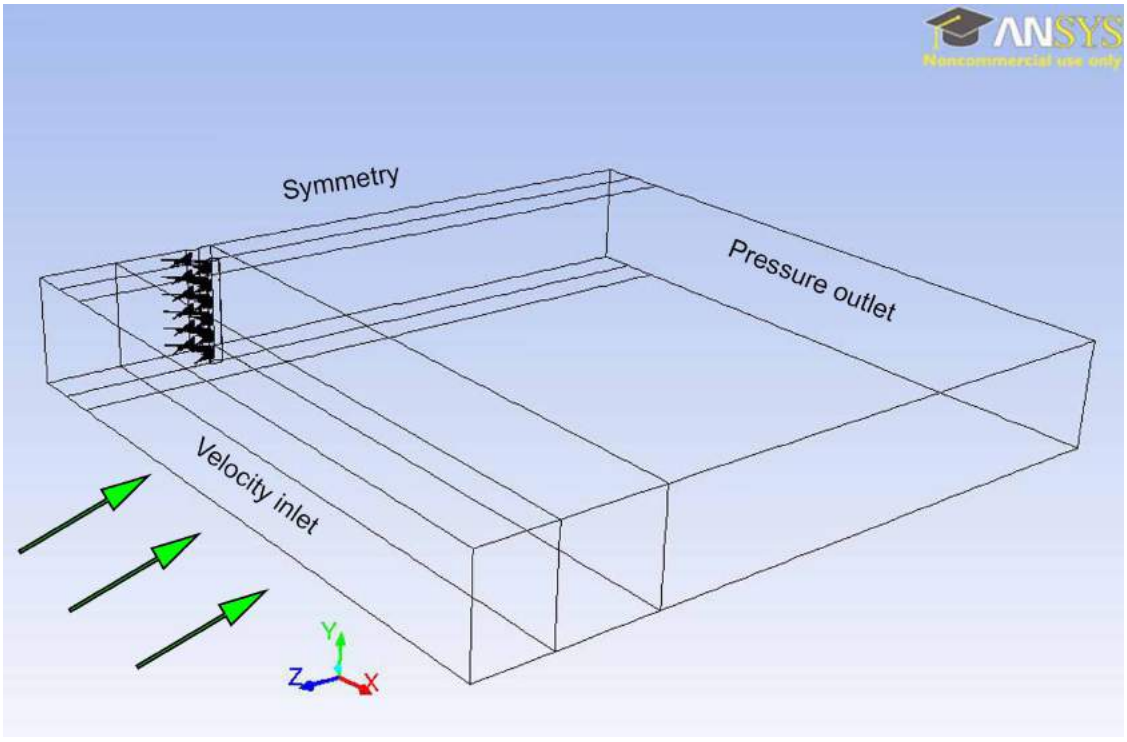

Figure 3.5. Setae with boxed boundary

Post-Processing

Here, we examined fluid pathlines, velocity vectors and contours, and drag coefficients of setae. Two planes (2D) comprising the height of the box and width from center to center of each cylinder along the x-direction were created at: i) the inlet upstream of enclosed setae; and ii) just downstream of the setae at the segment center. The mass flow rate along each plane was calculated and the proportion of inlet to segment plane mass flow rate was used to determine the amount of flow passing through the setae (i.e., leakiness). Drag coefficients of inner and outer setae are plotted against Reynolds number (Re) with base diameter of the longest setae as the characteristic length, L, and U, the dynamic viscosity of the fluid (i.e., 1.072e-03 kg/m-s for seawater at 20ºC; Vogel, 2003) (Fig. 3.9A,B).

Verification of Results

A variety of verification tests were performed to assess the appropriate element size for models and reliability of results from our CFD simulations.

2D tests

Grid number and quality typically guide the accuracy of ones results. The finer the mesh, the more accurate the results, however the more costly computationally and time-wise. A balance is needed between a mesh size that will produce results to the degree of accuracy desired while avoiding unnecessary additional elements. In our study, we used 2D tests to determine initial node number as well as to determine box parameters.

Minimum Node Number Required for models

To determine the minimum amount of nodes necessary to define our models without losing valuable information, we conducted several simple flow simulations in order to perform convergence testing. Using a series of models with varying node numbers, we ran simulations for each and monitored the pressure. Optimal node number was reached once there was no further change in pressure occurring with increasing node numbers. A rectangle with a circle disk centrally located of dimensionless diameter = 1 was used and tested with increasing node numbers along the disk edge.

Box parameters

Six disks of uniform dimensionless diameter = 1 arranged parallel to each other was created and solved using the finite element software CADYF (Etienne et al. 2006) (Fig. A6). Fluid entered the domain on the left, and flowed to the right. The zone of perturbation of fluid from the disks was analyzed by vertically increasing the domain size until the domain is wide enough for the deviated fluid to return naturally back to its initial horizontal direction. By manually increasing the height of the domain, a height of 80D (D being the diameter of the disk) was found to be satisfactory.

Grid refinement test

Three mesh sizes of approximately 3 million elements (ME), 7ME, and 9ME representing a coarse, medium, and fine mesh respectively were tested on each barnacle model. The mass flow rate at the segment was monitored for each case and final mesh sizes to which increasing the element size showed no significant changes in mass flow rates was found to be 6808487 cells for the sheltered and 7439983 cells for the exposed (Table 4).

Dimensional vs. Dimensionless

The coefficient of drag and fluid behaviour was compared using dimensionless and dimensional models to validate values obtained. Both simulations produced identical coefficients of drag within 3 digits of confidence and fluid behaviour in both simulations were identical.

Symmetry test

Our models defined symmetry in order to minimize mesh sizes, however defining symmetry, particularly where flow possibly diverges, leads to a possibility of forcing flow to be laminar at the symmetric boundaries where it otherwise may show vortices or recirculating flow. Three full adjoining cirri leg sections representing the equivalent symmetrical model was created to observe the effect of symmetry on results. Mass flow rates at the segment, directly downstream of setae and fluid patterns were compared. Both models had mass flow rates within 1% difference and displayed identical flow behaviour. Figure 2.6 represents our half model with the symmetric view applied.

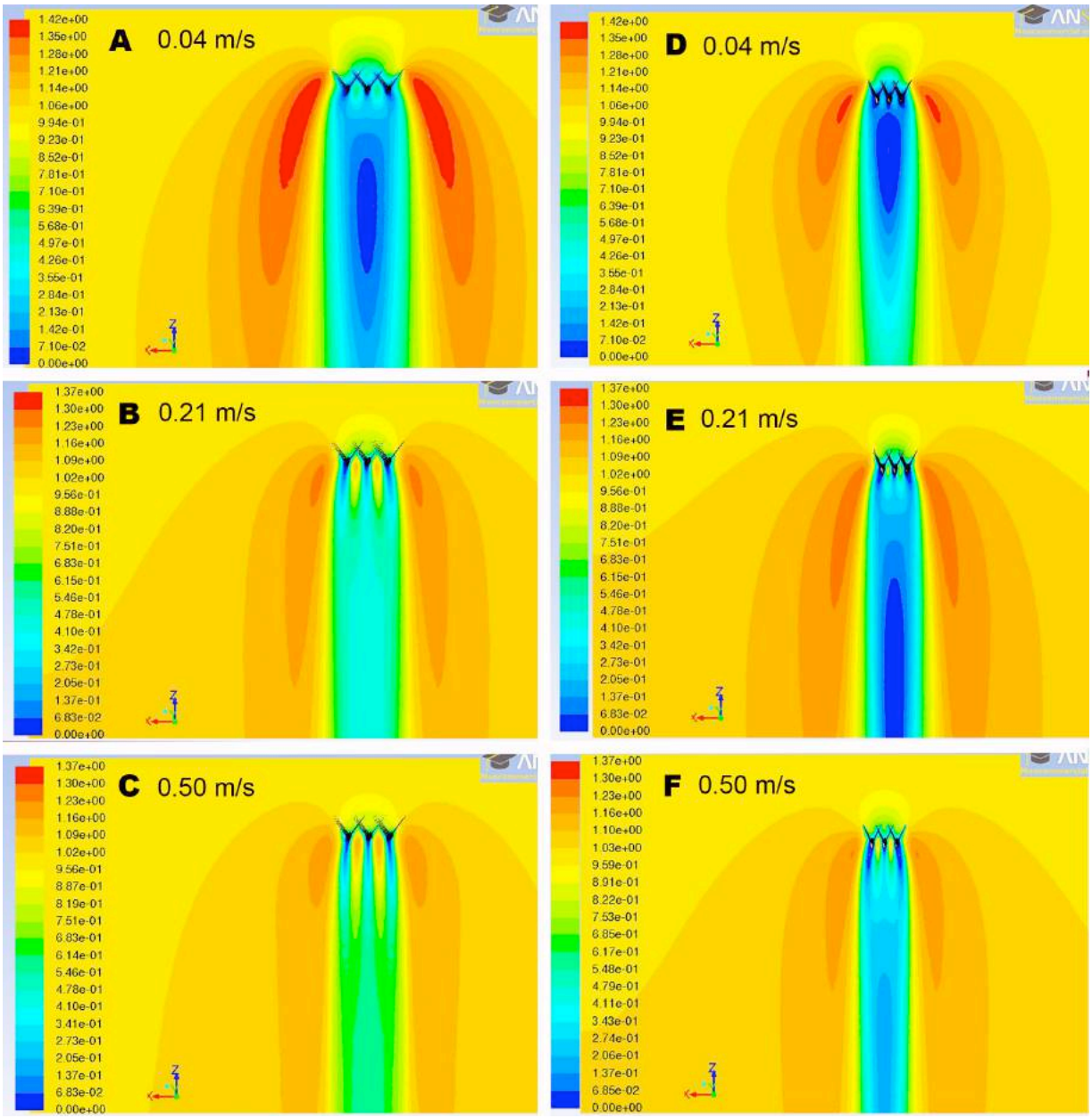

Figure 3.6. Velocity contours. Top view of velocity contours passing through intersecting setae with symmetric view applied to represent scale of simulations. A-C sheltered, D-F exposed at corresponding velocities.

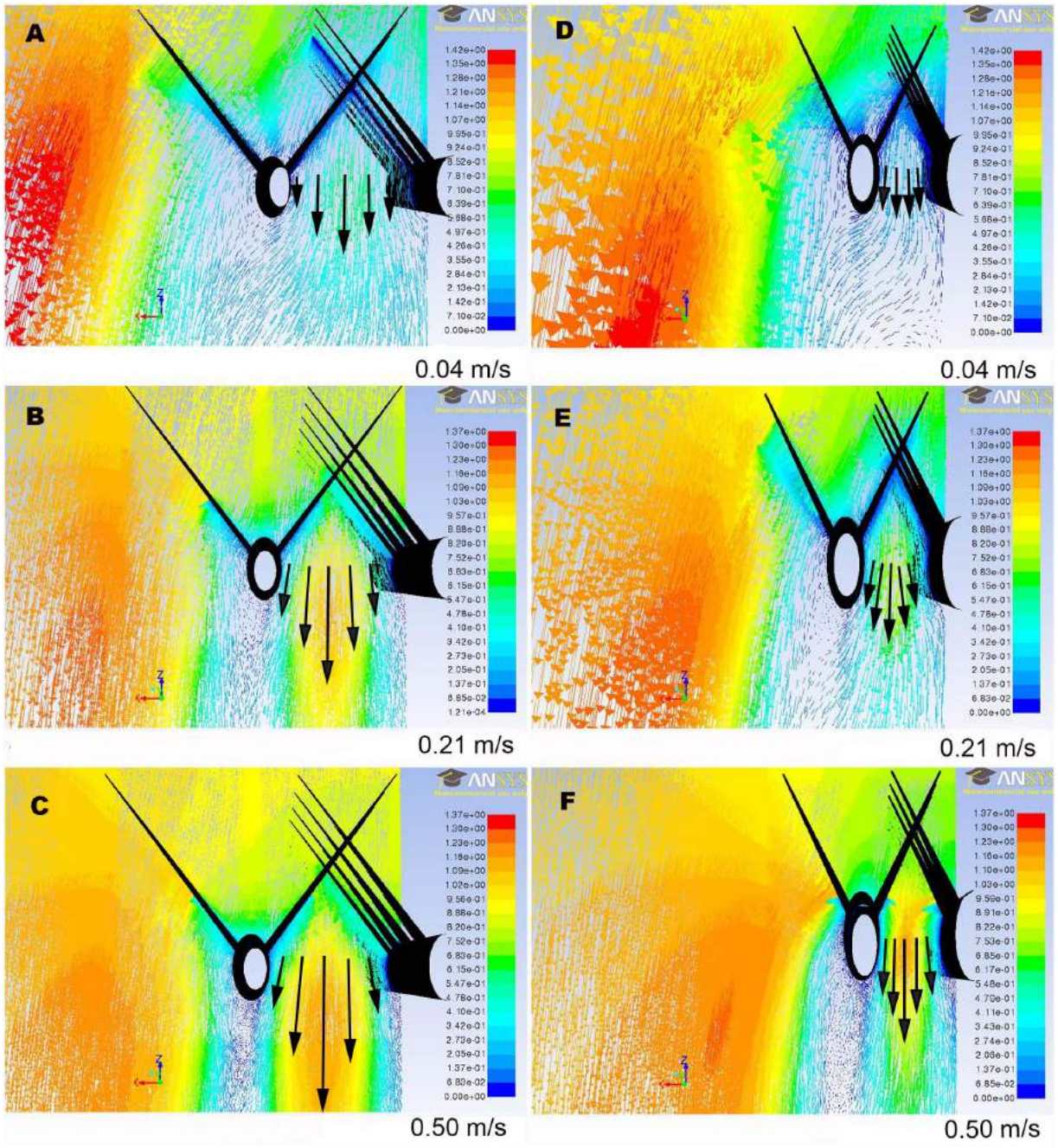

Figure 3.7. Velocity vectors. Magnified view of velocity vectors passing through setae. A-C sheltered vector profiles; D-F exposed vector profiles. Since flow fields are symmetric, only a single enclosed seta section shown. Arrow lengths denote relative velocities.

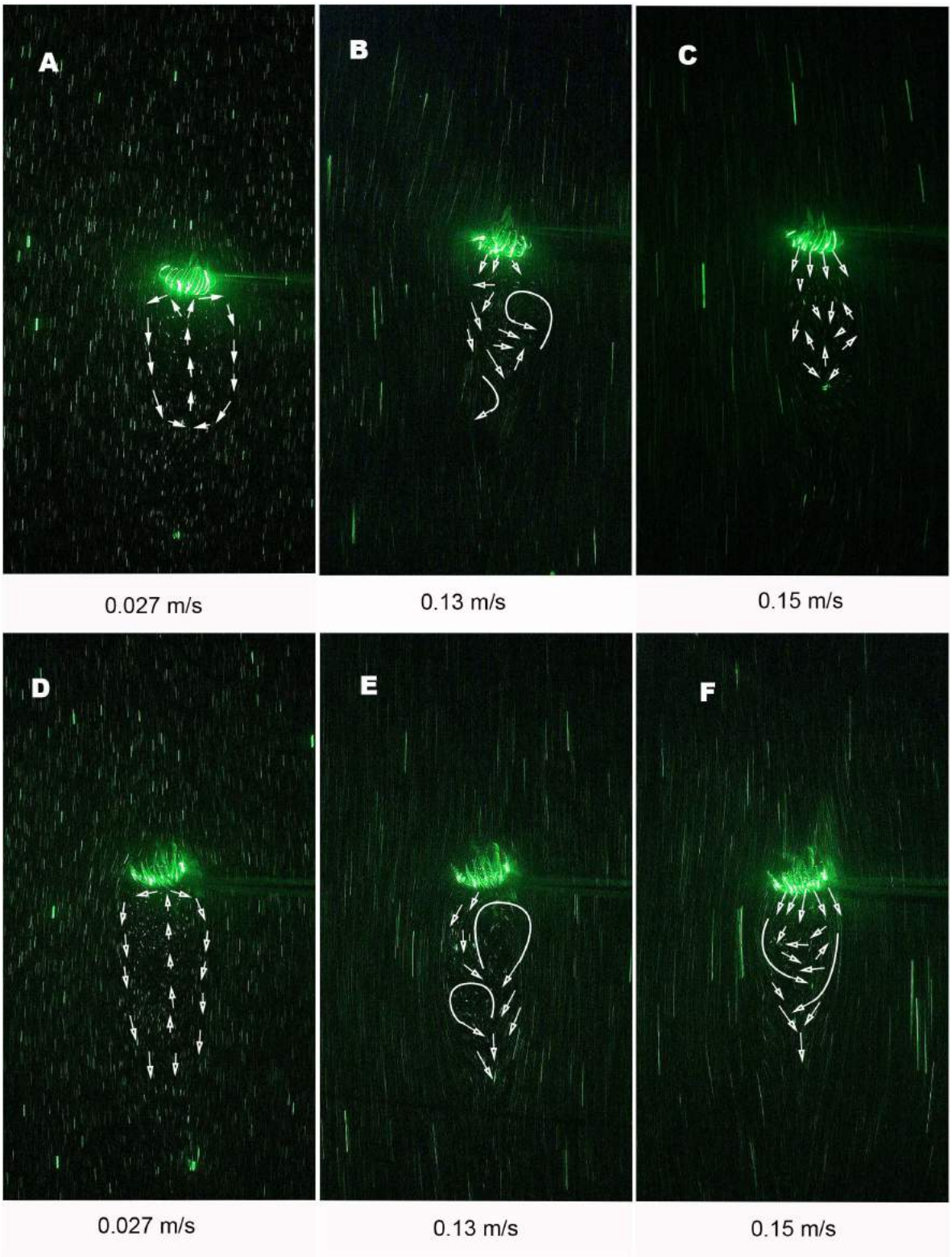

Figure 3.8. PIV of wake behaviour. Sheltered filter (A-C) and exposed filter (D-F). A, D show slow recirculating vortices; B, flow is passing through the filter, altering wake and flow separation point is pushed rearward; C, full leakiness with a short, turbulent wake and flow separation pushed further rearward; E, flip-flopping wake; F, short, turbulent wake with flow separation.

3.4 RESULTS

Computational Fluid Dynamic simulations revealed detailed flow behaviour at fine scales that have proven difficult to observe on animals. Due to computational limitations and to the modular nature of barnacle appendages, only a small 3D portion of the barnacle feeding fan was modeled. Observations on whole animals using PIV provided a larger flow field, though with less resolution. In situations where results from CFD and PIV could be compared, there were several congruent findings. This congruence provides some confidence that observations unique to the CFD simulations are valid.

Flow dynamics

A horizontal two dimensional plane passing through the intersecting setae was simulated with CFD to examine flow behaviour. Figures 3.6 and 3.7 reveal a top-view of the velocity contour and vectors respectively passing through the setae along the horizontal plane of the two barnacle models at all velocities tested. For comparison, the identical view was analysed with PIV (Fig. 3.8).

Flow behaviour

The general flow behaviour around the barnacle cirri of both phenotypes are similar in both our PIV experiments and CFD simulations. Flow is laminar upstream of cirri and depending on velocity (or Re) and phenotype, either: i) contours around the cirri, or ii) passes through the cirri. Laminar flow separates on the cirri and encloses vortices attached to cirri (i.e. vortex streets) followed by a laminar wake downstream (Fig. 3.6, 3.8; Video A1, A2). Fundamental differences in flow between the sheltered and exposed barnacles, are more evident in CFD simulations, most notably in the shear gradients next to structures and the wake area. CFD also provided drag coefficients, and more quantifiable detail on leakiness.

Shear gradient near structures

When fluid moves past a solid surface, the fluid contacting the surface does not slip relative to the surface and a velocity or shear gradient develops between the surface and the free stream (i.e. boundary layer) (Cheer & Koehl, 1987). CFD simulations show thicker, more shallow shear gradients around exposed model structures overall, while sheltered reveal the

contrary (Fig. 3.7). Regardless of the model, an increase in Re results in a more narrow and steep shear gradient (Fig. 3.7). The fine details of this boundary layer change are difficult to detect with PIV video analysis, though a decrease in velocity directly adjacent to both barnacle surfaces is apparent (Video A1, A2).

Wake characteristics

Wake behaviour and size vary depending on velocity (or Re) and less so according to phenotype (Fig. 3.7, 3.8; Video A1, A2) in PIV and CFD experiments. Wakes were observed for Re = 0-5 for cirri and 0-12 for setae (Fig. A7). CFD simulations of exposed models display a wake with very slow velocities (i.e. close to zero) in the low and medium velocities, and in the lowest velocity of the sheltered model (Fig. 3.6A,D,E). PIV reveal slow moving wakes behind cirri at comparable velocities, and counter-rotating vortices (Fig. 3.8A,B,D,E; Video A1, A2).

As velocity increases, PIV reveal both exposed and sheltered wakes displaying vortex shedding periodically, more notably in exposed, and faster recirculating vortices, which are deflected to opposite sides in an alternating way, also termed 'flip-flopping' (Meneghini, 2001) (Video A1,A2). The onset of flip-flopping occurs at lower velocities in sheltered at an observed velocity of 0.11 m/s (Re = 1.89), while in exposed at 0.11 m/s (Re = 2.63) (Video A1,A2). Flip-flopping ceases at 0.15 and 0.13 m/s for exposed (Re = 3.51) and sheltered (Re = 2.24) barnacles respectively. At this point, full leakiness is observed and wakes appear small, symmetric, turbulent, and the flow separation point (i.e. the place the wake starts to form) is pushed rearward (Fig. 3.8A-F).

Coefficient of Drag

Drag represents the hydrodynamic force inclining a body to move in the direction of fluid relative to the body (Koehl, 1996). The coefficient of drag (C^d) is a dimensionless number that characterizes all the factors that affect drag (Vogel, 2003). Although it is difficult to calculate using PIV, C^d for setae were easily calculated in CFD and provide insight on the functional morphology of the two wave-extreme barnacles. The C^d of the inner and outer setae were plotted against various Re (Fig. 3.9A,B).

C^d for the inner setae decrease with increasing Re for all models tested (Fig. 3.9A). That of the sheltered geometry decrease quicker than the exposed geometry. At a Re of one, comparable to the lowest velocity tested, sheltered models have a C^d 1.3 times greater that of exposed than exposed (Fig. 3.9A,B). As Re increases, C^d of exposed models surpasses that of sheltered at approximately Re = 3, and maintains the higher C^d with increasing velocity (Fig. 3.9A). The difference at higher velocities is not significant. The slope of the C^d for the outer setae of sheltered models is similar to that of the exposed models (Fig. 3.9B). The exposed models remain slightly higher with increasing Re, however the difference between the two is not significant

Leakiness

The leakiness in CFD was determined by examining the proportion of mass flow rates at the inlet with that passing directly downstream of inner setae. The percentage of mass flow rate passing through setae was plotted against Re (Fig. 4.0). As Re, increases, the leakiness of filters increases for all models, with sheltered filters showing a higher percentage passing through setae overall (Fig. 4.0). At very low Re (i.e. 1), sheltered barnacles reveal nearly three times higher fluid passing through the enclosed region than exposed (Fig. 4.0). As Re increases, this difference is less pronounced and approaches one another with increasing Re. The higher velocity in between gap spaces of filters observed in CFD velocity profiles may be interpreted as fluid passing between the segments and setae (i.e. leakiness) (Fig. 3.6, 3.7). At the lowest velocity (Re = 0.69), sheltered filters may be interpreted as having very slight leakiness (i.e. slightly leaky paddles), however exposed barnacles at the same velocity (Re = 0.96), show very slow, or creeping flow, indicating little to no leakiness and thus, paddle-like behaviour (Fig. 3.7).

The highest rate of increase in CFD for leakiness of sheltered barnacles occurs within the Re range 1-3.8, after which, increasing Re result in little changes on leakiness (Fig. 4.0). This suggests the transition from paddle to sieve-like behaviour with full leakiness occurring at the higher end of the Re scale. Exposed CFD models show the greatest rate of increase for leakiness occurring between Re range of 1-5 (Fig. 4.0).

PIV analysis assumed full leakiness to occur once particles were observed to pass directly through the center of a filter. Onset of leakiness was rated on a scale from 0-1, with 0

being completely non-leaky to 1 being fully leaky. At the lowest velocity tested (i.e. 0.027 m/s), both barnacle filters behave as non-leaky paddles (Fig. 4.1A-C; Video A1, A2). As velocity approaches 0.04 m/s, comparable to our lowest CFD velocity tested, sheltered barnacles (i.e. Re = 0.89) revealed very slight leakiness which increased up to velocity 0.13 m/s (Re= 2.24), after which complete leakiness was observed (Fig. 4.1 C-E; Video A1). Exposed barnacles reveal onset of leakiness to occur at 0.11 m/s (Re = 2.63) with full leakiness at 0.15 m/s (Re = 3.5) (Fig. 4.2, 4.3; Video A2). CFD estimates for leakiness fall within our PIV range observed.

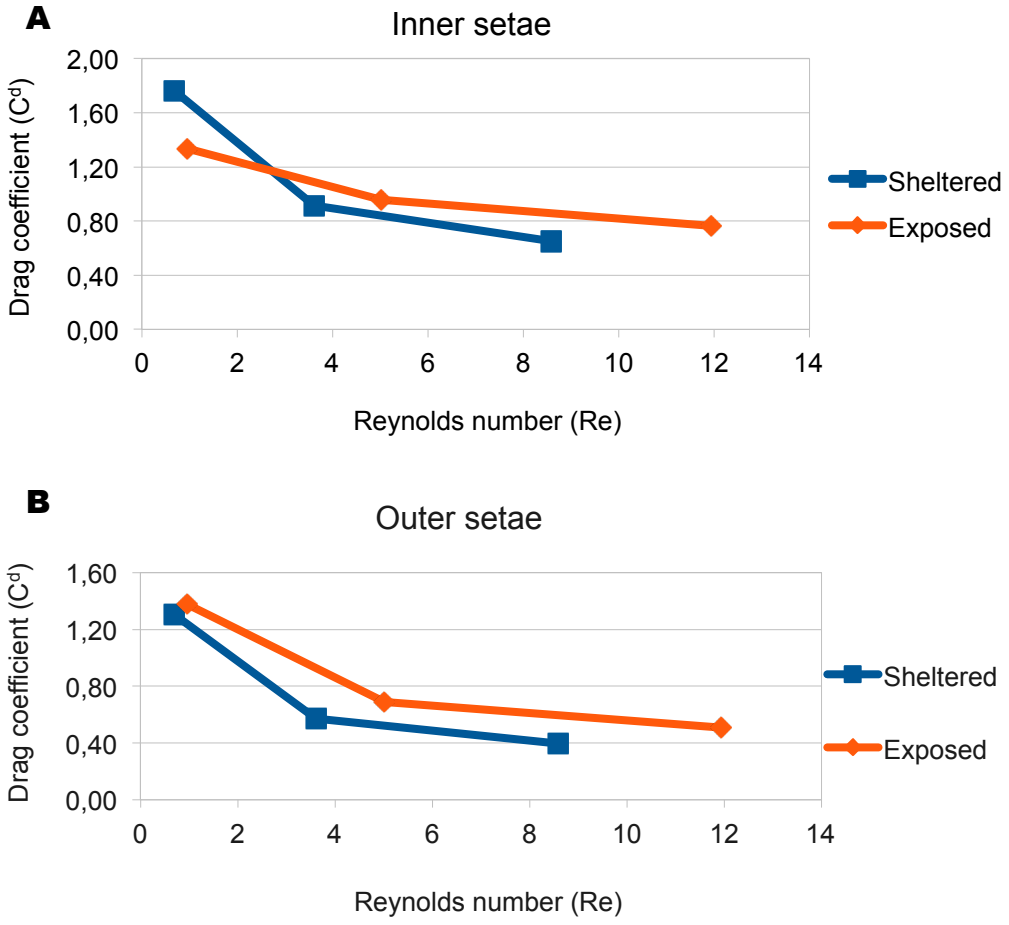

Figure 3.9. Drag coefficient plotted against Re. A, inner and B, outer setae.

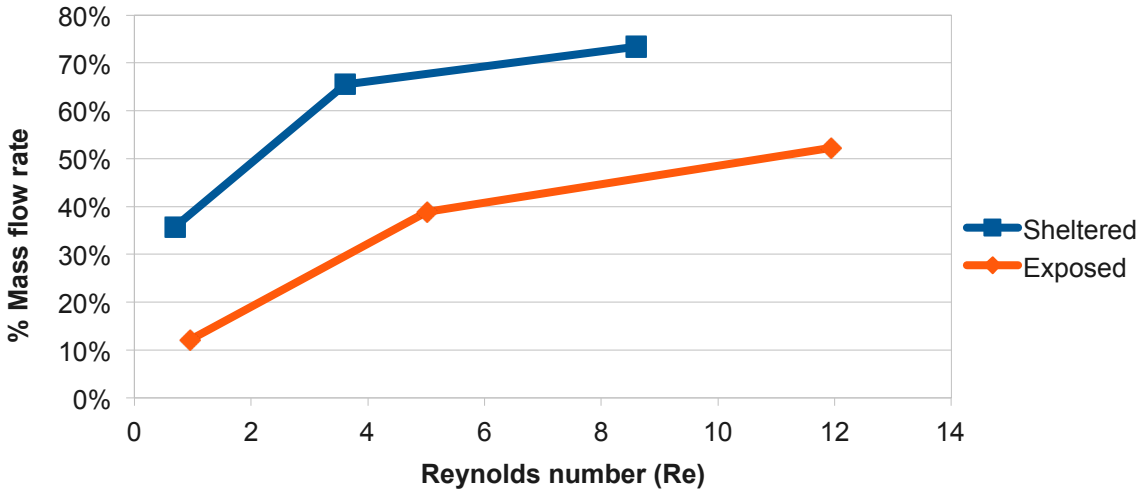

Figure 4.0. CFD Percent of mass flow rate passing through setae at increasing Re.

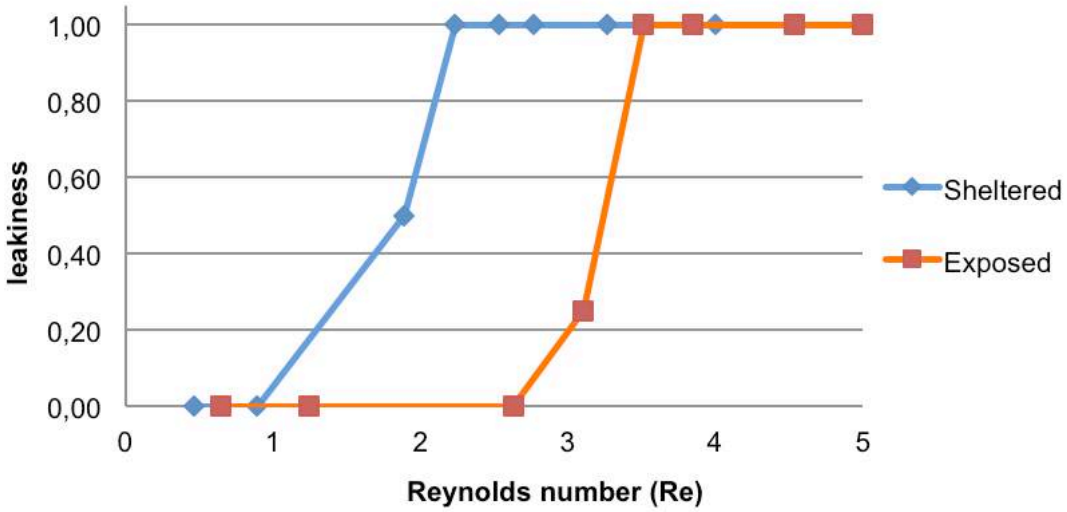

Figure 4.1. PIV observed leakiness with increasing Reynolds number.

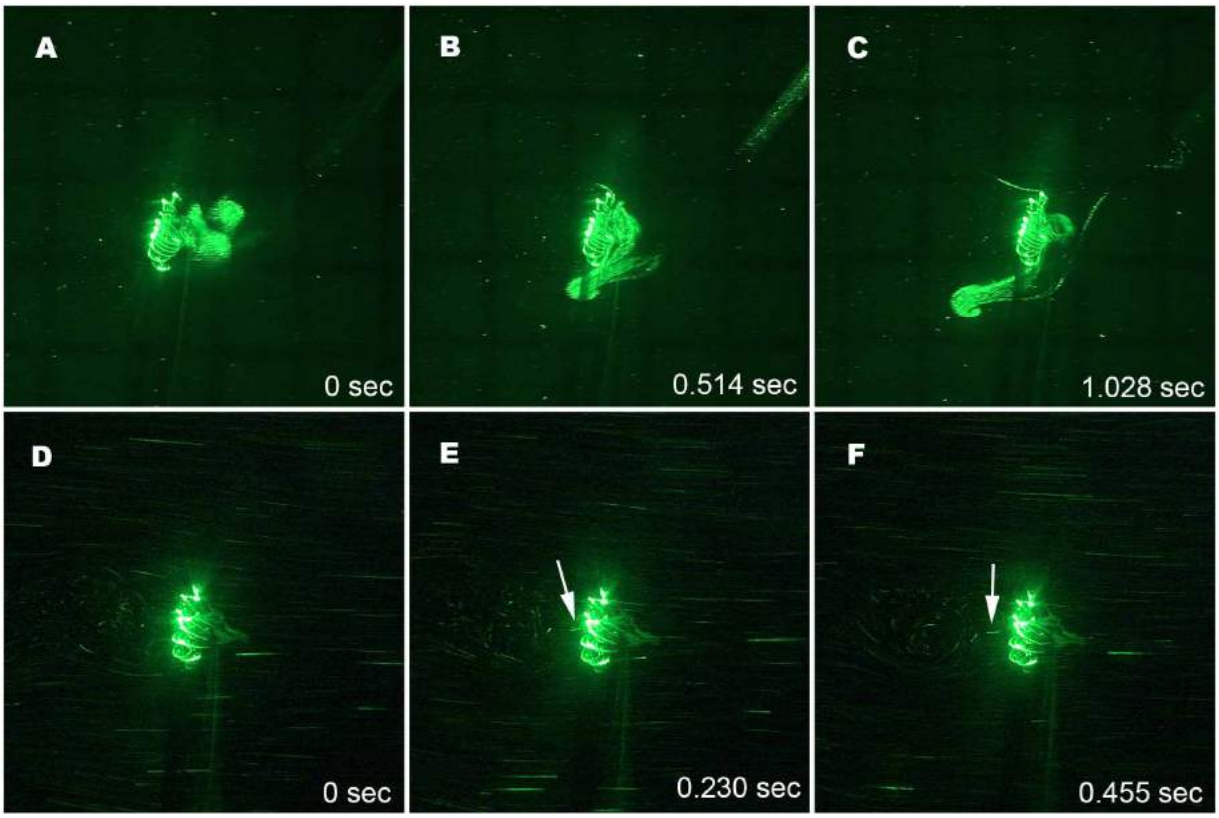

Figure 4.2. PIV flow fields representing paddle and sieve-like behaviour in a sheltered barnacle filter. A-C show paddle-like behaviour as a seeding cloud approaches and passes around the perimeter of filter at slow flow (i.e. 0.027 m/s, Re = 0.46). D-E show sieve-like functioning at faster flow (i.e. 0.13 m/s, Re = 2.24), with arrows denoting movement of a particle passing directly through the center of filter.

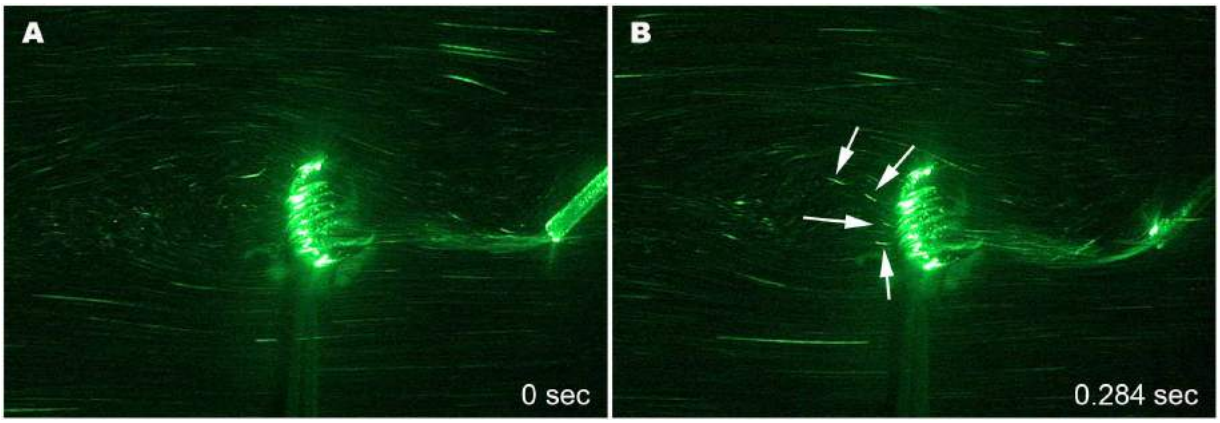

Figure 4.3. PIV flow fields of exposed filter at 0.15 m/s (Re = 3.5). Sieve-like behaviour with A, showing flow field directly before seeding and B, directly after with arrows denoting particles passing directly through the center of filter.

3.5 Discussion

This study set out to compare the filtering mechanisms among two phenotypically distinct, wave-extreme *Balanus glandula* barnacles through comparisons of the flow dynamics, coefficients of drag, and leakiness of each filter. As with previous work done on flow dynamics of barnacles filters using traditional flume experiments, visualisations of flow fields have been limited to flow speeds below 0.50 m/s (Trager et al., 1990; Pullen and LaBarbera, 1991; Trager et al., 1992; Sanford et al., 1994). Marchinko (2007) attempted to determine upper limit feeding velocities of barnacles, however equipment constraints resulted in this occurring only for sheltered individuals. Using computational fluid dynamics, flow was simulated through three dimensional models representing our wave-extreme filters. This not only simplified our analyses of the effects of morphology on a filters performance, but also unveiled flow details, normally difficult or impossible to observe in nature.

Shear gradients around structures

The steepness of the velocity gradient near a hair can greatly affect the efficiency of particle capture (Davies, 1973; Cheer and Koehl, 1987a). Particularly when Re are low, boundary layers are thick relative to the dimensions of the structure (Koehl, 1996). *Balanus glandula* from exposed sites have thick cirri segments and setae, with greater surface area, more closely spaced cirri, and smaller setae spacing ratios (Fig. 3.4, Table 4) compared to individuals from protected sites. A thick shear gradient relative to gaps between hairs at low Reynolds numbers (i.e. < 4) results, preventing much flow from leaking through and essentially creating paddles. At low Re, the thick shear gradients around structures produce a large viscous displacement effect where flow is diverted farther away from surfaces due to the broad viscous region (White, 2011), consequently pushing particles away and making the filter ineffective as a sieve to strain particles (Koehl and Strickler, 1981; Cheer and Koehl, 1987a). This demonstrates the inefficiencies of exposed geometries filtering in low Re conditions. As Re increases, shear gradients decrease overall and particles come in closer contact to filtering structures, increasing feeding efficiencies.

The reverse is true for sheltered barnacles characterized by narrow cirral segments and setae, and large gaps between setae (Fig. 3.4A). This morphology facilitates an increased mass flow of fluid through the feeding structures (Fig. 3.4). The narrow filter results in a steep shear

gradient and particle capture is more likely to occur with the close interaction of particles from the free-stream and filtering surfaces (Cheer and Koehl, 1987a; Vogel, 2003). As sheltered barnacles typically experience low Re, thin shear gradients are necessary in order to effectively capture particles. The disparate morphology of wave-extreme barnacles are adaptations for feeding at contrasting flow velocities.

Leakiness interpreted from wake behaviour

The wake generated in the downstream side of barnacle feeding appendages informs us of the leakiness between fibers and is influenced by Re and gap spacing (Kang, 2003). A large, slow-moving wake with counter-rotating eddies was observed in PIV on animals and CFD models for both exposed and protected barnacles at low velocities (i.e. 0.027 - 0.053 m/s). This is comparable to wakes formed by flow over solid bluff objects (Seto, 1990; Meneghini et al., 2001; Zhang and Zhou, 2001; Kang, 2003). In both cases, little flow passes between hairs resulting in a paddle-like function. A 2D CFD simulation comparing flow through 6 uniform diameter cylinders arranged in a side-by-side arrangement normal to flow against an array of 6 cylinders of decreasing diameters at Re = 0.5 revealed similar large recirculating vortices behind segments for the uniform cylinder arrangment (Fig. A6). This indicates the uniform cylinders are acting as a bluff object at this low Re, however the decreasing diameters permit flow to pass through at the same Re (Fig. A6). The decreasing cylinder simulations is analogous to the setae arrangement in barnacles, demonstrating the incredible ability for nature to design biological filters for optimal flow performance.

At low Re, when cylinders are very close together, their boundary layers can interfere mutually and a repulsion force may act between them, blocking flow (Bearman and Wadcock, 1973; Seto, 1990; Meneghini et al., 2001; Zhang and Zhou, 2001). At the lower end of velocities tested, Re < 1, the difference in setae spacing ratio (G/D) had little consequence on performance as both behaved as paddles, indicating similar and likely high cylinder interferences. As G/D was < 3 for both exposed and protected models (Table 4), with sheltered having slightly higher ratios overall, it can be interpreted that at this G/D in low Re (i.e. <1), the cylinders in a filter act as a single bluff body, and gap flow between them is deflected.

As flow increases, repulsion between cylinders diminish and the asymmetric, flip-flopping wake pattern observed with PIV for both phenotypes indicate more gap flow (i.e.

flow passing through hairs) influencing wake patterns (Kang, 2003) (Video A1, A2). The deflection of the gap flow causes one narrow and one wide vortex street to be formed which are irregular and unsteady (Kang, 2003). As flow separation and flow between cirri is not yet evident, gap flows are assumed to be weak, therefore filters are behaving as slightly leaky paddles. As velocity increases, the turbulent wakes with flow separation points positioned further rearward from cirri, indicate steady flow passing through gap spaces therefore full leakiness of filters. Sheltered demonstrate a lower threshold for this wake pattern at a velocity of 0.13 m/s (or Re =2.24) (Video A1, A2).

Drag of filter

The size and shape of cirri and setae affect the drag imposed on the feeding filter. At low Re, the tighter intermingling and larger spacing ratio of inner setae in sheltered models result in more flow interference from neighboring setae due to a broad viscous region, consequently leading to higher drag in sheltered compared to exposed.

In exposed models, the interstices between interlocking setae is larger resulting in less flow interference at low Re and thus less drag. As Re increases, drag and viscous layers are reduced overall, and as drag forces increases with projected area, naturally the larger exposed filter takes on a greater drag (Seto, 1990) (Fig. 3.9A).

Although exposed barnacles have thicker structures, the shorter length and smaller angle of the setal pairs minimizes the surface exposed to oncoming flow (Fig. 3.4), which reduces the net drag with respect to protected barnacles. These drag minimizing features are important for exposed barnacles that must effectively feed in high flow environments.

In both morphologies, setae located on the outer edge of distal cirri do not interact with other setae, resulting in lack of interference and similar drag forces among the two models (Fig. 3.9).

Leakiness and biological considerations

Previous studies have reported most filters to function as paddles at Re = 10^{-3} and as sieves as they approach Re = 1 (Cheer and Koehl, 1987a; Koehl, 1996). Here, we found the critical Re range for transition from paddle to sieve to occur between Re = 1- 3.5 for barnacle filters with full leakiness observed in sheltered at Re = 2.24 and exposed at 3.51. At very low

Re (i.e. < 1), the morphological differences between sheltered and exposed filters had little consequence on function. Both behaved as paddles, where thick viscous fluid and shear gradients prevented leakiness. As Re increased, the slimmer cirri and setae, larger G/D, larger opening between cirri, and more open setae configuration of the sheltered barnacle morphology result in steeper shear gradients and a lower velocity threshold for leakiness (i.e. Re ~ 0.89). This benefits sheltered barnacles which must effectively filter at very low Re with reported velocities as low as 0.0052 m/s (Re = 0.09) in certain sheltered environments (Marchinko and Palmer, 2003). The longer legs of sheltered barnacles reach past thick boundary layers associated with low Re to the free-stream flow and the thinner shear gradients permit increasing feeding efficiencies.

PIV analyses reveal exposed barnacles behaved as paddles up to Re = 3.1, at which point it transitioned to functioning as a fully leaky sieve at Re = 3.51 (Video A2). The higher transition point of exposed barnacles demonstrate its adeptness at high flow. At low Re, their thick, short, and compact geometry prevent flow through the filter. Likewise, the low profile keep them in the boundary layers and limit access to the free stream for filtering. Feeding in exposed barnacles has been reported to only begin at 0.0725 m/s (Re = 1.39) (Marchinko, 2007), suggesting they will not feed at lower velocities, complicating comparative studies. The higher velocity and continuous influx of particle-filled water passing through exposed filters provide a larger volume of flow per unit of filter time, allowing them to reduce drag forces, but maintain the capacity to efficiently filter particles.

The simultaneous use of CFD and PIV allowed a thorough analysis of flow fields around two geometrically distinct filters, with each method complementing the limitations either encountered. CFD allowed us to view detailed flow dynamics directly adjacent to structures, sometimes challenging to interpret with PIV, and calculated drag forces, difficult to acquire from small animals.

Several studies in engineering and biomedicine addressing the validity of CFD with PIV results, have repeatedly demonstrated CFDs ability to accurately and reliably predict details of flow fields in *in vivo* models (Sheng et al., 1998; Watanabe et al., 2005; Hoi et al., 2006; Ferreira et al., 2007; Ford et al., 2008; Van Ertbruggen et al., 2008).

Previous studies examining barnacle filters also reveal many parallels to our results, providing further validation of our CFD predictions. Trager et al. (1990) observed flow

passing through sheltered barnacle filters at 0.035 m/s, which was also observed with CFD at comparable velocities. Geierman and Emlet (2009) found barnacle filters comparable to our sheltered barnacles to behave as sieves at 0.04 m/s. Although CFD velocity profiles suggest only slight leakiness passing through at 0.04 m/s (Re = 0.46) (Fig. 3.7A, 4.0), feeding behaviour has great influence. Geierman and Emlet observed live animals, opposed to our passive filters, and the majority of the time, animals actively fed at this velocity. Should specimens have remained in the passive position, we believe our results would also correspond similarly.

Our present study revealed several parallels between CFD and PIV results, specifically with general flow and wake patterns and demonstrating leakiness at comparable velocities at low Re, however, visualisation constraints of flow fields at higher velocities in PIV make it challenging for validation of CFD results. Our models as well represent only a section of the filter, whereas PIV analysis observed flow through the entire filter, resulting in modified flow patterns. Therefore, to make reliable and comparable observations between CFD and PIV to validate results, future studies should model a complete filter or a system with the same conditions and model representation for both methods.

Assumptions and limitations

The Re estimation for complete leakiness of each filter morphology provides a good approximation of the transitioning point in barnacle filter functioning, however as with other mathematical and physical models, our models are only as good as their underlying assumptions.

Feeding behaviour and wall effects

The focus of this study was to compute appendage morphologies, image flow fields, and establish leakiness. All analyses were performed on passive barnacle filters, and active feeding behaviour was not considered. The movement of an appendage relative to fluid and towards a wall (i.e. substrate, body surface, or neighbor) can increase the leakiness through a filter at low Re (Cheer and Koehl, 1987a; Loudon et al., 1994; Koehl, 1996). As barnacles are facultative suspension feeders, actively sweeping their filters in slow flow and passively extending filters held rigidly opposed to the direction of flow in faster moving water, sheltered

barnacles would normally actively feed at the lower end of our velocities tested. Therefore, our leakiness predictions are not applicable to active feeding. Similarly, changes in cylinder spacing ratio (G/D) may affect the leakiness of a filter moving relative to a wall (Loudon et al., 1994), though G/D does not appear to affect leakiness at low Re in unbound fluid (Cheer and Koehl, 1987b). As both our methods assumed unbounded fluid, leakiness may have been underestimated for barnacles in closely spaced micro-habitats.

Scale of model (width and length)

To minimize computational time and calculations, our simulations observed flow through a small central region of the actual barnacle filter, representing 3 cirri, each only 6 segments in length. This enabled us to analyse both intermingled setae and distal setae that are open to flow (Fig. 3.2). The width of a row of cirri or setae may alter shear gradients near surfaces depending on Re, and hence affect leakiness (Cheer and Koehl, 1987a). At Re < 1, an increase in the number of setae or cirri in a row reduces leakiness, however at Re >1, the addition increases leakiness, suggesting the simple change to the width of a row of hairs has opposite consequences at slightly different Re (Koehl, 1995). Similarly, at low Re (i.e. $< 10^{-2}$), if the length of a hair (i.e. setae or cirri) is longer, as with a full sized filter, fluid is free to move around the tips of setae and sides of the cirri row, creating thicker shear gradients in the center of filters (Cheer and Koehl, 1987a). Therefore, our small section may be an underestimate in this respect and modeling a larger or complete cirral filter and testing it with a wide range of Re may provide more accurate estimates on the leakiness.

Mechanical stiffness

At high velocities (Re > 4), both filters showed high leakiness overall with little consequence to morphological differences at increasing velocities however, the mechanical stiffness of structures was not considered. CFD models assumed rigid, smooth walls. The bending and deflection of biological filters greatly reduce its feeding efficiency at higher velocities due to its inability to maintain a proper feeding position. Sheltered barnacles have been observed to undergo major cirral deformation occurring above 0.21 m/s (Marchinko, 2007), which was confirmed in our PIV analysis, while exposed reveal only minor cirral

deformation at 0.49 m/s. These physical limitations represent relative feeding limitations and abundance or distribution of specific phenotypes.

3.6 Conclusions

Examining the leakiness of a filter provides insight on the conditions in which a functional swtich of filters occur. With barnacles, this applies to the disparate functioning of their phenotypically plastic legs in variable flow, but may also apply to filters which encounter variable Reynolds number as they grow and develop. The critical range for transtioning from a paddle to a sieve for wave-extreme *Balanus glandula* filters occurs between Re of 1-3.5 with sheltered geometries having a lower Re threshold for sieving. At very low Re (i.e. <1) and Re above 4, morphological differences appear to have no significant consequences on a passive filters leakiness. Within the critical transitioning range between Re 1 and 3.5 however, the slight morphological differences resulted in disparate functioning of filters. The longer, slimmer geometry of sheltered provided thinner shear gradients, to increase leakiness and feeding efficiency in low Re environments, while the shorter, stout, geometry of exposed barnacles act to both reduce drag forces and maintain efficient feeding positions in higher flows. The leakiness of barnacle filters has demonstrated how simple morphological changes can dictate a complete transformation in function. Setae diameters and spacing have great influence on the leakiness of a filter at these lower Re, however, the parameter having the most influence to a functional change is yet to be determined. With the functional transition range determined, this narrows the Re range for future studies attempting to further the investigation between morphology and performance.

CFD use facilitated drag calculations and imaging of the fine flow details between structures, otherwise difficult to obtain using PIV alone. Nevertheless, considering the various modeling assumptions, continuous validations of CFD against *in vivo* data are encouraged.

3.7 ACKNOWLEDGEMENTS

Thanks to E. Tixier, R. Yu, and S. Corbeil-Letourneau at École Polytechnique for all the helpful discussions with FVM and CFD, and to all the staff at the Bamfield Marine Sciences Centre for logistic support. This research was supported by National Sciences and Engineering Research Council of Canada (NSERC) Discovery Grants to C.B.C. and D.P.

3.8 AUTHOR CONTRIBUTIONS

The concept for this study was developed by C.B.C and M.V and in concert with D.P, the experimental approach designed. M.V and F.V performed experimental CFD modeling, simulations, and analysis. M.V performed field work and P.I.V experimentation and analyses. M.V, C.B.C, F.V, and D.P prepared and edited the manuscript.

3.9 REFERENCES

Anderson, D. T. (1994). Barnacles: structure, function, development and evolution. London: Springer.

Arsenault, D. J., Marchinko, K. B. and Palmer, A. R. (2001). Precise tuning of barnacle leg length to coastal wave action. *Proceedings of the Royal Society of London. Series B: Biological Sciences* **268**, 2149-2154.

Ayaz, F. and Pedley, T. (1999). Flow through and particle interception by an infinite array of closely-spaced circular cylinders. *European Journal of Mechanics-B/Fluids* **18**, 173-196.

Bearman, P. and Wadcock, A. (1973). The interaction between a pair of circular cylinders normal to a stream. *Journal of Fluid Mechanics* **61**, 499-511.

Cheer, A. and Koehl, M. (1987a). Paddles and rakes: fluid flow through bristled appendages of small organisms. *Journal of Theoretical Biology* **129**, 17-39.

Cheer, A. and Koehl, M. (1987b). Fluid flow through filtering appendages of insects. *Mathematical Medicine and Biology* **4**, 185-199.

Davies, C. N. (1973). Air filtration. Academic Press: New York.

Ferreira, C. S., van Bussel, G. and Van Kuik, G. (2007). 2D CFD simulation of dynamic stall on a Vertical Axis Wind Turbine: verification and validation with PIV measurements. In *45th AIAA Aerospace Sciences Meeting and Exhibit/ASME Wind Energy Symposium*.

Fluent 13, Ansys (Software) (2012). Canonsburg, Pennsylvania:Ansys.http://www.ansys.com.

Ford, M. D., Nikolov, H. N., Milner, J. S., Lownie, S. P., DeMont, E. M., Kalata, W., Loth, F., Holdsworth, D. W. and Steinman, D. A. (2008). PIV-measured versus CFD-predicted flow dynamics in anatomically realistic cerebral aneurysm models. *Journal of Biomechanical Engineering* **130**, 21015.

Frank, D. M., Ward, J. E., Shumway, S. E., Holohan, B. A. and Gray, C. (2008). Application of particle image velocimetry to the study of suspension feeding in marine invertebrates. *Marine and Freshwater behaviour and physiology* **41**, 1-18.

Gambit (version 2.4) (Software) (2002). Canonsburg, Pennsylvania: Ansys. http://www.ansys.com.

Geierman, C. and Emlet, R. (2009). Feeding behavior, cirral fan anatomy, Reynolds numbers, and leakiness of *Balanus glandula*, from post-metamorphic juvenile to the adult. *Journal of Experimental Marine Biology and Ecology* **379**, 68-76.

Hansen, B. and Tiselius, P. (1992). Flow through the feeding structures of suspension feeding zooplankton: a physical model approach. *Journal of Plankton Research* **14**, 821-834.

Happel, J. R. and Brenner, H. (1965). Low Reynolds number hydrodynamics: with special applications to particulate media. Dordrecth, The Netherlands: Springer

Hoi, Y., Woodward, S. H., Kim, M., Taulbee, D. B. and Meng, H. (2006). Validation of CFD simulations of cerebral aneurysms with implication of geometric variations. *Journal of biomechanical engineering* **128**, 844-851.

iMovie '11 (vers. 9.0.2). Video editing software. Apple Inc. 2010. Mac OS X 10.6.

Jorgensen, C. (1983). Fluid mechanical aspects of suspension feeding. *Marine Ecology Progress Series* **11**, 89-103.

Kang, S. (2003). Characteristics of flow over two circular cylinders in a side-by-side arrangement at low Reynolds numbers. *Physics of Fluids* **15**, 2486.

Koehl, M. (1993). Hairy little legs: Feeding, smelling, and swimming at low Reynolds numbers. *Contemporary Math* **141**, 33-64.

Koehl, M. (1995). Fluid flow through hair-bearing appendages: feeding, smelling and swimming at low and intermediate Reynolds numbers. *The Society for Experimental Biology* **49**,157-182.

Koehl, M. (1996). When does morphology matter? *Annual Review of Ecology and Systematics* **27**, 501-542.

Koehl, M. (2001). Transitions in function at low Reynolds number: hair‐bearing animal appendages. *Mathematical methods in the applied sciences* **24**, 1523-1532.

Koehl, M. and Strickler, J. R. (1981). Copepod feeding currents: food capture at low Reynolds number. *Limnology and Oceanography* **26**, 1062-1073.

LaBarbera, M. (1984). Feeding currents and particle capture mechanisms in suspension feeding animals. *American Zoologist* **24**, 71.

Lee, I.-b., Sase, S. and Sung, S.-h. (2007). Evaluation of CFD accuracy for the ventilation study of a naturally ventilated broiler house. *Japan Agricultural Research Quarterly* **41**, 53.

Loudon, C., Best, B. and Koehl, M. (1994). When does motion relative to neighboring surfaces alter the flow through arrays of hairs? *Journal of Experimental Biology* **193**, 233-254.

Marchinko, K. B. (2003). Dramatic phenotypic plasticity in barnacle legs (*Balanus glandula* Darwin): magnitude, age dependence, and speed of response. *Evolution* **57**, 1281-1290.

Marchinko, K. B. (2007). Feeding behavior reveals the adaptive nature of plasticity in barnacle feeding limbs. *The Biological Bulletin* **213**, 12-15.

Marchinko, K. B. and Palmer, A. R. (2003). Feeding in flow extremes: dependence of cirrus form on wave-exposure in four barnacle species. *Zoology* **106**, 127-141.

Meneghini, J., Saltara, F., Siqueira, C. and Ferrari Jr, J. (2001). Numerical simulation of flow interference between two circular cylinders in tandem and side-by-side arrangements. *Journal of Fluids and Structures* **15**, 327-350.

Miller, L. P. (2007). Feeding in extreme flows: behavior compensates for mechanical constraints in barnacle cirri. *Marine Ecology Progress Series* **349**, 227-234.

Pullen, J. and LaBarbera, M. (1991). Modes of feeding in aggregations of barnacles and the shape of aggregations. *The Biological Bulletin* **181**, 442-452.

Riisgård, H. U. and Larsen, P. S. (2010). Particle capture mechanisms in suspension-feeding invertebrates. *Marine Ecology Progress Series* **418**, 255-293.

Rubenstein, D. I. and Koehl, M. (1977). The mechanisms of filter feeding: some theoretical considerations. *American Naturalist* **111**, 981-994.

Sanford, E., Bermudez, D., Bertness, M. D. and Gaines, S. D. (1994). Flow, food supply and acorn barnacle population dynamics. *Marine Ecology Progress Series* **104**, 49-49.

Schneider, C. A., Rasband, W. S. and Eliceiri, K. W. (2012). NIH Image to ImageJ: 25 years of image analysis. *Nat Methods* **9**, 671-675.

Seto, M. L. (1990). Flow interference effects between two circular cylinders of different diameters. Msc. thesis. University of British Columbia.

Sheng, J., Meng, H. and Fox, R. O. (1998). Validation of CFD simulations of a stirred tank using particle image velocimetry data. *The Canadian Journal of Chemical Engineering* **76**, 611-625.

Shimeta, J. and Jumars, P. A. (1991). Physical mechanisms and rates of particle capture by suspension feeders. *Oceanogrophy Marine Biology Annual Review* **29**, l-257.

Southward, A. (1955). On the behaviour of barnacles II. The influence of habitat and tide-level on cirral activity. *Journal of the Marine Biological Association of the United Kingdom* **34**, 423-433.

Tamada, K. and Fujikawa, H. (1957). The steady two-dimensional flow of viscous fluid at low Reynolds numbers passing through an infinite row of equal parallel circular cylinders. *The Quarterly Journal of Mechanics and Applied Mathematics* **10**, 425-432.

Trager, G., Hwang, J. S. and Strickler, J. (1990). Barnacle suspension-feeding in variable flow. *Marine Biology* **105**, 117-127.

Trager, G. C., Coughlin, D., Genin, A., Achituv, Y. and Gangopadhyay, A. (1992). Foraging to the rhythm of ocean waves: porcelain crabs and barnacles synchronize feeding motions with flow oscillations. *Journal of Experimental Marine Biology and Ecology* **164**, 73-86.

Van Ertbruggen, C., Corieri, P., Theunissen, R., Riethmuller, M. and Darquenne, C. (2008). Validation of CFD predictions of flow in a 3D alveolated bend with experimental data. *Journal of Biomechanics* **41**, 399-405.

Vogel, S. (1996). Life in moving fluids: the physical biology of flow. New Jersey: Princeton University Press.

Vogel, S. (2003). Comparative biomechanics: life's physical world. New Jersey: Princeton University Press.

Watanabe, S., Kato, H., Lei, Z., Imamura, T. and Enomoto, S. (2005). CFD code Validation via Particle Image Velocimetry (PIV). *JAXA Special Publication*, 178-183.

White, F. M. (2011). Fluid Mechanics (7ed). p. 486 - 509.

Zhang, H. and Zhou, Y. (2001). Effect of unequal cylinder spacing on vortex streets behind three side-by-side cylinders. *Physics of Fluids* **13**, 3675.C6

4.0 APPENDIX

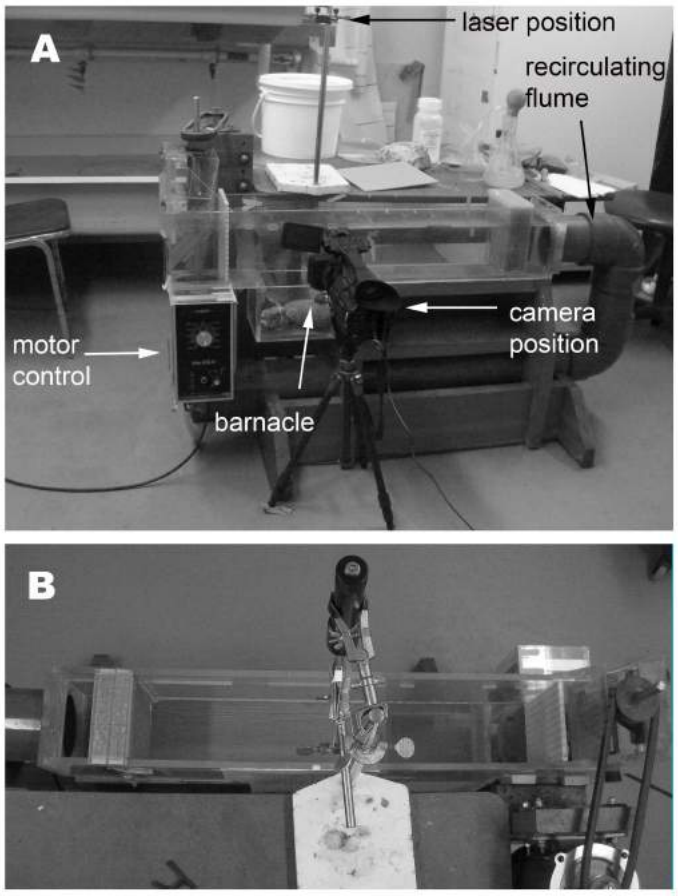

Figure A5. Experimental setup. A, recirculating flume showing camera, laser and barnacle positions. B, laser positioned on top of the flume and pointing directly down through an optical crystal to create the length-wise vertical PIV laser sheet.

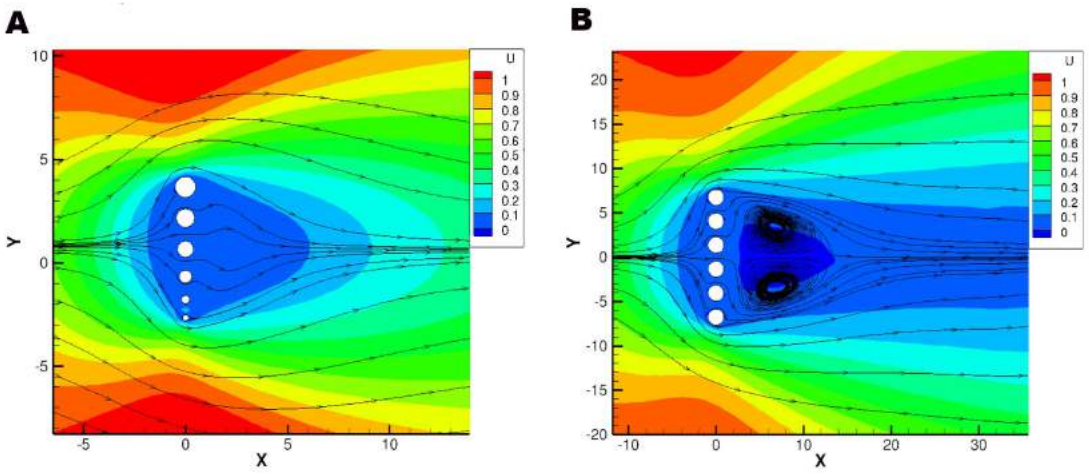

Figure A6. Velocity contours at Re = 0.5. A) Through decreasing cylinder diameters and B) through uniform diameter cylinders

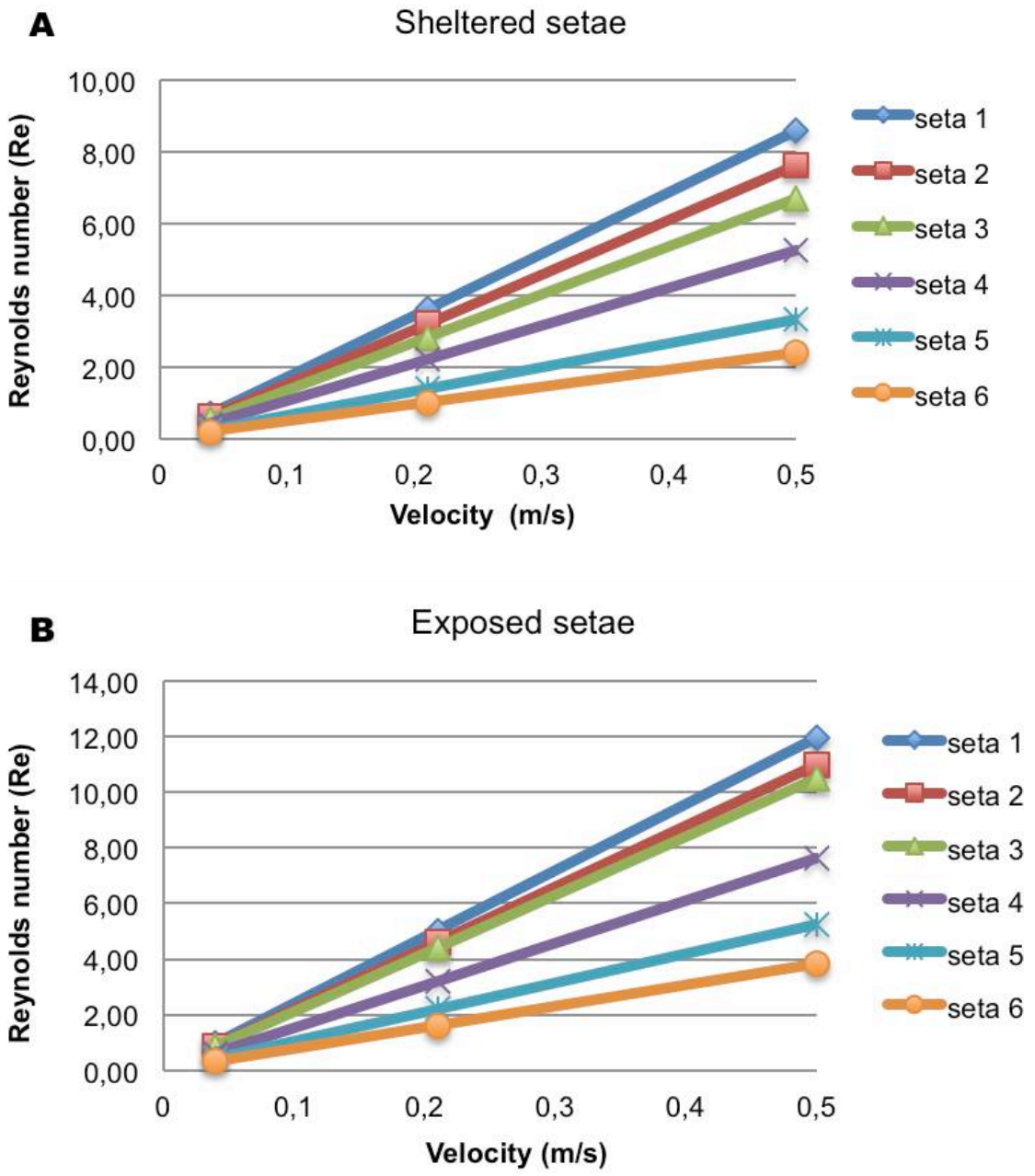

Figure A7. Setae Reynolds number with increasing velocities. A, sheltered setae and B, exposed setae.

Video A1. Summary of PIV flow fields in a sheltered barnacle filter. Velocities ranging from 0.027 m/s - 0.13 m/s

Video A2. Summary of PIV flow fields in an exposed barnacle filter. Velocities ranging from 0.027 m/s - 0.16 m/s

CHAPTER 4

4. EVALUATING CFD FOR BIOLOGY

Technology has allowed us to greatly improve biological research with advances in the former often linked to advances in the latter (Frank et al., 2008). Analytical applications such as electronic particle counters (EPC), flow cytometry (FCM), video-endoscopy, powerful microscopes, and particle image velocimetry (PIV) have all helped resolve many inherent difficulties, such as visualization or obstruction of flow. These technologies have likewise improved our understanding of suspension feeding mechanisms such as functional morphology of structures and kinematics of particle capture, transport, and ingestion (Frank et al., 2008 and references therein). The technological approach and the discoveries made by their use have paved the way for the development of conceptual models and further improvements on biological research.

Our studies used a computational fluid dynamics and finite volume methods approach to understand the flow dynamics and energetics of internal suspension feeders (i.e. the hemichordate pharynx) and external suspension feeders (i.e. barnacle legs). This interdisplinary approach is becoming more common in biological studies, however a full assessment, including advantages, accuracy for predicting biological behaviour, and limitations warrants further examination.

4.1 Computational Fluid Dynamics (CFD)

Computational fluid dynamics (CFD) is defined as "*the science of computing numerical solutions to partial differential or integral equations that are models for fluid flow phenomenon*" (Toro, 2009). Essentially, the computer numerically solves the laws that govern the movement of fluids in and around a subject system which is also created computationally (i.e. a geometric model) (Hirsch, 2007). The outcome is a virtual experiment, as opposed to

traditional experimental investigation, capable of calculating such elements as flow fields over surfaces, pressure distributions, velocity vectors and contours, stress, and drag, hence simplifying many case studies.

Both chapter 2 and 3 outline the major steps of using CFD, namely: 1) definition of the geometry, 2) discretizing the solution into finite elements 3) specifying boundary conditions and continuum, 4) definition of solver types and numerical method, and lastly, 5) post-processing.

Governing Equations

The Navier-Stokes (N-S) equations are the basic governing equations used to describe fluid motion for a viscous fluid whose equations are derived from the principles based on Newton's second law of motion for fluid (Acheson, 1990; Batchelor, 2000). The commercial CFD software package ANSYS FLUENT used in our studies use three dimensional solving for the N-S equation and solves for conservation equations of mass and momentum for all flows. Solving of the N-S equation can provide valuable information on flow patterns from velocity and pressure calculated at discretized points.

Finite Volume methods

Finite volume methods (FVM) were used in all of our studies for the discretization as they are available with commercial CFD software package ANSYS FLUENT and have easier formulation for unstructured meshes. Similarly to finite element and finite difference methods, values are calculated at discrete places, or nodes, on a meshed geometry. In the FVM, however, the governing equations are integrated over a "volume" around nodes with the assumption of a piece-wise linear variation of the dependent variables (Eymard et al., 2000). An advantage of FVM is that fluxes have more physical significance and are balanced across the boundaries for distinct volumes using the integrations, thus methods are conservative.

4.2 Biological use of CFD

Biology is one of the more recent domains to be added to the list of CFD users. Examples include using CFD to study tadpole swimming (Liu, 2002), hawkmoth hovering (Liu et al., 1998), ram suspension feeders (Cheer et al., 2001), the tidal flushing of animal

burrows (Heron and Ridd, 2001), and the propulsion efficiency in jellyfish (Etienne et al., 2010). As its primary use remains in industrial applications, software has been geared accordingly, and the challenges with modeling biological organisms, such as complex surface structure and geometry, material properties, and the conformation of organisms with movement make modeling more difficult. The accuracy, predictability, and therefore usefulness of CFD for biological studies still requires continuous validation. Chapter 3 nicely demonstrated CFDs potential of approximating biological phenomenon due to the parallels among CFD results and empirical data obtained using PIV investigation. It facilitated calculation of otherwise difficult variables such as drag in small animals and the fine flow details in between filter structures. Validation of CFD results with PIV have been repeatedly performed in many industrial and biomedical applications (Sheng et al., 1998; Watanabe et al., 2005; Hoi et al., 2006; Ferreira et al., 2007; Ford et al., 2008; Van Ertbruggen et al., 2008), providing confidence in the techology, however its limited use in biology requires further validation. The advantages and disadvantages of CFD use are discussed in the following section.

4.3 Advantages

Experimental studies are simplified

Traditional experimental approaches in a laboratory or field are sometimes met by numerous contraints and difficulties, as we will examine, leading to the potential for CFD use.

Delicate and fragile nature of animals - The soft, fragile state of certain animals make it difficult to collect, handle, and consequently observe in their natural setting or in the laboratory. Oikopleurid houses are frequently shed and/or damaged due to collection nets, upon handling, or during preservation in the laboratory (Alldredge, 1977).

Stressed animals - Animals may become very stressed or agitated in the laboratory when removed from their natural environment. The enteropneust *Harrimania kupferri* secretes copious amounts of mucus when added to fixative in the laboratory (Nørrevang, 1965) and ram suspension feeders becomes agitated when removed from their schools (Cheer et al., 2001).

Visualization - With animals only several millimetres or filtering structures sometimes in the micrometer size range, visualization of flow becomes extremely difficult (Cheer and Koehl, 1987a). Empirical data on flow fields inside cavities is extremely difficult to obtain and probes or other water flow measuring devices may be intrusive or interfere with water flow. Larvae amphioxus and ram suspension feeders are difficult to maintain in the correct feeding posture due to their constant movement, blurring flow fields, further complicating the acquisition of data (Lacalli et al., 1999; Cheer et al., 2001).

Controlled experiments - CFD enables users to create a controlled environment, facilitating systematic variation of a single factor while maintaining all other conditions constant; a task nearly impossible to perform in nature. The single modification on a reference model in our Chapter 2 study, minimized experimental variability between comparisons and allowed us to determine which characteristics have the greatest influence on power. Controlled experiments also allow the study of very large and very small systems and potentially hazardous or dangerous systems to become manageable to study.

Hypothetical situtaions - Hypothetical situations that may not exist in nature may be created to investigate a particular subject. Liu et al. (2002) created a hypothetical situation of making a fish swim in a tadpole mode over a larger Reynolds number range than normally found in nature in order to make comparisons on undulatory swimming methods (Liu et al., 1996).

Economical - Generally the more data, the more significant the analysis and results, however, associated with that comes increased time, laboratory fees, equipment, staff, and so on. CFD allows you to generate large volumes of data with ease at relatively low costs. Although the investment costs of CFD can be high, the total expense of running an experiment on the computer versus a full scale traditional experimental study is highly affordable in comparison.

Fast - CFD solutions generally require the repetitive manipulation of thousands, or even millions, of elements, impossible to calculate manually. Some basic CFD codes such as panel methods can complete in seconds to minutes (Malalasekera and Versteeg, 1995).

Accurate - In well known and modeled systems, CFD can reflect accurate and fast results. Betchel's (2003) predicted CFD calculations for head loss in a laminar flow pipeline was nearly identical to results of exact values calculated analytically, demonstrating CFDs possible precision and accuracy.

4.4 Disadvantages

Despite the many advantages of CFD, there exists some limitations and potential areas for errors to occur.

Designer's inexperience - A solution is only as good as its user. Poorly defined parameters within the code and general quality of the code along with problems in supplied geometry can lead to inaccuracies. Every numerical algorithm has its own characteristic error patterns which can only be determined with a thorough knowledge of the algorithms. There is still no formal way of estimating error introduced by inadequate design for a general flow, therefore initial definition of a particular problem requires very close attention.

Complex problems - The accuracy and complexity of a CFD problem depends in part on the mesh density. Increasing details, increases the accuracy but also computer power and calculation time. Users have to decide which parameters to include or omit without sacrificing accuracy of results. (i.e. temperature, 2D or 3D, pressure, air flow, and so on). Right choices requires good modelling skills and users must model to reduce complexity to a manageable level while still preserving significant features of the problem, which only comes with experience.

Biological shortcomings - Modeling biological organisms proves to be more complex than standard industrial questions in that biological organisms are made of soft, flexible, textured material in which shape conforms as it moves and surface roughness affects flow dynamics. CFD models are limited to smooth, rigid walls, limiting its ability to predict behavioural consequences such as structure buckling in certain flow conditions as discussed in Chapter 3. Animal behaviour is also difficult to mimic as animals respond differently to variable

conditions (i.e. passively feed in fast flow and actively feed in slow flow), therefore simulations are suited more for sessile organisms.

Validity of results - It is impossible to assess the validity of the models of physics and chemistry embedded in a program as complex as a CFD code or the accuracy of its final results by any means other than comparison with experimental test work. Once the validity for a particular problem is known (e.g. flow over a cylinder), however, a more in-depth examination into the problem may than be performed (e.g. flow over a cylinder at various Re) using CFD with relative confidence of results.

4.5 Future of CFD

Use of CFD as a supplement to experimental testing and validation of CFD results should be continually performed. Once the developement of a solid database of validated information exists for biological research, future studies may continue to expand on validated results and broaden CFD use to numerous areas in biological reasearch. The development of software should consider the biological community and include material options for defining models such as soft, flexible, or textured surfaces. With the development of computer technology, systems will become increasingly more powerful, efficient, affordable, user-friendly, and accurate, making it more appealing to use for biologists.

4.6 Conclusion

CFD is a powerful flow predicting tool that can provide detailed information of physical variables at both the macro and microscopic levels, giving a more in-depth understanding of physical phenomena. It has come a long way since its original use as a weather predicting tool in the beginning of last century, with its growth largely due to the huge development in computer technology, graphical user interfaces, affordability, and availability of commercial packages. Advances in CFD and its application to problems of increasing complexity is correlated with advances in computer storage and speed, therefore, the CFD community is in fact a potent force for driving the development of new supercomputers. CFD provides many advantages over traditional experimental methods, however, the codes are models that are close but not exact to real flow and should always be compared with

experimental data to continually validate results at the moment. Nevertheless, CFD may still serve as a powerful tool to use in conjunction with experimental investigation to provide in-depth analyses on fluid flow problems and advance research in otherwise difficult or unexplored areas of biology.

4.7 REFERENCES

Acheson, D. J. (1990). Elementary fluid dynamics: Oxford University Press.

Alldredge, A. L. (1977). House morphology and mechanisms of feeding in the Oikopleuridae (Tunicata, Appendicularia). *Journal of Zoology London.,* 181**(2)**, 175-188.

Batchelor, G. K. (2000). An introduction to fluid dynamics: Cambridge university press. 120 pp.

Cheer, A. and Koehl, M. (1987). Paddles and rakes: fluid flow through bristled appendages of small organisms. *Journal of Theoretical Biology* **129**, 17-39.

Cheer, A., Ogami, Y. and Sanderson, S. (2001). Computational fluid dynamics in the oral cavity of ram suspension-feeding fishes. *Journal of Theoretical Biology* **210**, 463-474.

Etienne, S., Garon, A., Pelletier, D. and Cameron, C. (2010). *Philiadium Gregarum* versus *Aurelia aurita*: on propulsion efficiency in jellyfish. From the 48th *American Institute of Aeronautics and Astronautics Meeting,* 1-8.

Eymard, R., Gallouët, T. and Herbin, R. (2000). Finite volume methods. *Handbook of numerical analysis* **7**, 713-1018.

Ferreira, C. S., van Bussel, G. and Van Kuik, G. (2007). 2D CFD simulation of dynamic stall on a Vertical Axis Wind Turbine: verification and validation with PIV measurements. Reno, NV, US. In *45th AIAA Aerospace Sciences Meeting and Exhibit/ASME Wind Energy Symposium*.

Ford, M. D., Nikolov, H. N., Milner, J. S., Lownie, S. P., DeMont, E. M., Kalata, W., Loth, F., Holdsworth, D. W. and Steinman, D. A. (2008). PIV-measured versus CFD-predicted flow dynamics in anatomically realistic cerebral aneurysm models. *Journal of Biomechanical Engineering* **130**, 21015.

Frank, D. M., Ward, J. E., Shumway, S. E., Holohan, B. A. and Gray, C. (2008). Application of particle image velocimetry to the study of suspension feeding in marine invertebrates. *Marine and Freshwater Behaviour and Physiology* **41**, 1-18.

Heron, S. and Ridd, P. (2001). The use of computational fluid dynamics in predicting the tidal flushing of animal burrows. *Estuarine, Coastal and Shelf Science* **52**, 411-421.

Hirsch, C. (2007). Numerical computation of internal and external flows: The fundamentals of computational fluid dynamics. Burlington, MA: Butterworth-Heinemann.

Hoi, Y., Woodward, S. H., Kim, M., Taulbee, D. B. and Meng, H. (2006). Validation of CFD simulations of cerebral aneurysms with implication of geometric variations. *Journal of Biomechanical Engineering* **128**, 844.

Lacalli, T. C., Gilmour, T. H. J. and Kelly, S. J. (1999). The oral nerve plexus in amphioxus larvae: function, cell types and phylogenetic significance. *Proceedings of the Royal Society of London, Series B: Biological Sciences* **266**, 1461-1461-1470.

Liu, H. (2002). Computational biological fluid dynamics: digitizing and visualizing animal swimming and flying. *Integrative and Comparative Biology* **42**, 1050-1059.

Liu, H., Wassersug, R. and Kawachi, K. (1996). A computational fluid dynamics study of tadpole swimming. *Journal of Experimental Biology* **199**, 1245-1260.

Liu, H., Ellington, C. and Kawachi, K. (1998). A computational fluid dynamic study of hawkmoth hovering. *Journal of Experimental Biology* **201**, 461-477.

Malalasekera, W. and Versteeg, H. (1995). An introduction to computational fluid dynamics-the finite volume method. Edinburg: Pearson education limited.

Nørrevang, A. (1965). On the mucuous secretion from the proboscis in *Harrimania kupfferi* (enteropneusta). *Annals of the New York Academy of Sciences* **118**, 1052-1069.

Sheng, J., Meng, H. and Fox, R. O. (1998). Validation of CFD simulations of a stirred tank using particle image velocimetry data. *The Canadian Journal of Chemical Engineering* **76**, 611-625.

Toro, E. F. (2009). Riemann solvers and numerical methods for fluid dynamics: a practical introduction: New York: Springer.

Van Ertbruggen, C., Corieri, P., Theunissen, R., Riethmuller, M. and Darquenne, C. (2008). Validation of CFD predictions of flow in a 3D alveolated bend with experimental data. *Journal of Biomechanics* **41**, 399-405.

Watanabe, S., Kato, H., Lei, Z., Imamura, T. and Enomoto, S. (2005). CFD code Validation via Particle Image Velocimetry (PIV). *JAXA Special Publication*, 178-183.

GENERAL CONCLUSIONS

The success of suspension feeding organisms in marine ecosystems is largely due to their multifaceted filtration system and adaptations to variable hydrodynamic conditions. Understanding the mechanical constraints, particle capture mechanisms and fluid dynamics with these biological filters has allowed us to interpret the functioning and general design principles of animals observed in nature as well as shed light on evolutionary questions.

Modelization of pumping water through multiple hemichordate pharynxs revealed the correlation between increasing energy demands with decreasing pharynx sizes and the inefficient flow circulation at both extremes of the size scale for ciliated pharyngeal filter feeding. These constraints explain both the the observed tendency for external feeding structures of small animals and the adoption of alternate feeding mechanisms of larger animals (i.e. muscular pump). The inefficient recirculation of fluid inside reconstructed *Cephalodiscus* models and its high energy costs to pump in its small size suggest the miniscule gill pores observed in pterobranchs are vestigial structures. This provided further support for the hypothesis of a larger acorn worm as the ancestor to all deuterostomes and as we are included in this phylum, it brings us closer to the discovery of our own origins.

CFD allowed us to specify pharynx diameter and pore changes to have the greatest affect on power expenditure as well as uncover the gill pores as the primary pump.

The paucity of reliable oxygen consumption rates in hemichordates made it difficult to validate our CFD results, thus future studies addressing this need will provide further validation. The results from this study suggests fluid mechanics act as a strong selective force driving the design principles of filtration systems in organisms of all sizes.

The change in function of bristled appendages from a paddle to a sieve depends both on morphology of an organism, either among different species or through ontongeny, and the

Reynolds number. The transition range for wave-extreme barnacle filters occurred at low Re between 1-3.5, with sheltered geometries transitioning earlier. With focus simply on geometry, within this critical Re range, the morphological differences between protected and exposed site barnacles, namely the setae spacing, length, and diameter, dictated the threshold for leakiness, while outside this range, any differences resulted in little consequences on filter performance. Determining this transitioning, now narrows the focus (i.e. Re range) for any subsequent research on barnacle morphology and performance. The large phenotypic plasticity between feeding legs may account for the functional change at different Re, however, the characteristic(s) having the most influence on change, remains to be determined. The large degree of plasticity of barnacles demonstrate they have adapted to different hydrodynamic conditions and justifies their abundance and success in oceans worldwide.

The use of computational fluid dynamics in our studies provided in-depth analyses on the mechanisms and fluid interactions of feeding appendages difficult to observe in nature. Its use undeniably facilitated our fluid studies and revealed fine details in spaces difficult to access. This innovative and interdisplinary approach may be necessary to uncover new discoveries and advance research in areas which have been exhausted through traditional methods. Despite certain limitations, CFD is a powerful tool to study fluid dynamics. Its future in biology is highly dependent on continual validation of results as well as the development of software to consider the biological community.

These studies demonstrate the different morphologies observed in nature likely resulted from strong selective forces experienced from their hydrodnamic conditions. Organisms have evolved to minimize their energy expenditure, drag, and pressure forces, and maximize feeding efficiencies. Understanding the relationship between morphology, performance, and their fluid dynamics reveal the large role fluid dynamics plays in both their form and functioning and how simple morphological changes can result in novel functioning.